

**NASA  
Technical  
Paper  
1950**

1981

# System Analysis Approach to Deriving Design Criteria (Loads) for Space Shuttle and Its Payloads

## Volume II – Typical Examples

Robert S. Ryan,  
Tulon Bullock,  
Wayne B. Holland,  
Dennis A. Kross,  
and Larry A. Kiefling  
*George C. Marshall Space Flight Center  
Marshall Space Flight Center, Alabama*

**NASA**

National Aeronautics  
and Space Administration

Scientific and Technical  
Information Branch

## TABLE OF CONTENTS

	Page
TYPICAL EXAMPLES .....	1
SECTION I. SPACE SHUTTLE.....	1
A. Characteristics.....	1
B. Approach .....	8
C. Shuttle System Loads.....	9
SECTION II. PAYLOAD LOADS.....	77
A. Space Telescope .....	77
B. Space Lab.....	88
SECTION III. CONCLUSIONS .....	99
BIBLIOGRAPHY .....	100

## LIST OF ILLUSTRATIONS

Figure	Title	Page
1	Shuttle configuration . . . . .	2
2	Space Shuttle MGVGT Orbiter/ET/SRB . . . . .	3
3	Space Shuttle MGVGT Orbiter/ET/SRB . . . . .	3
4	Space Shuttle MGVGT Orbiter/ET/SRB . . . . .	4
5	External tank schematic . . . . .	6
6	Trajectory shaping effect on loads. . . . .	8
7	Vehicle on pad . . . . .	10
8	SRB Aft Shirt, holddown bolt and foot pad . . . . .	12
9	Shuttle liftoff loads complexity . . . . .	13
10	SRB ignition thrust . . . . .	14
11	SRB thrust difference between two motors. . . . .	15
12	Number of free-free modes versus cantilever frequency. . . . .	16
13	Shuttle lift-off loads complexity . . . . .	17
14	MSFC & RISD lift-off envelope loads comparison. . . . .	20
15	MSFC & RISD lift-off envelope loads comparison. . . . .	20
16	MSFC & RISD lift-off envelope loads comparison. . . . .	21
17	Design loads interfaces and flow . . . . .	23
18	Analysis flow. . . . .	27
19	Systems dynamic laboratory environments and loads cycle. . . . .	27
20	Technical approach . . . . .	31
21	Gust directions considered . . . . .	31

## LIST OF ILLUSTRATIONS (Continued)

Figure	Title	Page
22	ET $M_y$ bending moment envelopes . . . . .	32
23	ET elastic transient contribution to $M_y$ . . . . .	33
24	Right SRB $M_y$ bending moment envelopes . . . . .	33
25	Right SRB elastic transient contribution to $M_y$ . . . . .	33
26	150 Real wind squatcheloid . . . . .	37
27	Monte Carlo analysis loads results . . . . .	38
28	Vortex shedding power spectral density plot. . . . .	40
29	SRB nominal reentry profile . . . . .	42
30	Test setup and results . . . . .	43
31	Resonance modes . . . . .	44
32	SRB motor frequency prediction model . . . . .	44
33	Environment as a function of angle of attack . . . . .	45
34	Sequence of events . . . . .	46
35	Sandia rocket sled test setup . . . . .	48
36	Drop test vehicle configurations . . . . .	49
37	SRB sequence of events-broadside deployment critical areas. . . . .	49
38	SRB sequence of events – deployment of mains critical areas. . . . .	50
39	Test objective targets. . . . .	52
40	Ultimate wing vertical bending moment (negative) ring hand wing B-52B/DTV configuration 1 . . . . .	52
41	DTV design loads . . . . .	53
42	Significant loading events . . . . .	54

## LIST OF ILLUSTRATIONS (Continued)

Figure	Title	Page
43	Typical initial impact dynamic events . . . . .	55
44	Cavity collapse loads . . . . .	56
45	SRB aft skirt water impact loads . . . . .	57
46	Nozzle configuration during water entry . . . . .	57
47	Simulation description . . . . .	58
48	SRB nozzle water impact response loads status . . . . .	58
49	SRB actuator water impact characteristics . . . . .	59
50	Typical actuator response . . . . .	59
51	SSME powerhead assembly . . . . .	61
52	High-frequency pressure transducer locations in engine . . . . .	62
53	LOX post shield configuration . . . . .	62
54	Maximum tension . . . . .	63
55	Force and loads characteristics on LOX posts . . . . .	64
56	LOX post loads block diagram . . . . .	65
57	Alternating stress versus lifetime . . . . .	66
58	HPFTP 1st stage blade cracking . . . . .	67
59	View of blade finite element grid with stress for a response case . . . . .	68
60	Aerodynamic interaction of strut/nozzle/blade configuration . . . . .	69
61	Aerodynamic flow past struts and nozzles . . . . .	69
62	Harmonic amplitude vs. harmonic number . . . . .	70
63	Relative amplitude vs. harmonic number, 15-strut case . . . . .	70
64	Alternating stress versus blade root temperature allowable . . . . .	72

## LIST OF ILLUSTRATIONS (Continued)

Figure	Title	Page
65	Description of nozzle system. . . . .	72
66	Steerhorn strains in transient operation. . . . .	73
67	Nozzle shell mode defined by Rocketdyne modal survey test . . . . .	74
68	Test configuration. . . . .	75
69	Nozzle model pressure pulses . . . . .	75
70	Space telescope. . . . .	78
71	Primary mirror loads . . . . .	80
72	Secondary mirror loads . . . . .	80
73	Analysis flow diagram . . . . .	81
74	Space telescope coordinate systems. . . . .	81
75	Interface forces . . . . .	82
76	Footpad forces time traces . . . . .	86
77	Net section load . . . . .	87
78	Multi-point release. . . . .	88
79	Single-point release . . . . .	88
80	Spacelab long module . . . . .	89
81	Pallet segment . . . . .	90
82	Design baseline configurations. . . . .	90
83	Sidewall mounted payloads for 5.7/5.8 triple pallet . . . . .	91
84	Location of nodal points for 89 DOF math model (internal) . . . . .	91
85	Typical Spacelab payload response . . . . .	95

## LIST OF TABLES

Table	Title	Page
1	Symmetrical Modes . . . . .	5
2	Anti-symmetrical Modes . . . . .	5
3	Derived Coefficients . . . . .	6
4	Liftoff Load Parameters . . . . .	11
5	Liftoff Program Capability Shuttle and Shuttle Payloads . . . . .	18
6	Varied Parameters and Combinations . . . . .	18
7	Loads Identified . . . . .	19
8	Design Criteria. . . . .	22
9	Basic Parameters . . . . .	25
10	Program Capability . . . . .	28
11	Analysis Approach. MAX Q. . . . .	29
12	Comparison with Rockwell Data. . . . .	34
13	Basic System Parameter Summary. . . . .	35
14	Preliminary Assessment of Aero Tolerances, Mach 1.25 . . . . .	36
15	Launch Probability for Q . . . . .	39
16	Load Summary . . . . .	40
17	SRB Reentry Acoustics-Fluctuating Pressures. . . . .	43
18	Decelerator Subsystem Requirements. . . . .	47
19	Data Summary - 80° Condition. . . . .	48
20	Development Test Philosophy. . . . .	50
21	Drop Test Program Objectives. . . . .	51
22	Primary Test Objectives Matrix . . . . .	51

LIST OF TABLES (Continued)

Table	Title	Page
23	Data Base for Water Impact Loads .....	54
24	Water Impact Loads Summary .....	60
25	Stress x 10 <sup>3</sup> .....	66
26	Comparisons of Steerhorn Peak Stresses .....	76
27	Hot-Firing Data Summary.....	76
28	Steerhorn Lifetime .....	77
29	Comparison of Results Maximum and Minimum Accelerations (GEES) in the OTA Lift Off Forcing Function Case LP604.....	82
30	Comparison of Results Maximum and Minimum Accelerations (GEES) in the OTA Landing Forcing Function Case LM35128 (Symmetrical Landing vs = 9.6 FPS).....	82
31	Design Values and Analysis Cycle Values .....	83
32	Multipoint Liftoff Loads.....	86
33	Developed Loads.....	93
34	Module-Mounted Payload Limit Linear Accelerations (g's) During Lift-Off and Landing.....	96
35	Pallet-Mounted Payload Limit Linear Accelerations (g's) and Angular Accelerations (rad/s <sup>2</sup> ) During Lift-Off and Landing.....	96
36	Sinusoidal Vibration Level .....	97
37	SL-1 Load Factors for Components Mounted in Racks No. 1 and No. 2.....	98



# SYSTEM ANALYSIS APPROACH TO DERIVING DESIGN CRITERIA (LOADS) FOR SPACE SHUTTLE AND ITS PAYLOADS

## TYPICAL EXAMPLES

This volume deals with loads analysis examples concentrating on special problem areas and areas that illustrate typical loads analysis approaches. Most examples come from Shuttle, its payloads, sub-systems, elements, and components.

### SECTION I. SPACE SHUTTLE

Marshall Space Flight Center has been heavily involved in the criteria development, loads philosophy approach, data interpretation, and independent trajectory, control, and loads analyses of the Space Shuttle vehicle. In addition, personnel have been members of Shuttle Systems Level II control panel, loads panel, performance panel, separation panel, aerodynamics panel, Ascent Flight Systems Integration Group (AFSIG), Systems Integration Review (SIR), and Program Review Change Board (PRCB). Although the major part of this section will deal with in-house independent loads analyses, some results of activities and analyses conducted by Johnson Space Center (JSC) and Rockwell International Corporation and reported in these working groups will be referenced.

#### A. Characteristics

##### 1. Dynamic Model

The Space Shuttle, from a loads analysis standpoint, is a very complex vehicle due to its multi-element, unsymmetrical design coupled with its multi-environment, multi-missions, and reusability requirements. It is a launch vehicle, orbiting space vehicle, and an airplane combined, weighing approximately 4.4 million pounds. The propulsion system consists of both solids (SRB's) and liquids with two liquid systems, the main liquid propulsion system consisting of the External Tank (ET) and three main engines (SSME's) and the Orbiter Maneuvering System (OMS). The two solids have a combined weight of 2.4 million pounds (1.2 million pounds each). The ET carries 1.4 million pounds of liquid oxygen (LOX) in the forward portion of the tank and 0.23 million pounds of liquid hydrogen (LH<sub>2</sub>). The Orbiter weighs 195,000 pounds and can carry up to 65,000 pounds into earth orbit.

Figure 1 depicts the Shuttle launch configuration from two viewpoints, side and top. The various elements are clearly shown as well as the element connections, such as struts, balls, etc. The multi-body point connections are one source of complication, statically and dynamically. Since each element has basic fundamental modes of oscillation constrained by the body or bodies it is attached to, this creates many overall vehicle modes

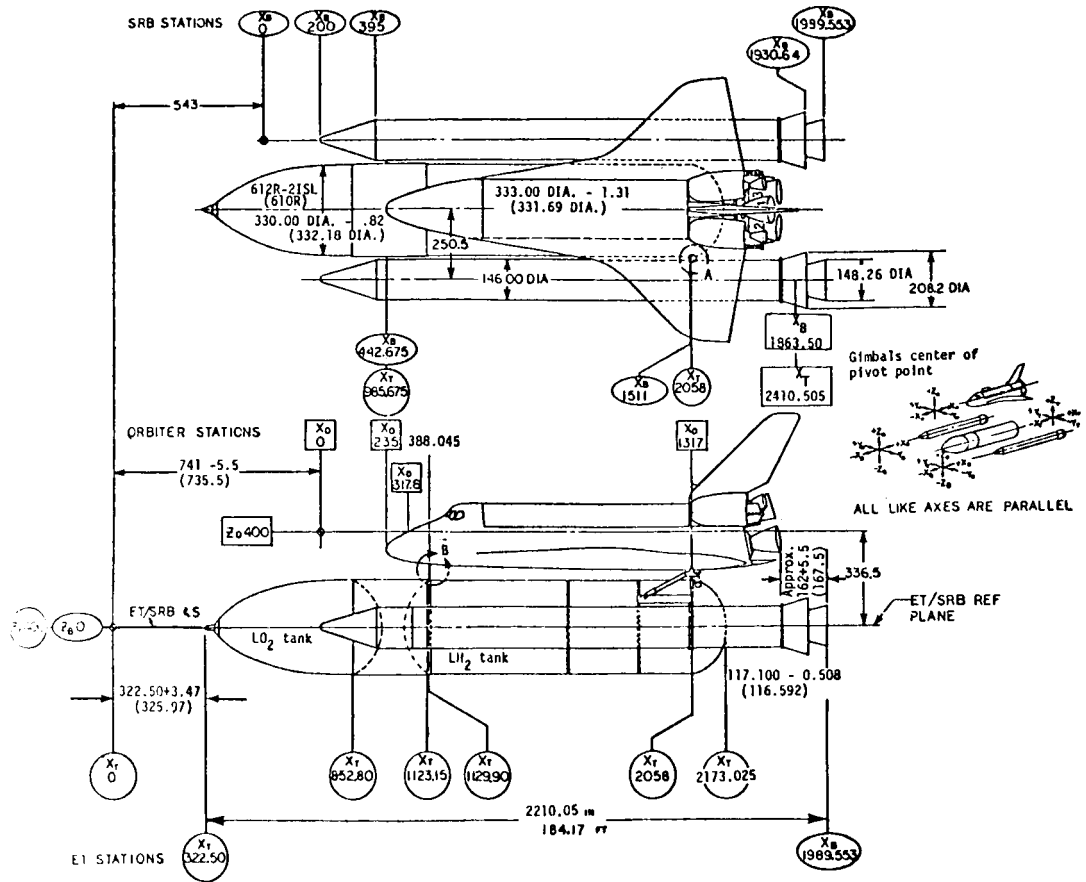


Figure 1. Shuttle configuration.

that shift significantly with small design changes due to element-to-element dynamic tuning. This means loads and response are very sensitive to these apparent small changes. Also, these same attachments and the overall configuration create asymmetries that cause cross-plane dynamic coupling. Longitudinal motion is coupled strongly with pitch and yaw motion. In addition, there is a strong static crossplane coupling. Figures 2, 3, and 4 are vector mode shapes for a 2.05 Hz mode measured in the full scale dynamic test conducted at MSFC. These vector mode shapes clearly show the strong crossplane coupling and the complex modal response.

Notice how the SRB's roll and pitch while the engines and OMS pods show pitch, yaw, and longitudinal motion. Some roll motion coupled with pitch is obvious for the tank while the Orbiter motion is primarily pitch and longitudinal. Because of the coupling potential of the multi-element modes in all directions, the modal density becomes very high requiring a large number of modes for loads analysis. This is illustrated in Tables 1 and 2 which contain the frequencies and mode shape descriptions for the high-gain modes found during full-scale testing. Both symmetrical and unsymmetrical modes are included.

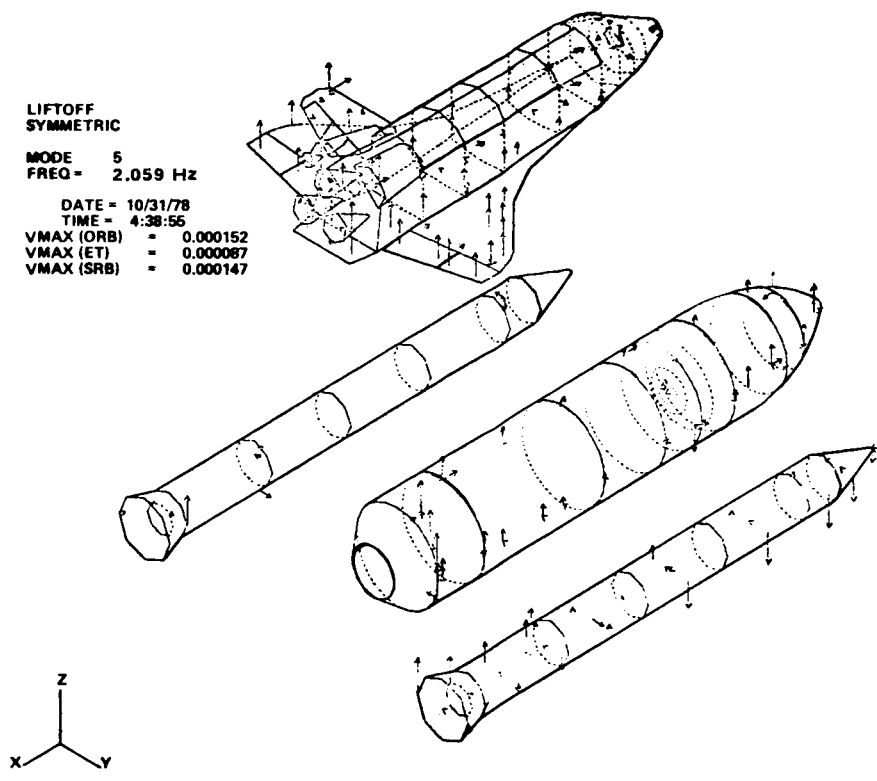


Figure 2. Space Shuttle MVGVT Orbiter/ET/SRB.

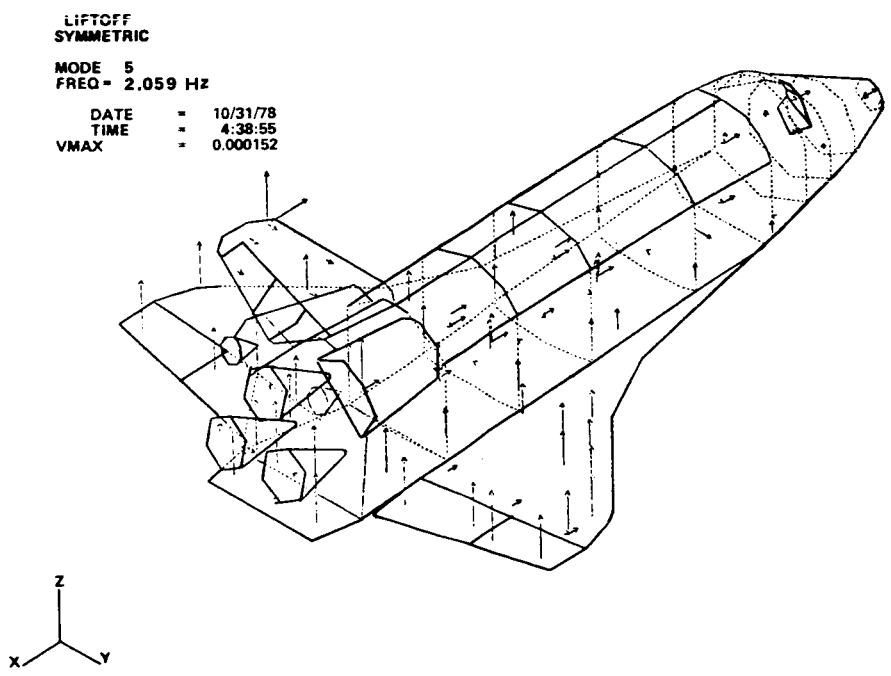


Figure 3. Space Shuttle MVGVT Orbiter/ET/SRB.

LIFTOFF  
SYMMETRIC  
MODE 5  
FREQ = 2.059 Hz  
DATE = 10/31/78  
TIME = 4:38:55  
VMAX = 0.000152

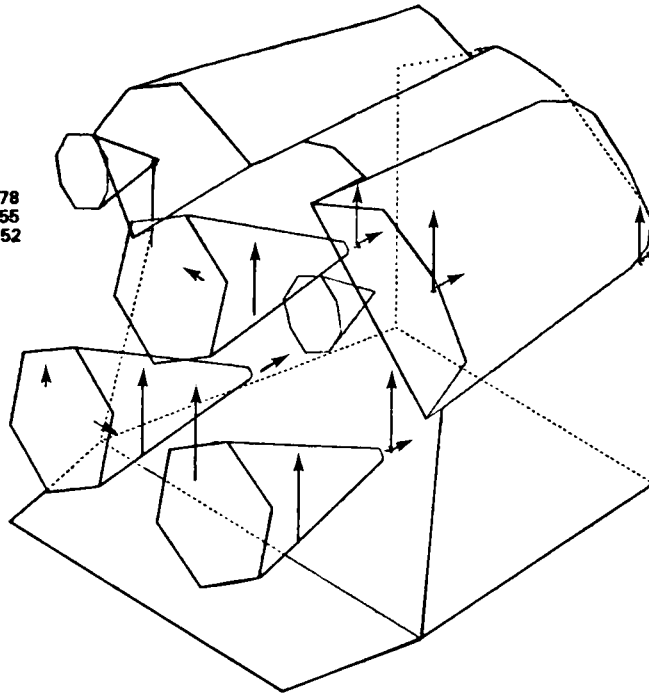
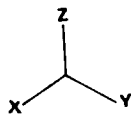


Figure 4. Space Shuttle MVGVT Orbiter/ET/SRB.

Another source of complications for loads analysis is the multi-body force application points. These forces are propulsion, aerodynamic, control, and inertial. For example, this means that forces in an attached member from both a static and dynamics consideration are the sum and differences of many large numbers. Anytime this happens, the sensitivity to small changes in characteristics is quite large. Figure 5 shows the interface forces and strut forces indicated as F's and P's, respectively. For the max q condition, loads determination can be made by summing the contributions due to externally applied forces. Table 3 gives a typical type set of coefficients derived to illustrate this effect.

If bending dynamics is important in one of these loads, then obviously the summation becomes very complex. This happens for the liftoff situation. This means that the complex load paths can lead to reduced loads, balancing main engine thrust with SRB thrust through ET fittings but at the expense of increased sensitivity and uncertainty in the loads.

Special couplings also exist between time sequencing, trajectories, propulsion, etc., that are very important but better discussed under the following sections dealing with the individual load events.

## 2. Control System

The Shuttle control system is a fundamental part of this coupling and the other items discussed above. The control system sends signals to each actuator of each propulsion element and mixes them in such a way as to provide maximum control torque for correcting

TABLE 1. SYMMETRICAL MODES

Test Mode			
Mode No.	Freq. (Hz)	Critical Damping Ratio	Critical Description
5	2.05	0.013	SRB Roll (0.34), Pitch (0.25), Yaw (0.16), Orbiter Pitch (0.08), ET-Z (0.13)
7	2.64	0.014	SRB Yaw (0.95), F1 Pitch (0.02)
9	3.02	0.017	SRB Pitch (0.38), Roll (0.27), F1-Z Bending (0.10), Orbiter-Z (0.07)
11	3.24	0.010	ORB Bending (0.33), X (0.36), SRB Z Bending (0.25)
12	3.88	0.015	SRB-X (0.60), Yaw (0.13), FWD F1 Shell (0.24)
23	4.39	0.001	SRB Z-Bending (0.22), Roll (0.08), F1 Fluid (0.17), Orbiter Bend (0.17)
14	5.26	0.016	SRB Z-Bending (0.47), F1 Bending (0.27), Orbiter Bending (0.17)
18	5.65	0.005	Orbiter Pitch, Bending, In-Phase Wing Bending (0.55), Orbiter X (0.18)
10	6.43	0.037	1st Wing Bending (0.68), Out-of-Phase Upper SSMI (0.13)
21	6.78	0.011	SRB Sym Haw and Y-Bending (0.85)
15	7.02	0.011	VERT Tail FWD/Alt Rocking (0.21), Out-of-Phase Wing Bending (0.18)
32	7.45	0.031	SSMI No. 3 Pitch (0.20), Out-of-Phase V.1, FWD/Alt Rocking (0.11)
27	7.77	0.009	1st LOX Tank Bulge, UPR F1 <sub>2</sub> (0.34), LOX Ogive (0.14)
16	8.42	0.016	SRB 2nd Z-Bending (0.62), Roll (0.05)
3	9.00	0.008	Orbiter Pitch and Bending (0.76), Out-of-Phase SRB Pitch (0.05)
26	11.94	0.025	SRB 2nd Y-Bending (0.71), Motor Case No. 3 Prop (0.00)
22	12.41	0.002	LOX Dome Bulge (0.0016), F1/L (0.15), LOX Tank (0.29)
19	14.52	0.010	FWD/Alt P/L X Out-of-Phase (0.14), FWR SSMI Pitch (0.16)
30	14.87	0.022	SRB Torsion (0.58), F1 (0.14)
31	14.87	0.030	Outb'd Elev RO1 Out-of-Phase With Inb'd Elev (0.22)
33	15.97	0.008	LOX Dome Bulge (0.0066), LOX Tank (0.30), SRB Axial (0.12)
17	15.97	0.027	Payload Pitch (0.12), OMS POD X (0.18), F1 (0.25)
25	16.15	0.012	OMS POS X (0.16), Out-of-Phase P/L X (0.07), Crew Mod X (0.03) and Z (0.05), F1 (0.28)
35	18.96	0.041	SRB Axial (0.43), LOX Dome (0.0092), F1 (0.48)
36	27.48		SSMI Axial, UPR Out of Phase with FWR (0.22), OMS POD (0.33), F1 (0.20)
39	30.53	0.014	SSMI Axial, FWR Out of Phase with UPR (0.28), OMS POD (0.06), F1 (0.35)
34	31.23	0.044	UPR SSMI Axial (0.31), OMS POD (0.19), F1 (0.24)
37	34.74	0.018	FWR SSMI (0.18) Axial In Phase with FWR (0.01), OMS POD (0.14), F1 (0.03)

TABLE 2. ANTI-SYMMETRICAL MODES

Test Mode			
Mode No.	Freq. (Hz)	Critical Damping Ratio	Critical Description
10	2.08	0.010	SRB Yaw and Y-Bending (0.163), ET YB (0.20)
8	2.24	0.010	SRB Pitch (0.33), Roll (0.18), Orbiter Y-Bend (0.29), Roll (0.03)
11	2.47	0.014	SRB Pitch (0.60), Roll (0.13), Orbiter Roll and Yaw (0.12)
15	3.37	0.016 0.022	SRB X (0.35), Y-Bend (0.16), Vert Tail Y-Bend (0.16)
27	3.53	0.005 0.007	Gear Trans, SRB Roll (0.08), F1 (0.09), Vert Tail Y-Bend (0.40)
5	4.12	0.014	SRB Roll (0.20), Z-Bend (0.09), ORB Yaw (0.44), Includ C M Y (0.10)
21	4.71	0.010	SRB Roll (0.27), Pitch (0.12), ORB Yaw and Roll (0.39)
28	4.98	0.016	Wing 1st Bend (0.38), SRB Y (0.14), SRB Z (0.10), FUS Y (0.08)
20	5.14	0.014 0.017	SRB Y-Bend (0.59), Z (0.13), Roll (0.03), F1 Y Bend (0.13)
1	5.45	0.013	SRB Z-Bend (0.43), Y-Bend (0.12), OMS POD Y (0.05)
25	5.57	0.016	Orbiter Yaw and Y-Bend (0.31), SRB Y-Bend (0.18), Z-Bend (0.15), Roll (0.04)
16	7.41	0.22 0.28	F1 Y-Bend (0.72), SRB Y-Bend (0.11)
24	8.30	0.010	Payload Y Out-of-Phase (0.21), FUS Torsion (0.21), Out-of-Phase Wing Bend (0.10)
18	9.28	0.011	F1 LOX Tank Torsion
2	10.10	0.028	SRB 2nd Z-Bend (0.60), Yaw (0.10), Axial (0.04)
19	10.65	0.022	SRB 2nd Y-Bend (0.61), Z-Bend (0.29)
31	13.89		Vert Tail Torsion (0.68)
17	14.56	0.010	Gear Train W SRB Torsion F1 Roll (0.53), SRB Torsion (0.36)
12	14.72	0.028	Gear Train W F1 Torsion (0.12), and SRB Torsion (0.59)
3	16.85	0.037	SRB 3rd Z-Bend (0.61), F1 Shell (0.24)
29	17.61		Crew MOD Y (0.06), Out-of-Phase FWD FUS Side Bend (0.29)
14	18.90	0.030	SRB Axial (0.78)
26	21.54	0.02	Fuselage Torsion, Side Bend, Yaw (0.25), OMS POD (0.17)
7	23.84	0.022	SRB 4th Z-Bend (0.65)
30	24.81	0.012	SRB 4th Y Bending (0.63)

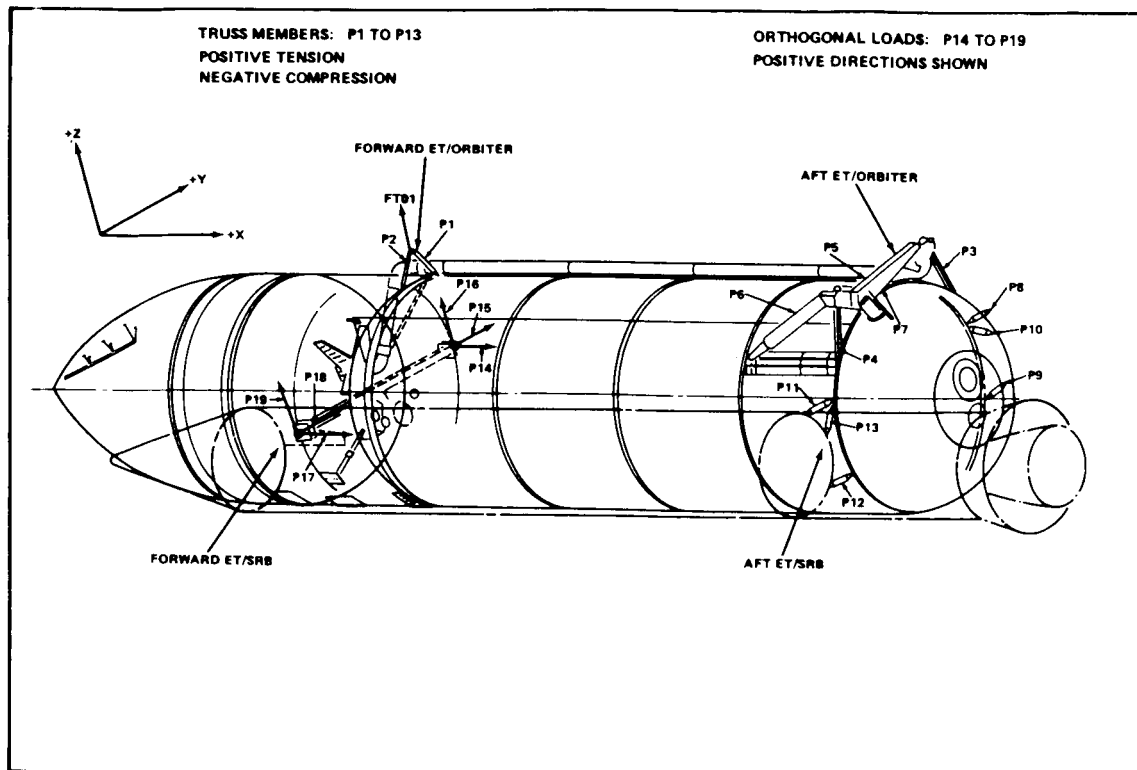


Figure 5. External tank schematic.

TABLE 3. DERIVED COEFFICIENTS

$$P_i = \sum_{j=1}^{18} C_{ij} V_j$$

VARIABLES	①	②	③	④	⑤	⑥	⑦	⑧	⑨
LOAD (LB)	$q$ (PSF)	$q + \Delta\alpha$ (PSF-DEG)	$q + \beta$ (PSF-DEG)	$T_1$ (LB)	$T_2$ (LB)	$T_3$ (LB)	$T_4$ (LB)	$T_5$ (LB)	$T_1 \delta P_1$ (LB-RAD)
P1	21.9	10.7	-8.7	-.086	-.064	.013	.007	.0035	-.088
P2	20.2	10.3	-11.5	-.037	.012	-.065	.0037	.007	-.089
P3	26.7	46.7	65.5	.162	.209	.132	-.036	-.006	.482
P4	72.4	45.7	-86.7	.165	.141	.207	-.012	-.031	.491
P7	-18.1	1.9	37.3	.0006	-.013	.014	.014	-.014	.0009
P10	37.8	37.8	35.2	-.012	.011	-.006	-.016	.002	.406
P13	53.8	37.6	-35.9	-.012	-.006	.011	.002	-.016	.408

VARIABLES	⑩	⑪	⑫	⑬	⑭	⑮	⑯	⑰	⑱
LOAD (LB)	$T_1 \delta Y_1$ (LB-RAD)	$T_2 \delta P_2$ (LB-RAD)	$T_2 \delta Y_2$ (LB-RAD)	$T_3 \delta P_3$ (LB-RAD)	$T_3 \delta Y_3$ (LB-RAD)	$T_4 \delta L_4$ (LB-RAD)	$T_4 \delta R_4$ (LB-RAD)	$T_5 \delta L_5$ (LB-RAD)	$T_5 \delta R_5$ (LB-RAD)
P1	.089	-.107	.111	-.105	.111	.019	.017	-.012	-.015
P2	-.089	-.107	-.111	-.109	-.111	-.015	-.012	.017	-.019
P3	-.687	.335	-.385	.675	-.386	.072	-.065	-.089	-.227
P4	.551	.768	.102	.272	.103	-.200	-.108	-.484	.043
P7	.342	-.179	.712	.181	.712	-.071	.043	-.044	.069
P10	-.364	.364	-.259	.483	-.258	.192	.100	-.389	-.480
P13	-.366	.485	.260	.365	.260	-.478	-.386	.100	.192

NOTES:  $\Delta\alpha = \alpha = 2$

P1, P2 = ORBITER/ET FWD STRUT LOADS  
P3, P4 = ORBITER/ET AFT VERT STRUT LOADS  
P7 = ORBITER/ET AFT DIAG STRUT LOAD  
P10 = RIGHT SRB/ET DIAG STRUT LOAD  
P13 = LEFT SRB/ET AFT DIAG STRUT LOAD

disturbances. These proportional control laws are based on vehicle disturbances sensed by position gyros in the Orbiter, rate gyro in the Orbiter and SRB nose, and accelerometers in the SRB and Orbiter (active during max q portion of flight only). During the max q portion of flight, three types of load relief control logic are used. The elevons on the wings have both a steady-state command position and a feedback loop to drive the hinge moment to deadband position about the command position. This load relief loop is required to keep the elevon hinge moment within reentry design limits and reduce wing loads. The pitch and yaw channels have a regular accelerometer feedback loop designed to reduce the angle of attack and side slip angles, thus loads. In addition, there is a roll command loop tied with side slip which rolls the vehicle such that the side slip angle goes into a pitch angle in a manner which ensures that the aerodynamic induced wing load is always in the direction of maximum wing capability. In addition, there is consideration given that load relief control (reducing  $\alpha$  and  $\beta$ ) introduces attitude errors. The system starts to correct these errors after max q. This reintroduces  $\beta$  (side slip) at a time where loads (low q) are not critical; however, this large  $\beta$  creates thermal problems and added insulation on the ET. Through special tailoring of the load relief control logic, it has been possible to keep both the loads and the thermal effects within bounds.

### 3. Trajectory

The trajectory is shaped for maximum performance under the constraints of crew safety and ET disposal. The crew safety conditions are Return to Launch Site (RTLS) and Abort to Orbit Once Around (AOA). The trajectory must be shaped such that under various failure modes, such as main engine out, capability exists to return to launch site or abort to orbit and land at the West Coast landing site or alternate sites. The choice of option is based on failure time, etc. (Ref. 55). Obviously, these conditions and constraints affect loads. In addition, the vehicle rolls shortly after liftoff to an Orbiter down position. This allows for increased performance due to the main engine cant (thrust vector) opposing gravity. The trajectory is also shaped to the monthly mean wind for the month of launch to reduce loads. Design trajectories were shaped for four generic missions for winter and summer month winds for both ETR (Eastern Test Range) and WTR (Western Test Range) in an attempt to bracket loads. As a part of the trajectory shaping, the Orbiter wing capability, which is much greater in one direction than the other, is taken into account such that the trajectory centers the wing capability with the induced environment characteristics such as winds. Figure 6, the  $q\alpha$  versus  $q\beta$  envelope, which is called a squatcheloid, illustrates this shaping.

The same situation exists in the yaw plane for the vertical tail and element-to-element strut loads. The trajectory is biased to center the  $q\beta$  parameter consistent with these capabilities relative to environments. Additional information will be given in these areas under "results."

### 4. Environments

The Space Shuttle environments are very complex from the loads standpoint, since they go from on-pad, liftoff, max q, orbit, reentry, and landing. On-orbit and reentry are not part of this report. At liftoff, the environments that influence loads are ground winds

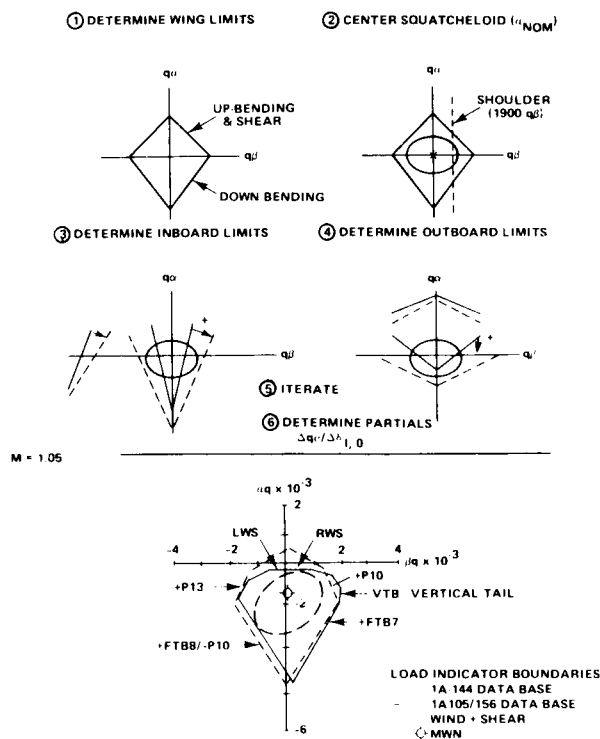


Figure 6. Trajectory shaping effect on loads.

(References 55, 56, 57), eccentric SSME thrust, SRM elongation due to internal pressures, and ignition overpressure arising from ignition of SSME's and SRB's and propulsion system induced acoustics. The SRB's igniting is the primary driver on liftoff loads. This was discussed briefly in Section I in terms of the AMTF test program. Additional discussion occurs in this section under "results."

During the maximum dynamic pressure regime (max q), the main external environment is the winds aloft (References 55, 56, 57). As a result of winds and dynamic pressure, flow effects create aeroelastic environments, such as acoustics and buffeting. Other atmospheric conditions, such as density changes, are included in the environments but not very critical to loads.

During landing, the critical environments are ground winds and runway roughness. Air Force derived criteria corrected to the Shuttle Orbiter configuration are the basis for these data (References 55, 56, 57).

## B. Approach

The approach taken for arriving at design loads concentrated in several areas that consist of the following: 1) criteria development, 2) data base development, 3) selection of analysis technique, and 4) interdiscipline integration. The main objective in these areas is to arrive at a set of design loads under 3-sigma vehicle parameter and environment variations.



Shuttle program management (Level II) set up a series of panels, working groups, and boards to address various technical problems. The major technical problems associated with the launch phase has been handled through the Ascent Flight Systems Integration Group (AFSIG) co-chaired by JSC and MSFC with technical representatives from all technical disciplines or technical subsystem managers from the two centers, Rockwell and the element contractors. This group reviews techniques and criteria, as well as integration trades required. Level II instituted technical panels that supported designs as well as AFSIG and SIR (Systems Integration Review). The technical panels that have interfaced with loads engineers are thermal, aerodynamics, performance, control, propulsion, separation, loads, and control.

As a result of these activities, detailed criteria were developed for each flight phase to meet the design objective. This was accomplished through the use of the generic missions discussed under trajectories. The detailed criteria, models, analysis techniques, data base, etc., will be discussed in detail under each load event. In all cases, the objectives were met and integrated as described generally here.

### C. Shuttle System Loads

#### 1. Liftoff

##### a. Design Criteria

Prelaunch and liftoff loads have a unique set of criteria. The prelaunch case is essentially ground winds other than the special case for Flight Readiness Firing (FRF) which is a 20-sec firing of the Shuttle main engines for propulsion system verification (applicable to STS-1 only and special cases later). The ground winds case without SSME firings is not a problem under enveloped wind conditions. The FRF case was kept within basic design loads through engine start and shutdown sequencing.

The liftoff case presents special problems in criteria development for meeting design objectives. This occurs because variations in timing, sequencings, etc., create a non-linear, time varying peak load that cannot be RSS'd in a classical way and treated with the A-factor approach to generate a 3-sigma time-consistent set of loads. The AFSIG decided that the best approach was to attempt to approximate the 3-sigma case by RSS'ing parameters such as thrust vector misalignments that met RSS criteria, then to combine all parameters in a 2-sigma worst-on-worst manner to approximate a 3-sigma, time-consistent loads case. The liftoff loads are due in large part to the liftoff twang and are therefore largely dynamic in nature. This means that the criteria must include any parameters that would drive these characteristics. The one exception made to this approach was the treatment of variations on the elastic modes and modal frequencies. In this case, the AFSIG decision, based on loads panel recommendations, was to use analytical modes of 1 percent damping. The verification loads cycle would use the test-verified analytical modes. Other key parameters were SRB to SRB thrust differential, SRB thrust and chamber pressure rise rate, winds, thrust vector misalignments, and ignition sequencing. As a result of the AFSIG criteria development, Rockwell International/Space Division published a parameter

design matrix. Table 4 is an extraction from this document for liftoff loads showing the parameters by discipline and the values of the variation. This table does not contain final values and is given only as typical.

In general, since liftoff loads are approximately 80 percent due to dynamics, it was decided to use time-consistent loads. The SRB design loads were an exception to this criterion. In this case, max/min loads were used to make them less sensitive to changes occurring downstream. This conservatism could be handled on the SRB without large impacts due to the payload to SRB weight trade. When the impacts are not too large, this is a good approach.

b. General Characteristics and Environments

The liftoff loads problem can best be understood by going into some depth in terms of the basic system. The configuration is supported on the Mobile Launcher Platform by the SRB's. Figure 7 shows the vehicle on pad.

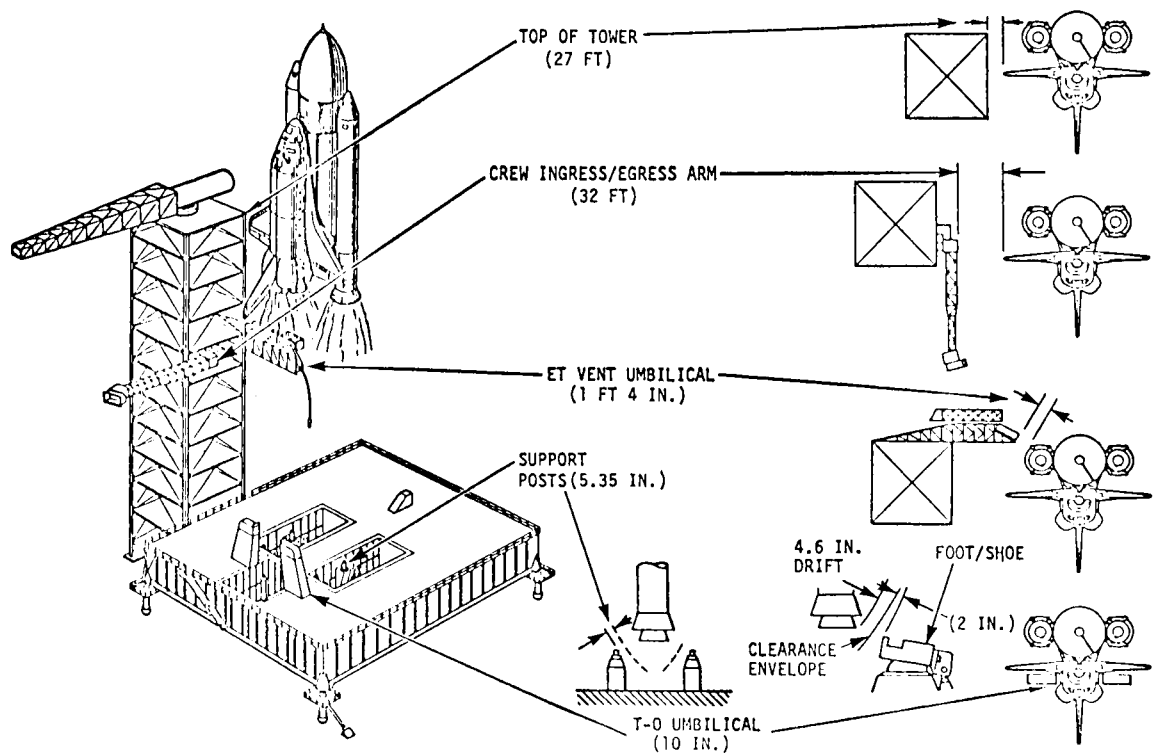


Figure 7. Vehicle on pad.

Due to the eccentricity of the Orbiter, bending loads are induced on the SRB's by SSME ignition. The resulting bending deformation stores a significant amount of strain energy which is relieved at liftoff. When the last SSME reaches 90 percent, an SRB ignition time base is established and then SRB ignition is set for 2.7 sec later. In the early

TABLE 4. LIFTOFF LOAD PARAMETERS

<u>SRM PROPULSION</u>	<u>ANALYSIS TOLERANCE</u>
o TC227A-75 THRUST VS. TIME CURVE PER SE-019-083-2H (SRB SYSTEMS DATA BOOK) FOR MAX/MIN GRAIN TEMPERATURES (TC227H 1 PROPOSED AS UPDATE)	{ 90°F (ETR) 40°F (WTR)
o THRUST LEVEL DEVELOPMENT UNCERTAINTY	± 3%
o STEADY-STATE THRUST MISMATCH BETWEEN SRM'S	35,000 LBS.
o FLIGHT-TO-FLIGHT THRUST LEVEL UNCERTAINTY	{ ± 5% SINGLE MOTOR ± 4.9% BOTH MOTORS
o THRUST BUILDUP RATE DEVELOPMENT UNCERTAINTY	REF: SD IL SRM76-037
o THRUST MISALIGNMENT	± 0.50° (BOTH); ± 0.70° (ONE)
<u>AERODYNAMICS</u>	
o GROUND WIND DRAG COEFFICIENTS PER SD72-SH-0060-2 (MATED VEHICLE AERO DESIGN DATA BOOK) AND ROCKWELL INTERNAL LETTER SAS/AERO/75-430	NONE
<u>MAIN PROPULSION</u>	
o 3 SSME'S AT 100% THRUST (RPL) TO 109% THRUST (FPL)	NONE
<u>MASS PROPERTIES</u>	
o MINIMUM PAYLOAD OF 2,500 LBS. (MISSION 3B)	NONE
o MAXIMUM PAYLOAD OF 32,000 LBS. (MISSION 3A)	NONE
o MAXIMUM PAYLOAD OF 65,000 LBS. (MISSION 3A)	NONE
<u>MISCELLANEOUS</u>	
o SRB/MLP HOLDDOWN BOLT PRELOAD (750,000 LBS.)	NONE
<u>FLIGHT CONTROL AND GUIDANCE</u>	
o ROCKWELL CONTROL #7 PER SD73-SH-0047-1 (INTEGRATED VEHICLE FLIGHT CONTROL SYSTEM DATA BOOK)	NONE
o ALL NOZZLES GIMBAL BUT SRB NOZZLE GIMBAL LIMITED TO 2° FOR FIRST 5 SECONDS	{ ± 0.17° (SRB) ± 0.23° (SSME)
o SRB MISTRIM TO 0° UNTIL SSV CLEARS THE LAUNCH PEDESTAL	NONE
o SRB TVC MISALIGNMENT	2 σ RSS EACH SRB IN WORST DIRECTION
<u>EXTERNAL ENVIRONMENT</u>	
o 95% WIND SPEED (ONE HOUR EXPOSURE)	NONE
o PEAK WIND SPEED	24 KNOTS (MAX)
o TUNED GUST (WORST CASE)	NONE
<u>VEHICLE DYNAMICS</u>	
o FIRST 50 BENDING MODES WITH 1% DAMPING	NONE
<u>FAILURE MODES</u>	
o NONE	
<u>ANALYTICAL APPROACH</u>	
o DIGITAL SIMULATION OF VEHICLE FLEXIBLE - BODY RESPONSE DUE TO APPLIED FORCES AND RELEASE OF BASE CONSTRAINTS	---
<u>COMBINATION METHOD</u>	
o SEQUENCE OF EVENTS SELECTED FOR MAX LOADS (WOW)	---
o RSS SIMILAR UNCERTAINTIES AS A GROUP THEN ADD GROUPS (+2 σ DEVIATIONS) IN WORST-ON-WORST COMBINATION	
<u>DOCUMENTATION OF RESULTS</u>	
o SD73-SH-0069-1, -2, -3, AND -4 STRUCTURAL DESIGN LOADS DATA BOOK	

design phases, SRB ignition command was given when the last engine reached 90 percent. At the same time as SRB ignition command, the eight SRB holddown bolts are fired. Figure 8 shows the SRB aft skirt and the holddown bolt and foot pad.

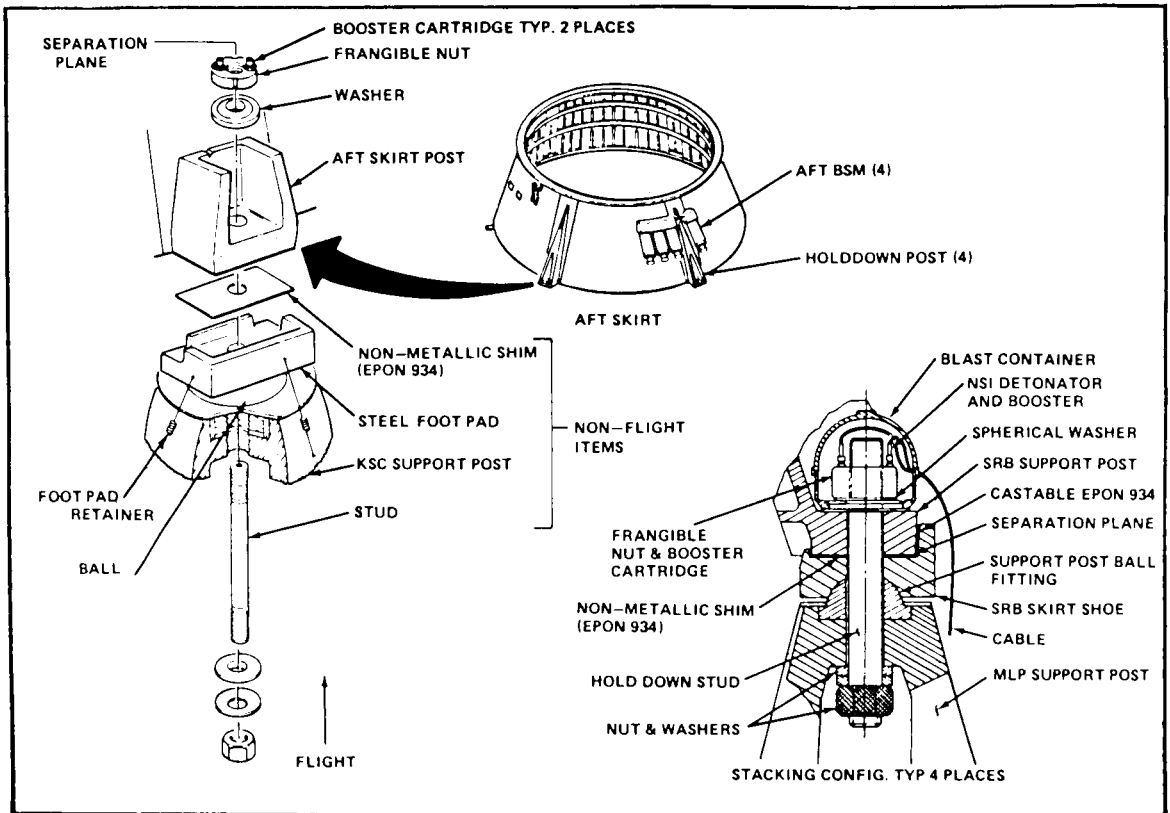


Figure 8. SRB Aft Skirt, holddown bolt and foot pad.

During liftoff, individual foot pads will release. This release is hard to model since the ball and cup can rotate and slide. Most of the loads work has been done at Rockwell, assuming all pads release simultaneously for each solid. This is accomplished by assuming that the moment goes to zero when the centerline of the solid goes from compression to tension. MSFC has modeled the individual footpad releases. All loads analyses results of the liftoff event for Shuttle systems given in this report used four points per SRB release model.

Figure 9 illustrates the moment stored at the SRB/MLP interface from SSME thrust buildup. Due to the fact that the system is dynamic, the vehicle responds in such a manner that if some time delay in SRB ignition is used, then a minimum moment can be achieved. This is at the expense of performance. IVBC-2 boundaries shown on the curve are the maximum and minimum moments at release for the case with no special SRB ignition time delays. The curve labeled  $T_s$  is a typical SSME thrust curve and the  $M_y$  with the

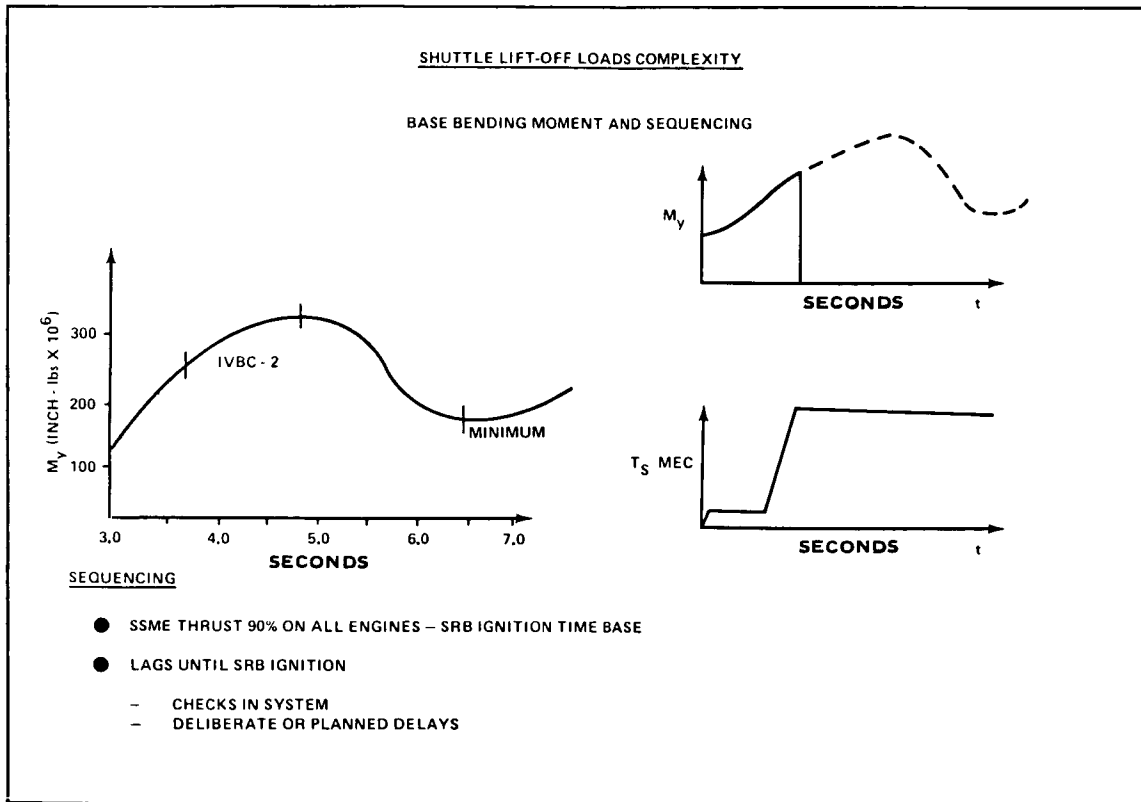


Figure 9. Shuttle liftoff loads complexity.

dotted portion illustrates how the moment is relieved at release. This asymmetry of both configuration and load paths, coupled with the requirement to verify the engine performance prior to liftoff commit, is a major source of energy for liftoff loads.

This problem is aggravated by the fact that the engines start and build up thrust sequentially, thus pushing the Orbiter and tank between the SRB's and bending them over in an unsymmetrical manner. Not only does the vehicle bend but the SRB's roll relative to the tank due to the coupling inherent in this configuration. These deflections coupled with the SRB thrust differential and rise rates create substantial additional twang loads in an unsymmetrical manner. Thrust misalignments add to this twang. It should also be pointed out that the internal SRB pressure is very large, building up very rapidly (slightly different for each SRB) and has a significant effect on these twang responses. The longitudinal loads on ET and the Orbiter are influenced significantly by the case elongation of the SRB's because of the rapid internal pressure change during thrust buildup. Figures 10 and 11 show the ignition phase of two paired SRB motors illustrating both thrust rise rate and internal pressure rise rate and thrust difference between two motors.

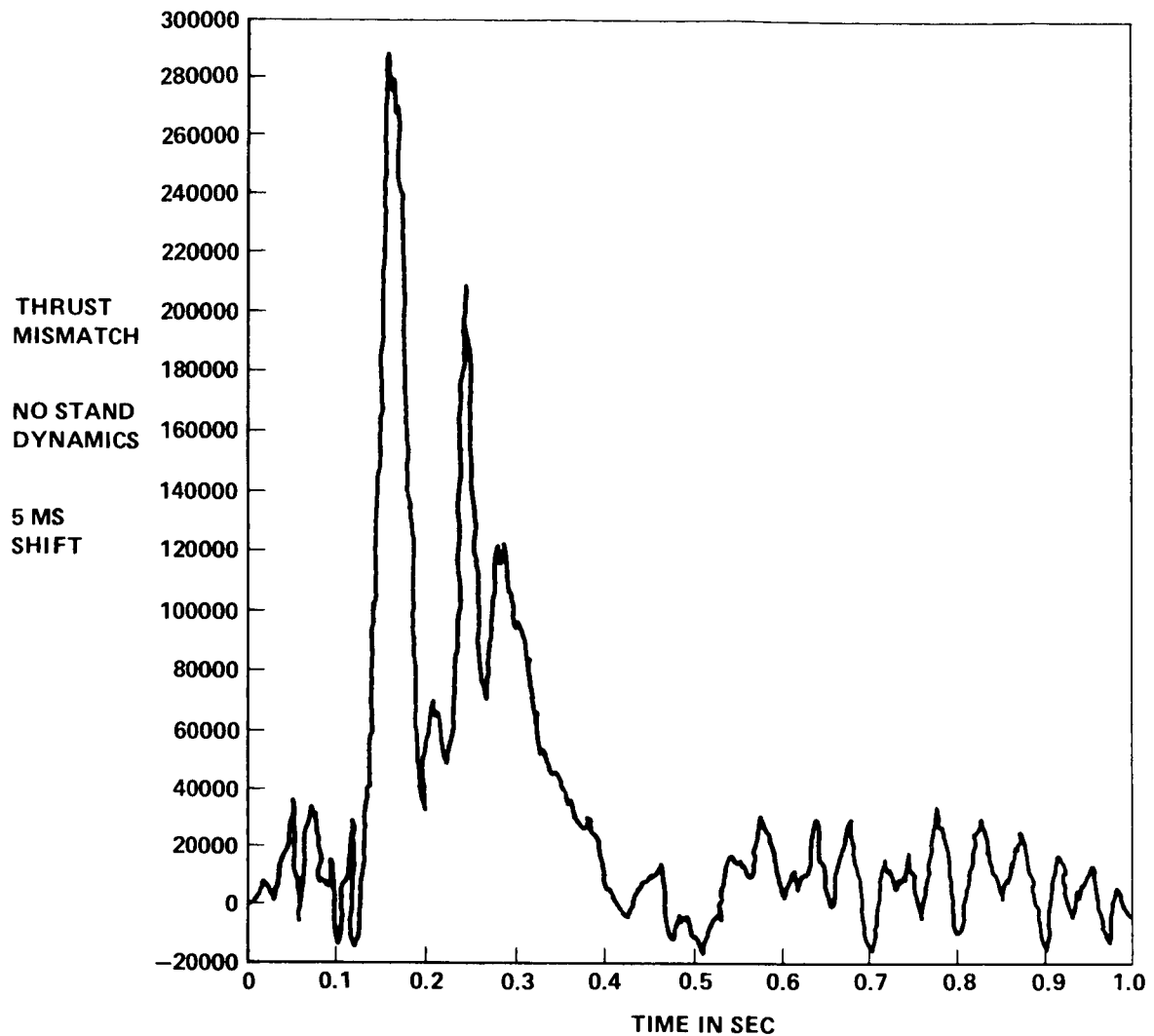


Figure 10. SRB ignition thrust.

One additional induced environment effect is significant for loads. The rapid rise of the SRB thrust creates a reflected acoustic wave (overpressure) due to the MLP bucket design, which loads the vehicle on one side more than the other. This overpressure travels up the vehicle as a wave, adding to the dynamic response as the vehicle releases. The test program to determine these environments was alluded to earlier. Much work had to be accomplished by JSC and Rockwell to get valid pressure distributions and generalized forces that would properly represent this phenomenon and produce correct loads. Obviously, phasing between the vehicle bending and the traveling wave could greatly alter loads. If worst phasing was assumed, loads increased significantly while best phasing could reduce loads. Best estimates of the actual phasing were made, then 2-sigma estimates of the possible differences were made. This was used in the loads analysis.

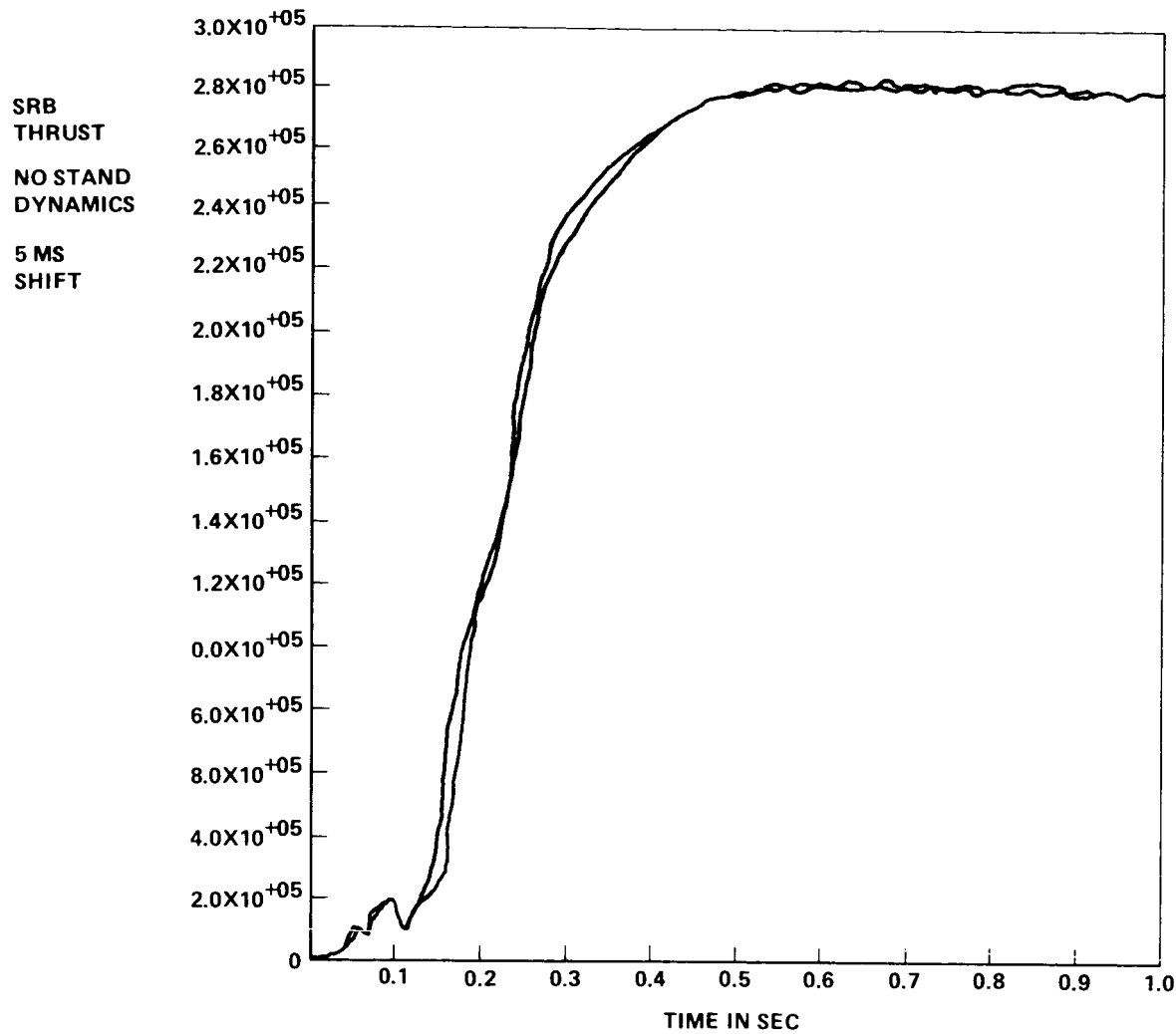


Figure 11. SRB thrust difference between two motors.

The bulk of all liftoff loads, etc., has been done by Rockwell and has served as the basis for most of the decisions discussed so far. MSFC has been accomplishing loads analyses in support of the Loads Panel and AFSIG. As active members, MSFC involvement was based on an independently developed liftoff model and loads analysis. In general, only results of the MSFC studies will be shown.

As the design has matured, the requirement has developed for pre-stressing the SRB/ET struts to reduce loads and prevent ET bulkhead buckling. Adding strut pre-stress to an analysis model is a complication but has been included.

c. Modal Model Requirements

It is clear by now that the liftoff analysis model is very complicated. One additional analysis complication, the large number of modes required for loads convergence, needs discussion; particularly since there is a change in boundary condition during the start of the twang, from clamped-free to a free-free condition. It was found that at least 90 modes below 20 Hz were required for load convergence. Figure 12 shows this convergence.

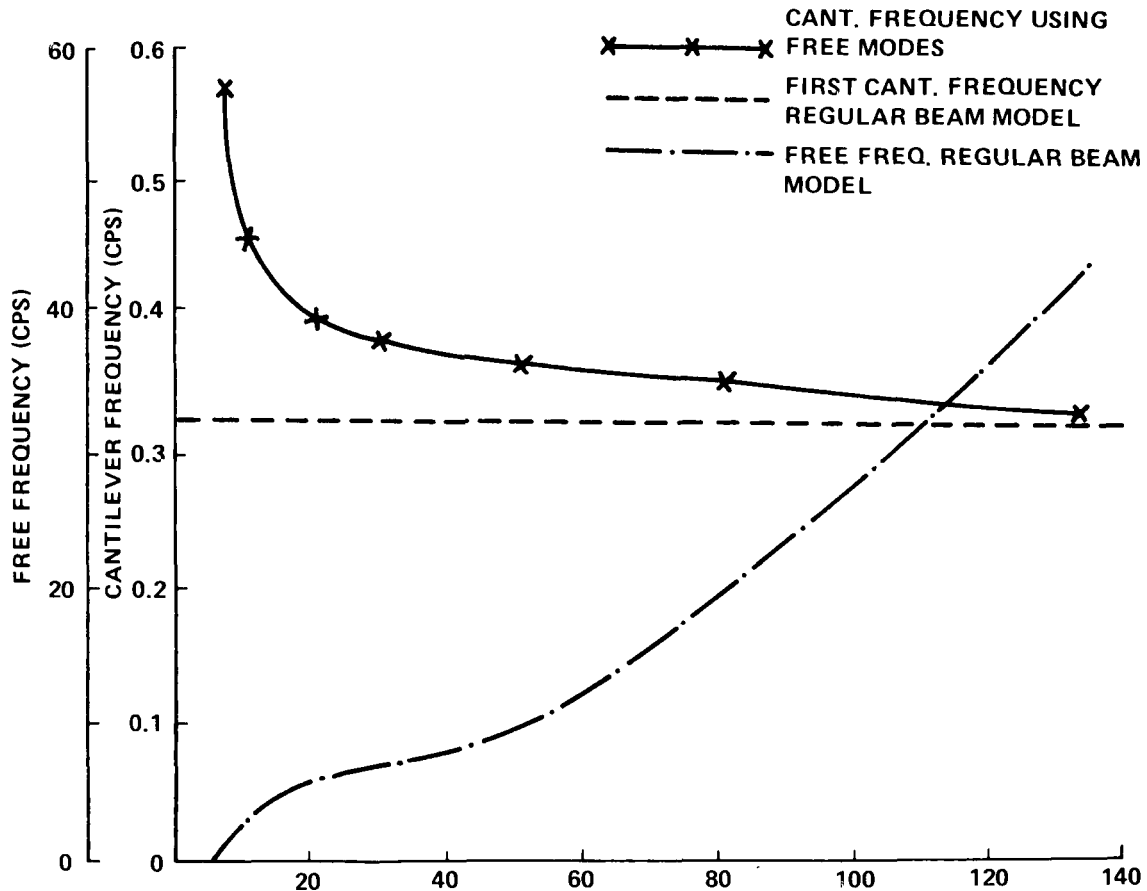


Figure 12. Number of free-free modes versus cantilever frequency.

Associated with this large number of modes is the sensitivity associated with small shifts in element modes creating dynamic tuning or detuning and thus large load changes. The SRB model was changed to reflect internal pressurization effects on the aft ET or SRB attach stiffness. This pressure effect changed only two systems modes by less than 5 percent on the frequency, yet had a pronounced effect on loads. Figure 13 compares the load for both models showing the large shift in loads, particularly the combined load due to moment and shear. Notice that with the model update (configuration 5.4A) that the moment does not dip down and phases much worse with the shear.



## DYNAMIC TUNING/MODAL CHARACTERISTICS (PHASING)

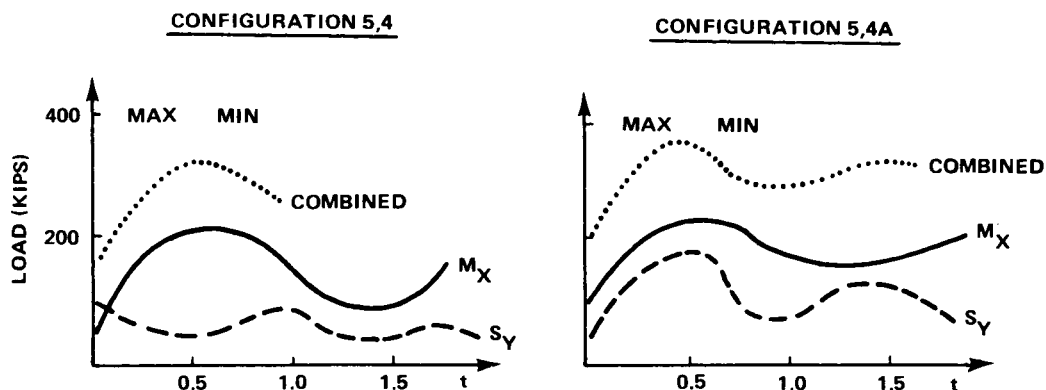


Figure 13. Shuttle lift-off loads complexity.

It is important to develop a comprehensive approach for combining the loads which resulted from several sources for liftoff. This same approach will be adaptable for max  $q$  regime also. In general, the loads combination problem does not occur for components, experiments, etc., above 1,000 pounds. For cases where loads combination is important, loads were specified by axis, the low-frequency load and the random load derived through Miles relationship, added together algebraically to achieve the design loads. The rationale for algebraically adding is that there are so many cycles of the high frequency that there would always be peak phasing.

### d. Simulation/Computer Programs

To do detailed time-consistent loads analysis for liftoff, two programs have been developed. The first is a modal coupling technique developed for changing elements or payload models and incorporating them into the system model quickly. The main feature of this program, developed by Dr. John Admire, is the use of optimized Raleigh Ritz eigenvalue routine, which has cut significantly the machine time for getting the coupled modes out. In addition, if one is conducting a sensitivity analysis by changing only the elements' characteristics, for example a payload, then the program uses the previously solved for modes as a starting point for the new modes, further reducing computer run time significantly.

The other is the liftoff loads time-response loads analysis program developed by Martin-Marietta Corporation. This program has modeled the MLP, each of the SRB hold-down posts, modal characteristics, and environments. Table 5 summarizes the program capability.

### e. Results

The first study dealt with loads sensitivity to various parameter variations. Table 6 summarizes the parameters varied and the different combinations.

**TABLE 5. LIFTOFF PROGRAM CAPABILITY  
SHUTTLE AND SHUTTLE PAYLOADS**

<b>DYNAMICS:</b>	<ul style="list-style-type: none"> <li>o Elastic Model of Vehicle and launch pad.</li> <li>o SRB internal pressure.</li> <li>o Time-consistent loads response.</li> <li>o Six-DOF elastic body.</li> </ul>
<b>CONSTRAINTS:</b>	<ul style="list-style-type: none"> <li>o Point-by-point fly away release.</li> <li>o Gimbal angle body.</li> </ul>
<b>ENVIRONMENTS:</b>	<ul style="list-style-type: none"> <li>o Winds and gust.</li> <li>o Overpressure.</li> </ul>
<b>AERODYNAMICS:</b>	<ul style="list-style-type: none"> <li>o Drag.</li> </ul>
<b>OVERALL CAPABILITY:</b>	<ul style="list-style-type: none"> <li>o Not dependent on configuration and payload.</li> </ul>

**TABLE 6. VARIED PARAMETERS AND COMBINATIONS**

**SHUTTLE LIFT-OFF LOADS ASSESSMENT - LOAD CASES**

CASE	PAYLOAD Wt (KIPS)	SSM THRUST	SSM "2g" Δt (SEC)	SRB THRUST "2g" HOLD (2) COL (DC) (2) NO(S)	SRB Δt "2g" (KIPS) (SRB TIME)	WIND MAG (KNOTS)	WIND DIR	SRB TB VECTOR MISALIGN (deg) ENG. BUFL PITCH BUFL IN BUFL OF L/DUG	
								LEFT	RIGHT
1	0	RPI	25 #2 late	C	0	24	180 270	δp S	δp S
2	68	RPI	25 #2 late	H	200	24	180 270	δout S	δout S
3	68	RPI	25 #2 late	C	200	24	180 270	δin S	δin S
1A	0	RPI	25 #2 late	C	0	24	180 270	δp S	δp S
2A	0	RPI	25 #2 late	H	200	24	180 270	δout S	δout S
3A	0	RPI	25 #2 late	C	200	24	180 270	δin S	δin S
2B	65	RPI	25 #2 late	H	200	24	180 270	δp +S	δp +S
2C	65	RPI	25 #2 late	H	200	24	180 270	δp +S	δp S
3B	65	RPI	25 #2 late	C	200	24	180 270	δp S	δp +S
3C	65	RPI	25 #2 late	C	200	24	180 270	δp +S	δp S
2D	0	RPI	25 #2 late	H	0	24	180 270	δ 0	δ 0
2I	0	RPI	25 #2 late	H	0	24	180 270	δp S	δp S
2I	68	RPI	25 #2 late	H	200	24	180 270	δout S	δ 0
2G	65	RPI	25 #2 late	H	200	24	180 270	δ 0	δout S
3D	65	RPI	25 #2 late	C	200	24	180 270	δin S	δ 0
3I	84	RPI	25 #2 late	C	200	24	180 270	δ 0	δin S
2K	65	RPI	25 #2 late	H	200	24	0 no wind on left wing	δout S	δout S
3I	65	RPI	25 #2 late	C	200	24	0 no wind on left wing	δin S	δin S
2I	65	RPI	25 #2 late	H	200	24	0 no wind on left wing	δp +S	δp S
3G	65	RPI	25 #2 late	C	200	24	0 no wind on left wing	δp +S	δp S
2I	0	RPI	25 #2 late	H	200	24	0 no wind on left wing	δp +S	δp S
2II	0	RPI	25 #2 late	H	200	24	0 no wind on left wing	δp S	δp +S
2I	65	RPI	25 #2 late	H	200	24	0 no wind on left wing	δin S	δin S
4	0	RPI	0	C	200	24	0 wind on both wings	δp +S	δp +S
4A	65	RPI	0	C	200	24	0 wind on both wings	δp +S	δp +S
4B	0	RPI	0	H	200	24	0 wind on both wings	δp +S	δp +S
4C	65	RPI	0	H	200	24	0 wind on both wings	δp +S	δp +S
5	43	RPI	25 #2 late	S	0	24	180 270	δ 0	δ 0

The SRB's are the source of much of the variations. SRB thrust and thrust rise rate are a function of propellant temperature which varies with the launch month. These variations have been characterized as hot and cold (H and C) depicting the hottest and coldest 2-sigma thrust. The last SSME to reach 90 percent is shown as SSME "2-sigma"  $\Delta T$ . Other significant parameters are SRB thrust misalignment labeled  $\delta_p$ , for pitch and  $\delta_{out}$  and  $\delta_{in}$  for yaw. Payload weight has some effect on loads and is shown as a parameter.

As mentioned earlier in this report, because of the nonlinear nature of the liftoff problem, it was decided to approximate the 3-sigma case by using 2-sigma worst-on-worst combination of each parameter. Table 7 is a listing of the element interface loads obtained with the cases from the table identified as causing the design load.

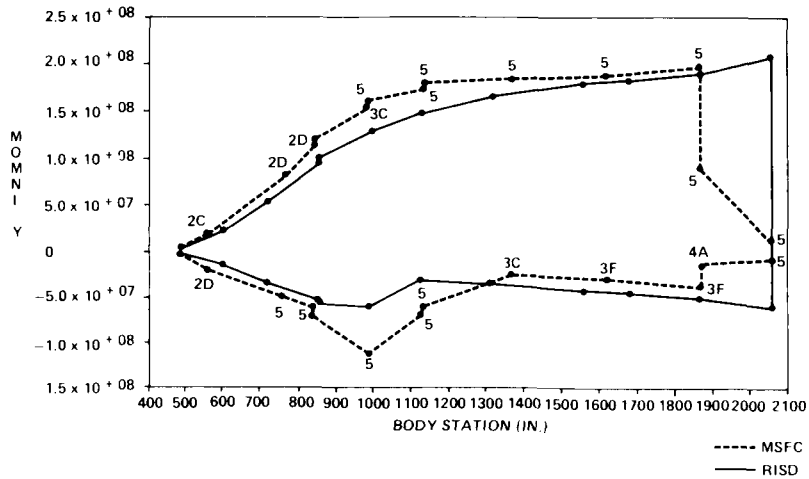
TABLE 7. LOADS IDENTIFIED

COMPRESSION LOADS					TENSION LOADS			
	MEMBER	(KIPS)	CASE NO.	SRB THRUST	MEMBER	(KIPS)	CASE NO.	SRB THRUST
FWD ET/ORB	P1*	-94.	5	N	P1	50.	2B	H
	P2*	-94.	5	N	P2	55.	2C	H
AFT ET/ORB	P3	-90.	2, 3, 2L	C&H	P3	257.	2D, 4B	H
	P4	-97.	2, 3, 2L	C&H	P4	264.	4B	H
	P5	-616.	2D, 2B	H	P5	140.	3F, 2K, 4C	C&H
	P6	-625.	4B	H	P6	140.	2, 3, 2L	C&H
	P7*	-20.	2J	H	P7	15.	2K	H
AFT ET/SRB	P8*	-223.	2G	H	P8*	261.	2D	H
	P9*	-209.	5	N	P9*	352.	2L	H
	P10	-144.	2B	H	P10	73.	2J	H
	P11*	-246.	2I	H	P11*	261.	2L, 2C	H
	P12*	-206.	5	N	P12*	374.	2L	H
	P13	-168.	2C	H	P13	50.	2H	H
FWD ET/SRB	X P14	-1319.	2K	H	X P14	-53.	5	N
	X P15*	-253.	2L, 5	H&N	X P15*	105.	5	N
	Z P16*	-186.	2H	H	Z P16*	244.	3C	C
	X P17	-1348.	2I	H	X P17	-51.	4	C
	Y P18*	-109.	2K	H	Y P18*	248.	2L, 5	N&H
	Z P19*	-178.	2J	H	Z P19*	246.	3B	C
*Member loads which are higher for lift-off than for other events.						H - Hot C - Cold N - Nominal		

One key load other than the SRB to ET interface loads and the forward Orbiter to tank interface force is the External Tank LOX tank shear load. The liftoff twang response loads the tank inertially creating large shear forces from the propellant against the tank wall. Figure 14 shows the shear force distribution in the x-direction. The two curves are a comparison between Rockwell analysis and MSFC analysis. The agreement is good considering that the Rockwell analysis considered overpressure and strut pretension which MSFC's did not.

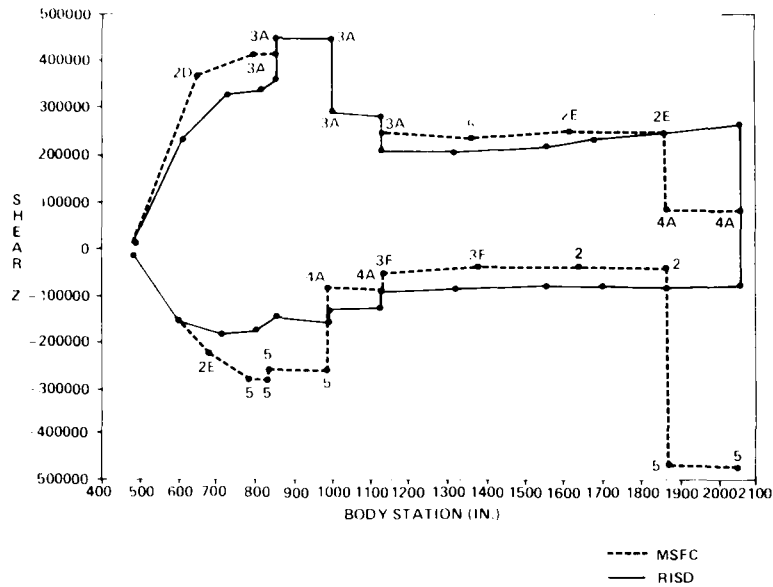
Figure 15 is the same type comparison for shear.

Just as critical for design is the moment introduced by the shear. Figure 16 gives the moment showing the critical design point between stations 900 and 1000.



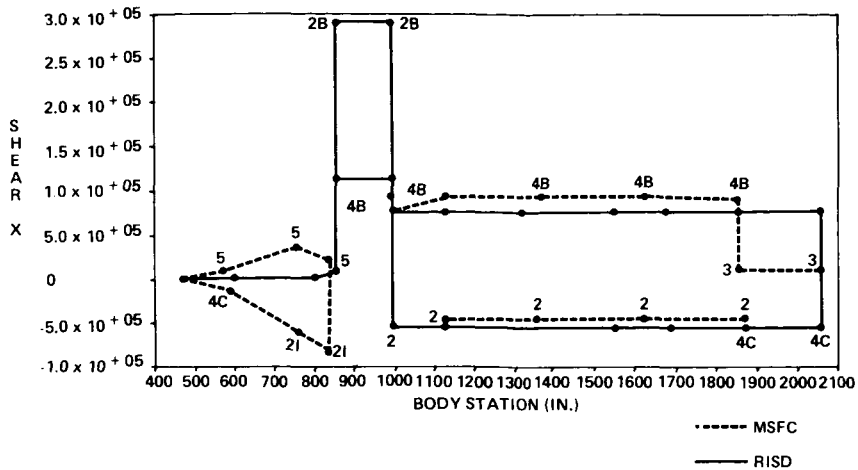
STATION INCH	MAX. CASE NUM.	MIN. CASE NUM.	STATION INCH	MAX. CASE NUM.	MIN. CASE NUM.	STATION INCH	MAX. CASE NUM.	MIN. CASE NUM.	STATION INCH	MAX. CASE NUM.	MIN. CASE NUM.
403.90	6	8	602.40	6	6	719.50	6	6	804.10	6	6
852.70	6	6	852.80	6	6	990.60	8	8	990.70	8	8
1129.00	2	8	1129.14	2	8	1321.00	2	17	1560.00	2	17
1685.00	2	17	1871.00	2	17	2057.90	1	17	2058.00	13	15

Figure 14. MSFC & RISD lift-off envelope loads comparison.



STATION	MAX.	MIN.	STATION	MAX.	MIN.	STATION	MAX.	MIN.	STATION	MAX.	MIN.
483.90	6	6	602.40	6	6	719.50	6	6	804.10	8	8
852.70	8	8	852.80	9	16	990.60	9	16	990.70	13	17
1129.00	13	17	1129.14	13	17	1321.00	13	17	1560.00	2	17
1685.00	9	17	1871.00	9	17	2057.90	9	17	2050.00	17	13

Figure 15. MSFC & RISD lift-off envelope loads comparison.



STATION INCH	MAX. CASE NUM.	MIN. CASE NUM.	STATION INCH	MAX. CASE NUM.	MIN. CASE NUM.	STATION INCH	MAX. CASE NUM.	MIN. CASE NUM.	STATION INCH	MAX. CASE NUM.	MIN. CASE NUM.
403.90	4	15	602.40	4	15	719.50	4	15	804.10	4	15
852.70	4	15	852.00	6	8	930.00	6	8	990.70	9	17
1129.00	9	17	1129.14	9	17	1321.00	9	17	1560.00	9	17
1685.00	9	17	1871.00	9	17	2057.90	9	17	2058.00	16	13

Figure 16. MSFC & RISD lift-off envelope loads comparison.

The significant result of this study was twofold: (1) it added confidence to design loads generated by Rockwell since an independent model and analysis gave comparable results, and (2) it showed the requirement for a large number of cases (27) to bracket all loads for design.

The second study conducted dealt with answering the questions, alluded to earlier, whether it was adequate to approximate liftoff using a single point release model MLP, or was a four-point release model required? This comparison is given in the payloads section under Space Telescope loads.

Late in the Shuttle Program due to certain design problems in the Orbiter OMS pod area and payload design loads, it was decided to conduct special liftoff load alleviation studies. Rockwell did these studies and reported the results in the AFSIG and the loads panel.

The major results were that the most reliable and major contributor under the engineer's control was the SRB ignition time relative to the moment stored in the vehicle due to SSME thrust buildup. Loads for basic structure were reduced approximately 30 percent while payload net load factors dropped from 30 to 100 percent. Based on these results, a 2.7-sec SRB ignition lag time relative to the last SSME reaching 90 percent was adopted.

In summary, the liftoff analysis has clearly demonstrated that multibody point connected systems are very sensitive to element-to-element dynamic tuning. This

implies a strong requirement for accurate models and environments coupled with detailed sensitivity analysis. How conservative the 2-sigma worst-on-worst design approach turns out to be can only be ascertained from actual flight data. Loads were very sensitive to thrust slope, time between SRB thrust buildup, phasing of various modes [small changes in modal characteristics and SSME buildup (simultaneous and engine lag)], and SRB ignition commit times.

## 2. Maximum Dynamic Pressure (Max q)

The maximum dynamic pressure regime (max q) is probably the most interesting from a systems engineering standpoint. It challenges the control engineer to reduce loads and thus structural weight, the flight mechanics engineer to maintain performance while reducing dynamic pressure without increasing thermal environments, the aerodynamicists to adequately define the induced environments, the environments engineer to accurately and efficiently model the atmosphere including winds, and the loads engineer to accurately model and efficiently predict the loads including detailed aeroelastic effects. This obviously dictates close interdiscipline cooperation and communication, systems simulation approaches, adequate trade studies, etc. Also important for the max q regime is correct assessment of protuberance loads and venting loads. Included in the protuberance loads are not only static forces but also unsteady forces due to vortex shedding, buffeting, and flutter. Figure 17 depicts the various discipline interactions, data requirements, tests, environments, etc., involved in loads analysis.

Close inspection of Figure 17 shows an interaction or cross talk between the disciplines, environments, etc. Also indicated are the required interfaces between loads, flight operations, and test. Fatigue loads, isolation requirements, and quality and acceptance criteria are key parts of loads work. As a result of an understanding of this complex system interaction, the AFSIG developed a set of design criteria.

### a. Design Criteria

The design criteria were formulated first in general terms and then as a very detailed parameter matrix. Table 8 describes the general criteria.

TABLE 8. DESIGN CRITERIA

<p>HB04q</p> <p>0 - TRAJECTORY BASED</p> <p>    MONTHLY MEAN WIND AND DIRECTION</p> <p>    SRB MONTHLY TEMPERATURE THRUST PROFILE</p> <p>    <math>q_0</math> AND <math>q_0</math> SQUARE ROOT PEAK MEAN LOADS</p> <p>0 - 95% WIND SPEED 50% SHEARS, 3 M SEC GUST BASE EFFECTS</p> <p>    ADDITIONAL SHEARS AND GUST EFFECTS ISSUED WITH OTHER PARAMETERS</p> <p>0 - RND 2 THREE SIGMA PARAMETERS</p> <p>0 - BODY TO BODY AEROEFFECTS - INTERFERENCE LOADS ONLY</p> <p>0 - LOAD RELIEF CONTROL TORQUE</p> <p>    LATERAL ACCELERATION</p> <p>    YAW ROLL CROSSFEED</p> <p>    WHEEL ALIGNMENT TORQUE</p> <p>0 - BENDING DYNAMICS ADDED DIRECTLY TO RIGID BODY LOADS</p>
--

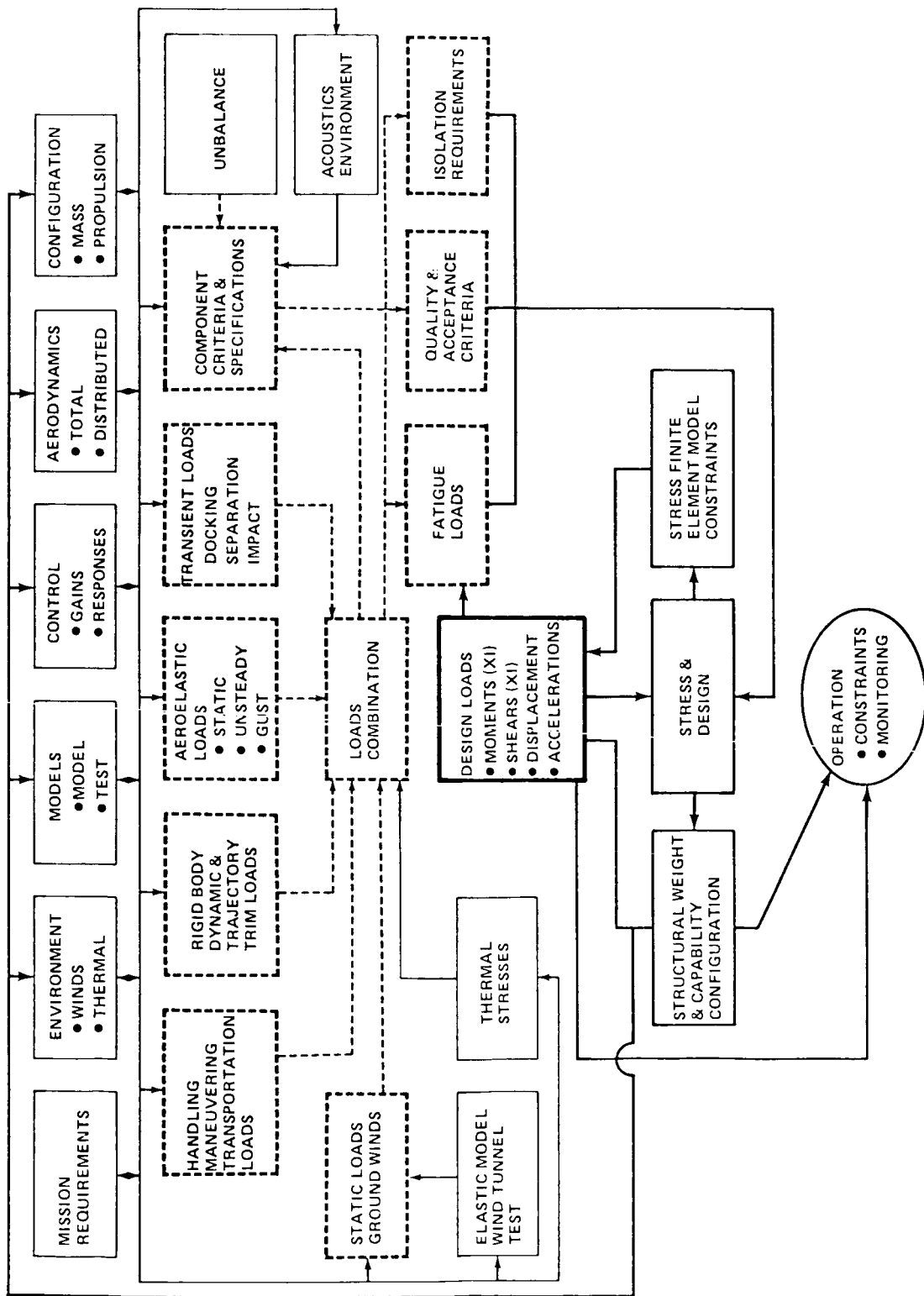


Figure 17. Design loads interfaces and flow.

Two items on this chart require further comments. The term squatcheloid is a JSC/Rockwell coined term for a  $q\alpha$  versus  $q\beta$  envelope. The envelope shape is determined by the wind magnitude and direction. The squatcheloid can be shifted to the right or left ( $\pm q\beta$ ) for yaw plane winds and up or down ( $\pm q\alpha$ ) for pitch plane winds through trajectory shaping. Squatcheloid placement as noted above is the shifting of the squatcheloid to minimize design loads through trajectory shaping. The last line, bending dynamics, added directly means that bending dynamics response to wind gusts is calculated separately from the rigid body trajectory control induced loads and is added peak-loads-to-peak-loads directly. This approach is conservative but not penalizing since gust induced dynamic loads constitute only about 10 percent of the rigid body loads. If the load contributors were nearly equal, then a total trajectory, control, elastic body time-consistent analysis would be required for loads. Also, aeroelastic effects such as lift growth, gust penetration, etc., are insignificant and can be ignored (results to be given later).

A detailed parameter matrix was developed by Rockwell through the AFSIG as was done for the liftoff case. Table 9 lists the basic parameters and their tolerances. Some changes in value have occurred; however, the purpose of including the matrix is not to give final values but to show the scope of the problem.

#### b. Simulation and Computer Programs

Several programs have been developed for handling loads predictions. In general, matrix formulations are used for loads analysis. Computer programs are coded using the FORMA Library as their basis. FORMA (Fortran Matrix Analysis) is a library of subroutines for the solution of the matrix operations encountered in structural analysis and was originally developed by the Martin-Marietta Corporation.

A general program exists for gust response. Either time response or power spectral response (generalized harmonic analysis) can be accomplished. This program can take up to the computer's capacity in modes and treat aeroelastic effects such as gust penetration, lift growth, etc.

The basic rigid body trajectory, control, loads response program is a joint program developed between the Aerophysics, Control, Structural Dynamics Divisions, and the Systems Analysis and Integration Laboratory. Since the first three groups are the same laboratory, this consolidated approach was easy to implement. Through close working relationships and a steering committee chaired by the laboratory lead engineer, this effort was carried out. Data flow is a major problem for this type of analysis. To handle this efficiently, particularly for a system with many aerodynamic surfaces, understanding was required by all disciplines. As a result, the approximately 20,000 pieces of aerodynamic data which were a function of Mach number, elevon position, side-slip angle, and angle of attack were put in a format on magnetic tape compatible with the control dynamics simulation fed directly to the program.

The same approach was used with the control dynamics output. Time responses for all key parameters, such as angle of attack, rigid body accelerations, and gimbal angles were stored on tape and used as input to the loads program. Additional



TABLE 9. BASIC PARAMETERS

<u>SRM PROPULSION</u>	<u>ANALYSIS TOLERANCE</u>
o TC227A-75 THRUST VS. TIME CURVE PER SE-019-083-2H (SRB SYSTEM DATA BOOK) FOR BULK GRAIN TEMPERATURES (TC227H IS PROPOSED AS UPDATE)	{ ETR - 81° F (MEAN)/83.4° F (MAX) WTR - 52° F (MEAN)/44.5° F (MAX)
o FLIGHT-TO-FLIGHT PROPELLANT BURNING RATE	{ ± 5.3% (ONE SRM) ± 4.7% (TWO SRM'S)
o THRUST LEVEL DEVELOPMENT UNCERTAINTY	± 3%
o THRUST OSCILLATION (DYNAMIC FACTOR ASSUMED FOR LOADS ANALYSIS)	± 5%
o STEADY-STATE THRUST MISMATCH BETWEEN MOTORS	85,000 LBS. (REF VOL X, FIG 3.3.2.1.2e)
o THRUST MISALIGNMENT	± 0.75° PER SRB
o FLIGHT-TO-FLIGHT THRUST LEVEL DISPERSION	{ ± 5% SINGLE MOTOR ± 4.9% BOTH MOTORS
<u>AERODYNAMICS</u>	
o PRESSURE DISTRIBUTION TEST DATA MATCH WITH AERODYNAMIC COEFFICIENT TEST DATA	± 3%
o ELEVON DEFLECTION SCHEDULE #6 (HINGE MOMENT LIMITING FEEDBACK) PER ROCKWELL INTERNAL LETTERS ACDA/FSA/76-527 AND 531	$\Delta\delta_{e0} = f(\Delta C_{HM} = 0.02)$ AERO DATA ADJUSTED TO NEW ( $\delta_{e0} + \Delta\delta_{e0}$ )
o SD72-SH-0060-2 (MATED VEHICLE AERO DESIGN DATA BOOK)	NONE
o INCLUDE AERODYNAMIC TOLERANCE EFFECTS ON COEFFICIENTS: WIND TUNNEL DEVIATIONS PLUS POWER-ON-DEVIATIONS PLUS REYNOLDS NUMBER EFFECTS	VALUES PER PRCB BRIEFING ON 8/18/76 MCR 3378 "5.3 ASCENT LOAD ADJUSTMENTS"
<u>MAIN PROPULSION SYSTEM</u>	
o 3 SSME THRUST LEVEL THROTTLING RANGE	50% (MPL) TO 100% (FPL)
o THRUST OSCILLATION (DYNAMIC FACTOR ASSUMED ONLY FOR LOADS ANALYSIS)	± 5%
o EQUAL THROTTLE SETTINGS ON ALL SSME'S	NONE
o WITH ONE SSME OUT, THE TWO REMAINING SSME'S OPERATE AT 109% THRUST	NONE
o THRUST MISALIGNMENT	± 0.3° PER SSME
o MIXTURE RATIO (6:1)	NONE
o VARIATIONS IN ET PROPELLANT LOAD LEFT AT MECO RESULT FROM OFF-NOMINAL SRM/SSME PERFORMANCE AND SSME THROTTLING HISTORY	NONE
<u>MASS PROPERTIES</u>	
o MINIMUM PAYLOAD OF 2,500 LBS. (MISSION 3B)	NONE
o MAXIMUM PAYLOAD OF 32,000 LBS. (MISSION 3A)	NONE
o MAXIMUM PAYLOAD OF 65,000 LBS. (MISSION 1)	NONE
<u>FLIGHT CONTROL AND GUIDANCE</u>	
o ROCKWELL CONTROL #7 PER SD73-SH-0097-1 (INTEGRATED VEHICLE FLIGHT CONTROL SYSTEM DATA BOOK)	NONE
o ELEVON SCHEDULE #6 (HINGE MOMENT LIMITING FEEDBACK)	± 0.02 HINGE MOMENT COEFFICIENT
o PLATFORM MISALIGNMENT	± 0.5°
o ACCELEROMETER MISALIGNMENT	± 0.5°
o ACCELEROMETER NULL OFFSET (TIME VARIABLE)	{ 0.010 TO 0.025 g (PITCH) 0.008 TO 0.015 g (YAW)
o ACCELEROMETER MDM BIAS	0.0248
o IMU ATTITUDE ERROR	± 0.0083°
o ACTUATOR HYSTERESIS	1.5MA
o RATE GYRO MISALIGNMENT	± 2°

TABLE 9. (Concluded)

<u>FLIGHT CONTROL AND GUIDANCE (CONTINUED)</u>	<u>ANALYSIS TOLERANCE</u>
o RATE GYRO HYSTERESIS	± 0.02 DEG/SEC
o RATE GYRO MDM BIAS	± 0.12 DEG/SEC
o RATE GYRO ZERO OFFSET	± 0.15 DEG/SEC
o SRB AND SSME FORWARD LOOP GAIN	± 10%
<u>EXTERNAL ENVIRONMENT</u>	
o 95% SEASONAL WINDS BASED ON MONTHLY WIND ELLIPSE DATA FOR WTR AND ETR (TMX-73319)	NONE
o BASIC $q\alpha/q\beta$ : 95TH PERCENTILE WIND ENVELOPE PLUS 3 M/SEC GUST PLUS 50TH PERCENTILE SHEAR RANDOM $q\alpha/q\beta$ : FCS SYSTEM EFFECTS; 6 M/SEC GUST (i.e., 9 M/SEC MINUS 3 M/SEC) AND SHEAR UP TO 99TH PERCENTILE DISPLAY $q\alpha/q\beta$ ENVELOPES: BASIC PLUS FCS EFFECTS; BASIC PLUS 6 M/SEC GUST AND SHEAR UP TO 99TH PERCENTILE	
<u>VEHICLE DYNAMICS</u>	
o FIRST 50 BENDING MODES WITH 1% DAMPING	NONE
o AEROELASTIC EFFECTS	NONE
o FLUTTER STABILITY X FIRST 20 MODES X CONTROL SYSTEM FEEDBACK REPRESENTED X PARAMETRIC VARIATION OF ACTUATOR STIFFNESS	NONE
<u>FAILURE MODES</u>	
o NUMBERS 1, 2, OR 3 SSME OUT ANYTIME AFTER LIFT-OFF	----
o TVC FAILURE BY-PASS TRANSIENT	
<u>ANALYTICAL APPROACH</u>	
o TRAJECTORY LOGIC SUPERIMPOSES ENGINE-OUT SQUATCHELOID ON NO-FAILURE SQUATCHELOID	
o CONDUCT LOADS SURVEY AROUND SQUATCHELOID USING RIGID-BODY SQUAWKR PROGRAM TO CALCULATE MAX/MIN WING AND ELEVON LOADS AND ORB/ET AND SRB/ET FITTING LOADS	
o FLEXIBLE-BODY DYNAMIC RESPONSE CALCULATED FOR FINAL LOADS	
<u>COMBINATION METHOD</u>	
o $q\alpha/q\beta$ FCS TOLERANCE ADDED ( $\pm 700$ PSF-DEG $q\alpha$ ; $\pm 700$ PSF-DEG $q\beta$ )	
o 85% GUST TIMED 6 SEC AFTER SSME FAILURE IN 85% MAX SHEAR OR FULL GUST 6 SEC AFTER SSME FAILURE FOLLOWED BY FULL DESIGN SHEAR AFTER SSME FAILURE. SEQUENCE OF EVENTS SELECTED FOR MAXIMIZING LOADS	
o SRB THRUST DISPERSIONS:	
$\Delta T = \Delta T_{\text{MEAN TEMP}} + \Delta T_{\text{OSC}} + \sqrt{\Delta T_{\text{TEMP}}^2 + \Delta T_{\text{TEMP}}^2 + \Delta T_{\text{LIFT}}^2}$	
<u>DOCUMENTATION OF RESULTS</u>	
o SD73-SH-0069-1, -2, -3, AND -4 (STRUCTURAL DESIGN LOADS DATA BOOK)	
o SD73-SH-0097-1 (INTEGRATED VEHICLE FLIGHT CONTROL SYSTEM DATA BOOK)	

aerodynamic data to account for body-to-body variations as well as other aero distributions were also required. These were again fed directly to the loads program. Specialized load indicators were supplied to the control dynamics simulation for quick look assessment and cross checking. Figure 18 illustrates these flows between loads and control.

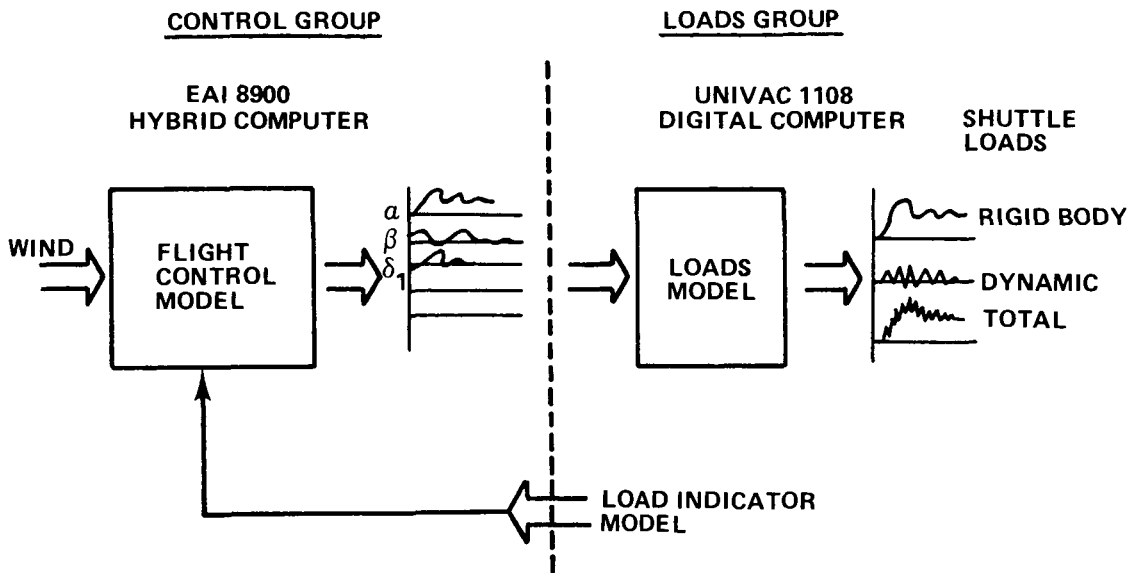


Figure 18. Analysis flow.

The control dynamics program was implemented on the hybrid computer because of speed and operator interactive capability. Figure 19, given earlier and repeated

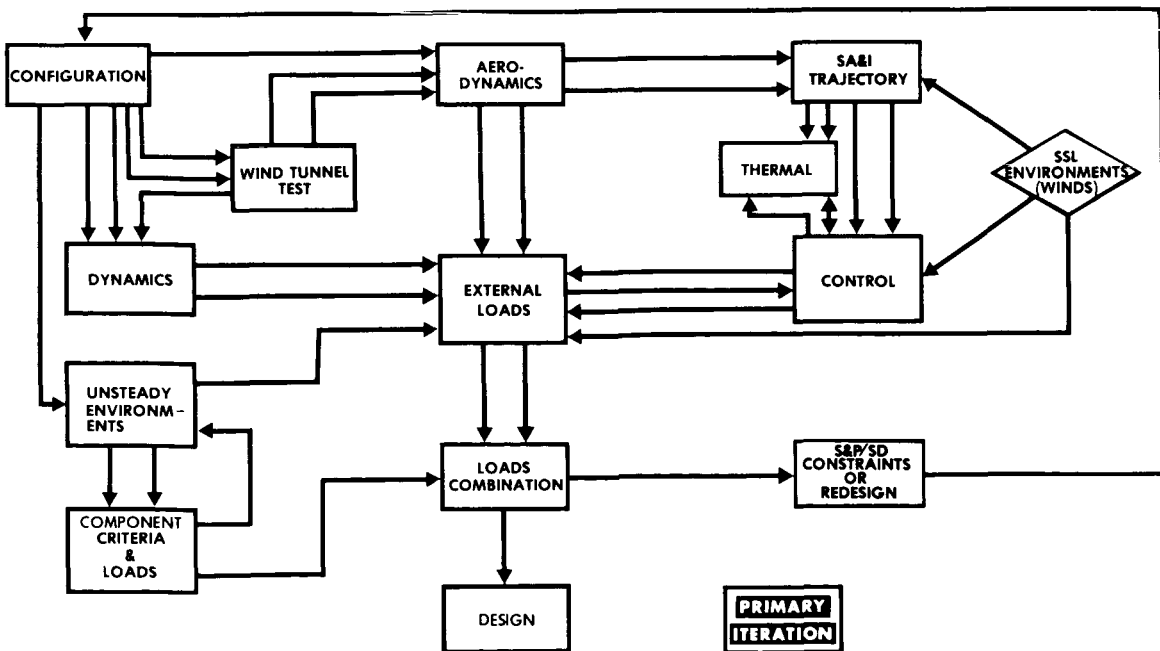


Figure 19. Environments and loads cycle.  
(Ref. Figure 7, Vol. 1)

here, shows this overall approach developed. Shown are the various disciplines and the organizational laboratories involved in each discipline; namely, Systems Analysis and Integration Laboratory (SA&I), Structures and Propulsion Laboratory (S&P), and Space Science Laboratory (SSL).

It should be pointed out that environments, such as winds, can be modeled in many ways. A good understanding between the environmentalists and the loads engineer is mandatory. MSFC has built this understanding through many years of cooperative effort. The results of these many efforts were published by AGARD (Reference 34).

The basic capability of these loads related programs is summarized in Table 10.

TABLE 10. PROGRAM CAPABILITY

O	CONTROL		
	-	TOTAL RIGID-BODY GAINS	
	-	VEHICLE LOAD RELIEF	
	o	PITCH AND YAW ACCELEROMETER	
	o	YAW/ROLL CROSSFEED	
	o	ACTIVE ELEVONS	
	-	ACTUATOR DYNAMICS	
	-	BENDING MODE FILTER CHARACTERISTICS	
O	AERODYNAMICS		
	-	TAPE OUTPUT TO ALL DISCIPLINES	
	o	MACH NUMBER	- M 0.6 TO 3.0
	o	ELEVON DEFLECTION	- $\delta_e$ 10 TO -10 DEGREES
	o	ANGLE OF ATTACK	- $\alpha$ -6 TO +4 DEGREES
	o	SIDE SLIP	- $\beta$ $\pm$ 10 DEGREES
O	ENVIRONMENT		
	-	VECTOR WIND MODEL	
	-	MEASURED WIND ENSEMBLES	
O	TRAJECTORY		
	-	SIX DEGREE WITH TRIM COMMANDS	
	-	TOTAL RIGID-BODY AERODYNAMICS	
O	DYNAMICS (HYBRID)		
	-	SIX DEGREE RIGID-BODY	
	-	FIFTEEN NODE POINTS OR INTERFACES (LOADS)	
	-	THREE SSME'S AND TWO SRB'S GIMBAL	
O	DYNAMICS (DIGITAL)		
	-	DISTRIBUTED AERO	
	-	STATIC ELASTIC EFFECTS	
	-	UP TO 100 ELASTIC MODES	

Notice that this program will handle easily the synthetic vector winds or measured individual winds. MSFC has on tape 150 individual measured winds for each month which can be used for response analysis. The winds are measured by use of Jimsphere balloons and have details down to 25 meters, thus including gusts, speeds, and directions (Reference 35). This means that either an A-factor type RSS'ing or Monte Carlo analysis is accomplished. The A-factor has been the basic approach used as shown in the analysis approach summary (Table 11); however, for the final STS-1 loads analysis, the Monte Carlo approach was used to parallel work done at Rockwell.

The basic decision made through AFSIG was that the A-factor RSS'ing would be used for generating design loads, while the Monte Carlo and individual measured Jimsphere winds would be used for final verification and operations. Table 11 is a summary of the approach and key steps.

TABLE 11. ANALYSIS APPROACH. MAX Q.

O	BASIC APPROACH
	- TIME CONSISTENT, RIGID-BODY LOADS ANALYSIS USING RSS LOADS SENSITIVITY VALUES TO TOLERANCE VARIATION FOR DESIGN LOAD AND THE A-FACTOR APPROACH TO OBTAIN COMPATIBLE RSS TIME RESPONSE.
	- ADD ELASTIC BODY FACTORS DIRECTLY USING RIGID-BODY RESPONSE AS FORCING FUNCTION.
O	KEY STEPS IN APPROACH
	- DEVELOP AERODYNAMIC DATA FROM WIND TUNNEL TEST
	o TOTAL COEFFICIENTS
	o ELEMENT RIGID-BODY COEFFICIENTS
	o DISTRIBUTIONS
	- SHAPED TRAJECTORY TO CRITERIA AND CONSTRAINTS
	- DEVELOP RIGID-BODY LOAD PARTIALS
	- USING SYNTHETIC VECTOR WIND MODEL, PICK CRITICAL WIND AZIMUTH FOR EACH LOAD FOR NOMINAL WIND AND PERTURBATED WIND. 50% SHEAR, 3 M/SEC GUST, AND 99% SHEAR AND GUST.
	- DETERMINE LOAD PERTURBATIONS ASSOCIATED WITH EACH CRITICAL LOAD AND WIND AZIMUTH.
	- DETERMINE RSS LOAD AND A-FACTOR FOR EACH LOAD.
	- USING A-FACTOR ON EACH INPUT PERTURBATION, DEVELOP CORRESPONDING TIME CONSISTENT DYNAMIC RESPONSE AND STORE ON TAPE.
	- USING RESPONSE TAPE, DETERMINE SYSTEM LOADS FOR EACH CASE INCLUDING BODY-TO-BODY AERO TOLERANCES AND ELASTIC BODY EFFECTS.
	- LOADS FROM CONTROL RESPONSE ARE COMBINED WITH LOADS DUE TO:
	o ELEMENT AERO TOLERANCES
	o SRB THRUST UNCERTAINTY
	o SRB AND SSME THRUST OSCILLATION
	o ELASTIC TRANSIENTS
	- STATIC AERO-ELASTIC EFFECTS ASSUMED NEGLIGIBLE

Two points need further discussion: loads combination and the body-to-body aerodynamic tolerances. The term delta load  $B_{1-A}(\Delta L_{B_{1-A}})$  is the load contribution due to the system parameter dispersions given in Table 11 for a 95 percent wind speed plus 1-sigma shear and gust. Load A is the load due only to 95 percent wind speed and 1-sigma shear and gust. The AFSIG chose this criterion to remove conservatism used in the past based upon 95 percent wind speed with 3-sigma shear and gust as the baseline winds for RSS'ing other parameter variations. The second term under the radical is the body-to-body aerodynamic tolerance effects. This was a consideration given only to the element-to-element interface loads. This term is zero for all other loads. The rationale for using body-to-body aerodynamic tolerances is that the interface loads are very sensitive to small changes in the total aerodynamic forces and moments on each element, making up to half the total magnitude of the interface loads. The approach used was to take a total vehicle force and moment coefficient and, through independently varying the individual element forces and moment coefficients within tolerance bands while maintaining the overall total coefficient, determine sets of rigid body element force and moment distribution for use in loads calculation. This delta load is also under the radical for RSS'ing since it is a tolerance. The delta load due to thrust is that part of the SRB thrust variation that can be considered as a development tolerance and should not overly penalize the design. The delta load due to thrust oscillation was an allowance made for thrust oscillations. Here it was assumed that a  $\pm 5$  percent variation on thrust would envelope all thrust oscillation induced loads. As discussed earlier, bending dynamic loads were calculated separately and added directly. This loads combination approach, etc., was developed and baselined in AFSIG.

### c. Results

#### (1) Aeroelastic Effects

The first study dealt with the vehicle response to wind gusts and aeroelastic effects (Reference 26). This analysis used an early set of structural dynamic modes (90 elastic body modes plus 6 rigid-body degrees-of-freedom) in conjunction with a preliminary set of aerodynamic pressure distributions based on zero degrees elevon deflection. The aerodynamic data were linearized about the operating angle of attack ( $\alpha$ ) and side slip angle ( $\beta$ ). The various wind models came from References 28 and 35. The structural response of an elastic vehicle to the synthetic wind shear is essentially quasi-static, whereas the response to the gust shape is a dynamic transient. The total loads were thus determined in two steps:

Step 1. Determine static elastic loads at the time of gust onset based upon a rigid trajectory simulation of the wind shear. The rigid body trajectory simulation included the time variation of the system parameters.

Step 2. Determine the transients response and loads due to the gust shape by employing a perturbation solution. The system parameters are assumed to be invariant over the time frame of the perturbation solution. The frequencies of the sinusoidal wind gust were tuned to select modes. These two steps are illustrated in Figure 20. Figure 21 shows the gust directions considered.

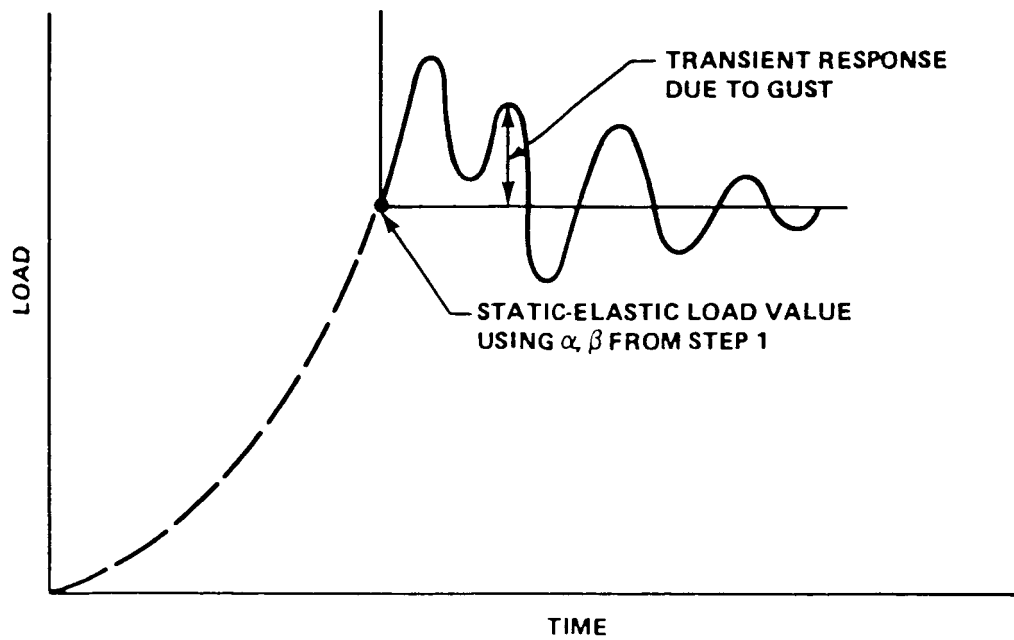


Figure 20. Technical approach.

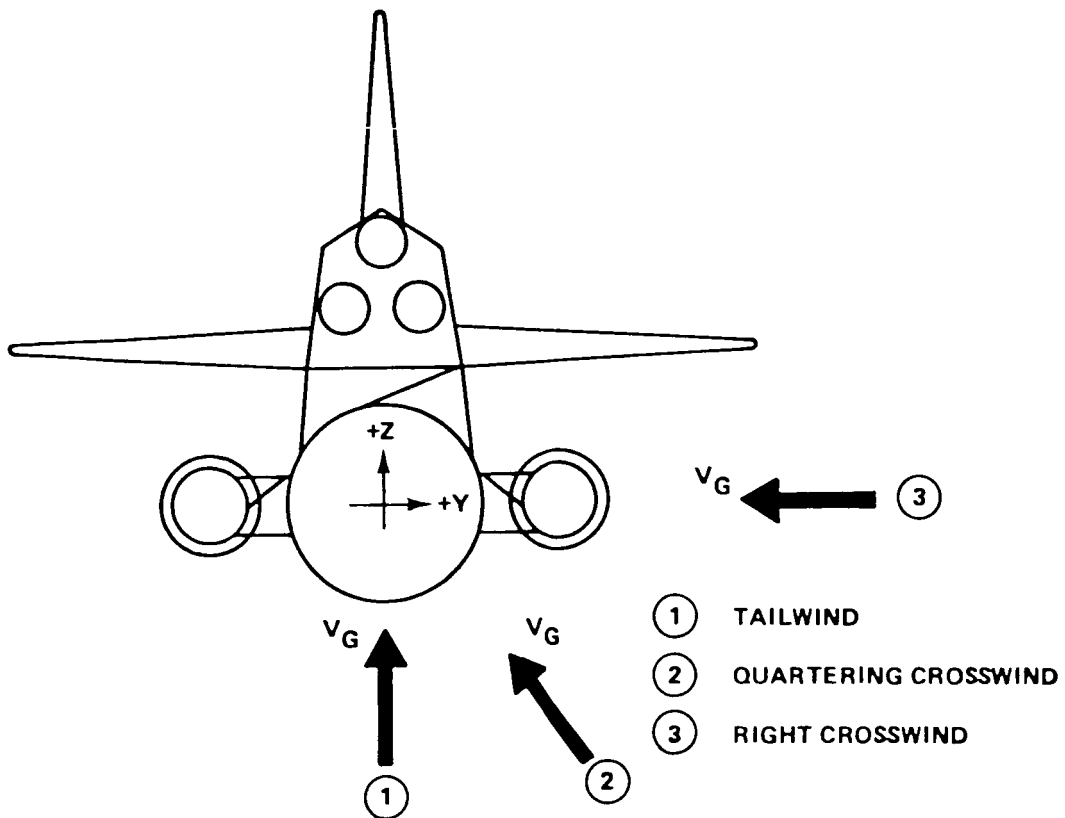


Figure 21. Gust directions considered.

The results of this study are generally plotted as ratios of dynamic transient loads to total static and transient elastic loads.

$$\text{Ratio} = \frac{\text{Peak value of elastic transient load}}{\text{Peak value of total load}}$$

A typical example of the results is depicted in Figures 22 and 23. Plotted are the total ET y-direction bending moment and the ratios for both the synthetic rectangular gust and the tuned sinusoidal gust. The system (AFSIG) baselined the use of the rectangular gust assuming that the sinusoidal-tuned gust was too severe a requirement. Notice the big difference between the two gust effects on the ET  $M_y$ . Rectangular gusts gave a maximum of 20 percent, while the sinusoidal gave a maximum of 50 percent.

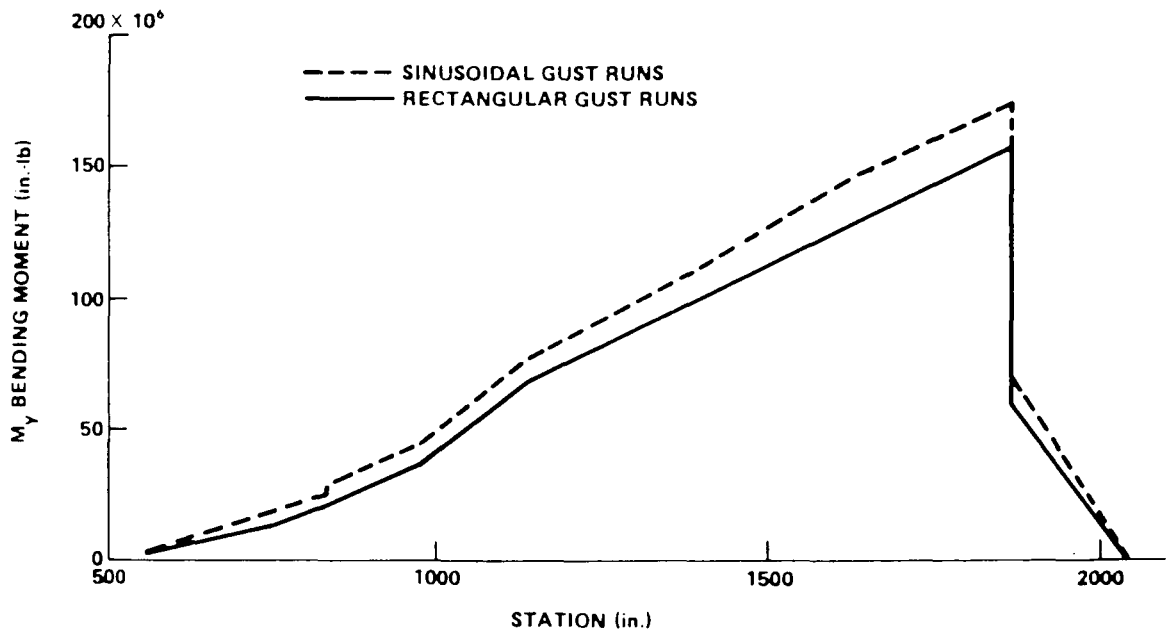


Figure 22. ET  $M_y$  bending moment envelopes.

These trends were observed for the Solid Rocket Motor, Figures 24 and 25.

Element interface forces and Orbiter wing root moment ( $M_x$ ), fuselage moment ( $M_x$ ), and vertical tail moment ( $M_x$ ) were also compared. Table 12 summarizes these results.



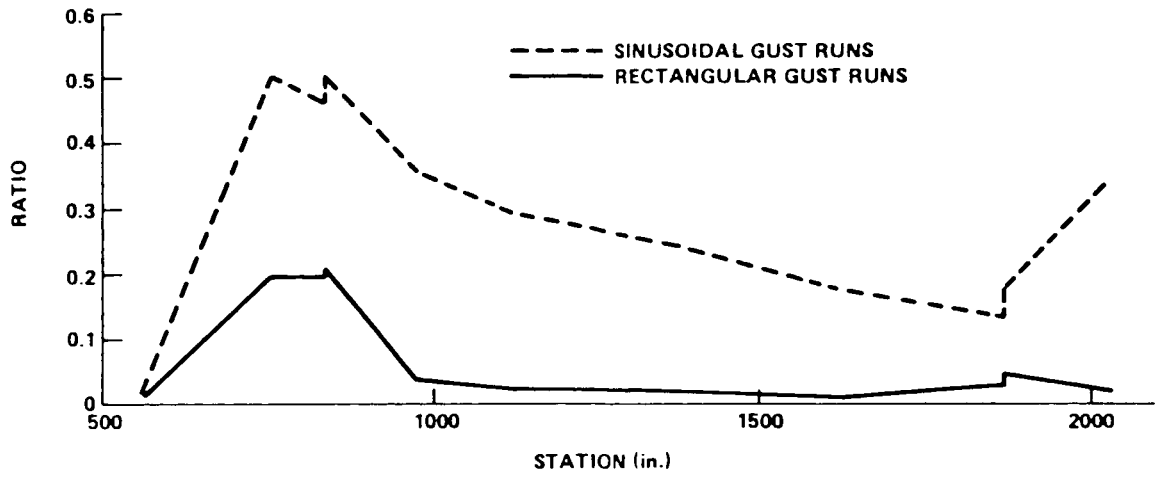


Figure 23. ET elastic transient contribution to  $M_y$ .

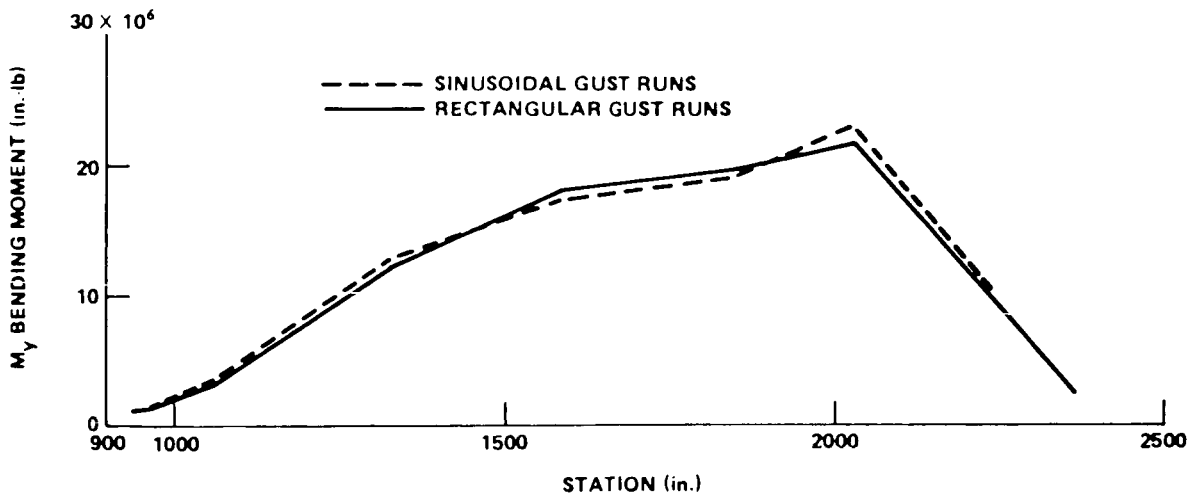


Figure 24. Right SRB  $M_y$  bending moment envelopes.

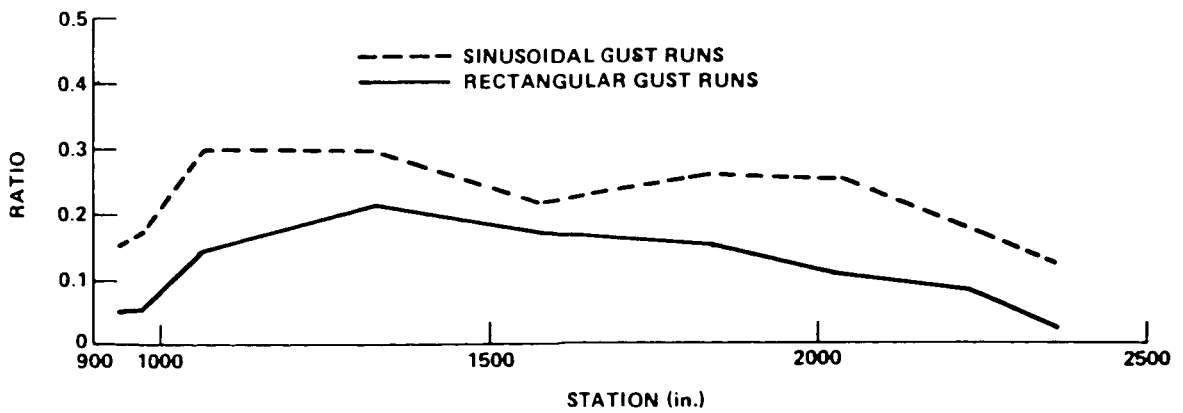


Figure 25. Right SRB elastic transient contribution to  $M_y$ .

TABLE 12. COMPARISON WITH ROCKWELL DATA

Load	MSFC Values			Rockwell Values (lb)	Source of Rockwell Data
	Static (lb)	Dynamic (lb)	Total (lb)		
ET/Orbiter Forward Attach FZ1 or FT01	-66099	-11690	-77789	-65314	Dec. 74 Loads Dump
ET/Orbiter Aft Attach FZ2 or FT03	-434682	-22580	-457262	-243403	↓ Dec. 74 Loads Dump
FZ3 or FT04	-430137	-30410	-460547	-438597	
FY2 or FT05	40629	9946	50575	0	
FY3 or FT06	47348	11540	58888	112858	
Wing Root $M_x$	$22.45 \times 10^6$	$1.61 \times 10^6$	$24.06 \times 10^6$	$32.00 \times 10^6$	Loads Status MCR 1346
Fuselage $M_x$	$35.18 \times 10^6$	$3.06 \times 10^6$	$38.24 \times 10^6$	$17.83 \times 10^6$	↓ Loads Status MCR 1346
Vertical Tail $M_x$	$5.35 \times 10^6$	$0.68 \times 10^6$	$6.03 \times 10^6$	$8.83 \times 10^6$	

Notes: Static loads results are from the squatcheloid assessment accomplished in Reference 4.

Dynamic loads are from the rectangular gust results contained herein.

Several conclusions were drawn from this study:

- (a) Static elastic effects were negligible.
- (b) Gust penetration effects were negligible.
- (c) Lift growth effects can be neglected since they would reduce loads.
- (d) Tuned sinusoidal gusts are very large and too conservative.
- (e) Transient gust loads are small and, therefore, can be added peak-to-peak without considering elastic body response in the trajectory simulation (basic for criteria and approach baselined by AFSIG).

## 2. Rigid Body Interface Loads

The second independent study conducted by MSFC concentrated on the interface loads using an updated set of aerodynamic data and vehicle control system. A detailed comparison was made between wind effects and vehicle parameter effects on loads. Table 13 summarizes the effects of basic system parameters on loads.

TABLE 13. BASIC SYSTEM PARAMETER SUMMARY

LOAD VALUES IN KIPS	P1(+)	P3(+)	P4(+)	P7(+)	P7(-)	P10(+)	P13(-)	FT01(+)	
ACCEL. MISALIGN.	3.6	27.2	37.1	14.7	5.4	25.2	26.9	1.8	
ENGINE MISALIGN.	3.2	11.2	19.2	11.7	12.2	40.4	40.3	3.2	
AERO	5.6	46.8	26.1	18.3	9.4	55.6	30.0	3.8	
THRUST	1.6	4.8	44.9	5.7	6.4	4.7	6.1	13.4	
GAINS	0.6	4.5	5.7	2.2	2.6	3.0	4.3	0.3	
Δ RSS	9.9	58.3	70.0	27.7	-19.4	75.3	-64.8	15.2	15.2
B[0.85* (99% SH, 9 M/SG)]	59.1	308.7	349.3	80.5	-74.8	167.2	-187.5	67.8	72.1
A(50% SH, 3 M/SG)	53.8	267.7	287.6	61.6	-51.8	133.7	-147.4	62.0	62.4
Δ WIND	5.3	41.0	61.7	18.9	-23.0	33.5	-40.1	5.8	9.7
$[(\Delta \text{RSS})^2 + (\Delta \text{WIND})^2]^{1/2}$	11.2	71.3	93.3	33.5	30.1	82.4	76.2	16.3	18.0
MACH	1.25	1.25	1.05	1.25	1.10	1.25	1.25	1.10	1.05
WIND AZIMUTH	15	15	215	15	200	15	40	265	265

The aerodynamic tolerance effect shown on this chart only covers the tolerances in total vehicle aerodynamics. In general, the vehicle tolerances create a larger load delta than does the delta wind load due to going from 1-sigma shear and gust to 3-sigma shear and gusts. The thrust variation affects only P<sub>4</sub> while engine misalignment, accelerometer misalignment, and aerodynamic affect all loads. Control system gain variations had a negligible effect. The maximum load Mach number and wind direction are given in the last two rows. Some component of cross wind is necessary to peak interface loads.

The effect of body-to-body aero tolerances is shown in Table 14. These tolerances have a large effect on loads varying from 16 percent to 74 percent of the base load.

### (3) Monte Carlo Analysis

The last study conducted dealt with the final verification and flight operations using the detailed individually measured wind profiles (Jimsphere). As mentioned previously Shuttle Systems Level II, at the recommendation of AFSIG, baselined a verification and operations approach using the individual measured wind ensembles for the month of launch and load indicators. The load indicator consists of a load algorithm and the corresponding limit values (in general, test verified). By using these load indicators, launch commit decisions can be made very quickly without doing detailed stress analysis. The following is a typical example of a load indicator.

TABLE 14. PRELIMINARY ASSESSMENT OF AERO TOLERANCES, MACH 1.25

<u>LOAD</u>	<u>INCREMENT</u>	<u>BASE LOAD</u>	<u>%</u>
P1	37.0	60	62
P2	37.0	60	62
P3	71.0	319	22
P4	93.0	324	29
P7	59.0	80	74
P10	31.0	172	18
P13	31.0	190	16

$$P_2 \text{ compression} = -0.1801 M_x^2 + 0.39 M_y^2 - 2.634 F_w^2 + F_v^2 \\ + 0.177 F_{TO1} + 0.233 F_{TO2} \quad 42.8 \text{ Ksi}$$

where  $M_x$  and  $M_y$  = moments X and Y imposed on yoke or Orbiter

$F_w$  = Drag force on strut

$F_v$  = Force in strut caused by vortex shedding

$F_{TO1}$  and  $F_{TO2}$  = interface load in Z and Y directions, respectively.

Using this approach requires detailed interfaces and communication with elements in developing and verifying the load indicators; however, the merits are obvious. Additionally the load indicator approach is useful for Monte Carlo analysis to predict launch probabilities. Also, day of launch I-loads update (day of launch wind biasing) can be based on these indicators.

The baselined (Level II) approach for flight operations is:

(a) Run vehicle response to the 150 measured winds ensemble using nominal values for all system parameters determining peak loads and 3-sigma loads.

(b) Run vehicle response to the 150 measured winds ensemble with Monte Carlo sampling of all vehicle parameter tolerances and aerodynamic variations determining peak loads and 3-sigma loads.

(c) Determine vehicle parameter variations and aerodynamic variation effects independent of winds by taking differences between (a) and (b) above.

(d) Determine wind persistence effects between 8-hour matched wind pairs.

(e) Using results of steps (c) and (d), modify the load indicator limits to give wind only nominal vehicle limit load.

(f) Run vehicle response for the measured wind profile taken 8 hours prior to launch and make launch commit decision. A final verification can be made with the 1½-hour wind profile.

As mentioned previously, two constraints for launch are imposed from the loads viewpoint: (1) a flutter constraint  $q \leq 660$  psf, and (2) loads less than limit values as provided by load indicators. Figure 26 shows results obtained using a 150 measured wind ensemble for  $q\alpha$  and  $q\beta$ . In general, design loads were based on  $q\alpha$  and  $q\beta$  envelopes; therefore, these envelopes from the measured winds are good indicators of capability. They do not, however, include aerodynamic variation effects and are not the total picture. The outer solid line corresponds to the basic  $q\alpha/q\beta$  squatcheloid and indicates that, in general, most of the wind-induced responses fall within the design.

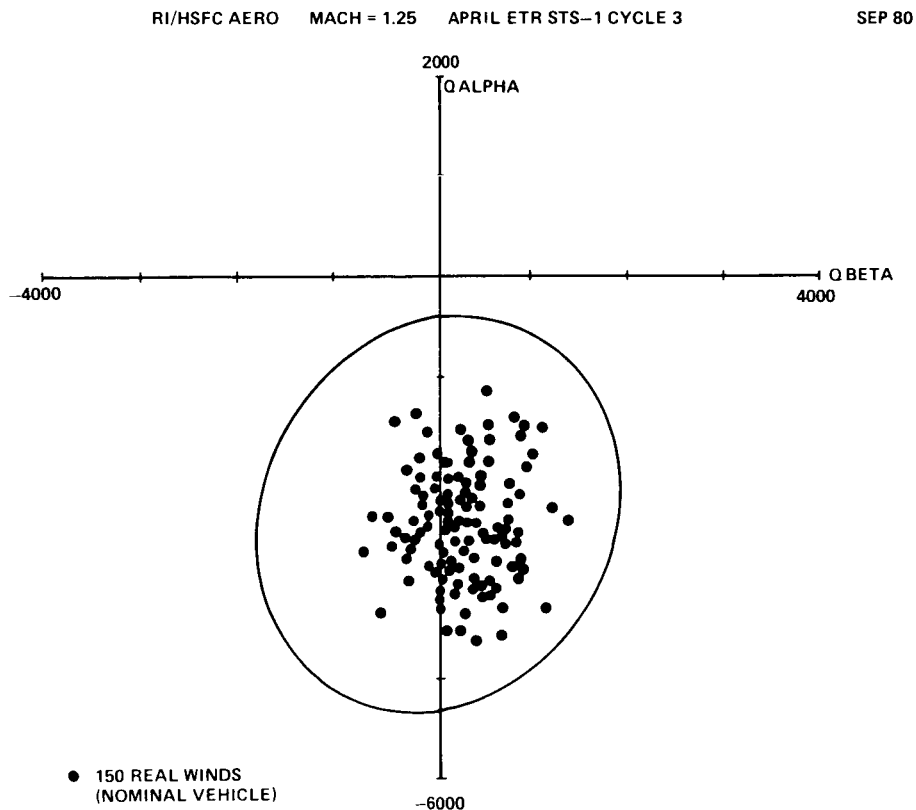


Figure 26. 150 Real wind squatcheloid.

Taking the next step, running the load indicator responses, the total picture can be obtained. Figure 27 is a plot of the load indicator amplitude for the Orbiter to ET forward bipod struts P1 and P2, plotted versus probability. Notice that the graph shows both the nominal (winds alone) and the random (winds plus random variation of vehicle parameters). The winds alone have a small influence, while the parameters plus winds have a large influence. Also, the parameter variations will both increase and decrease loads, hence the random values cross the nominal (winds only) at approximately to 50% level, which is where they should cross.

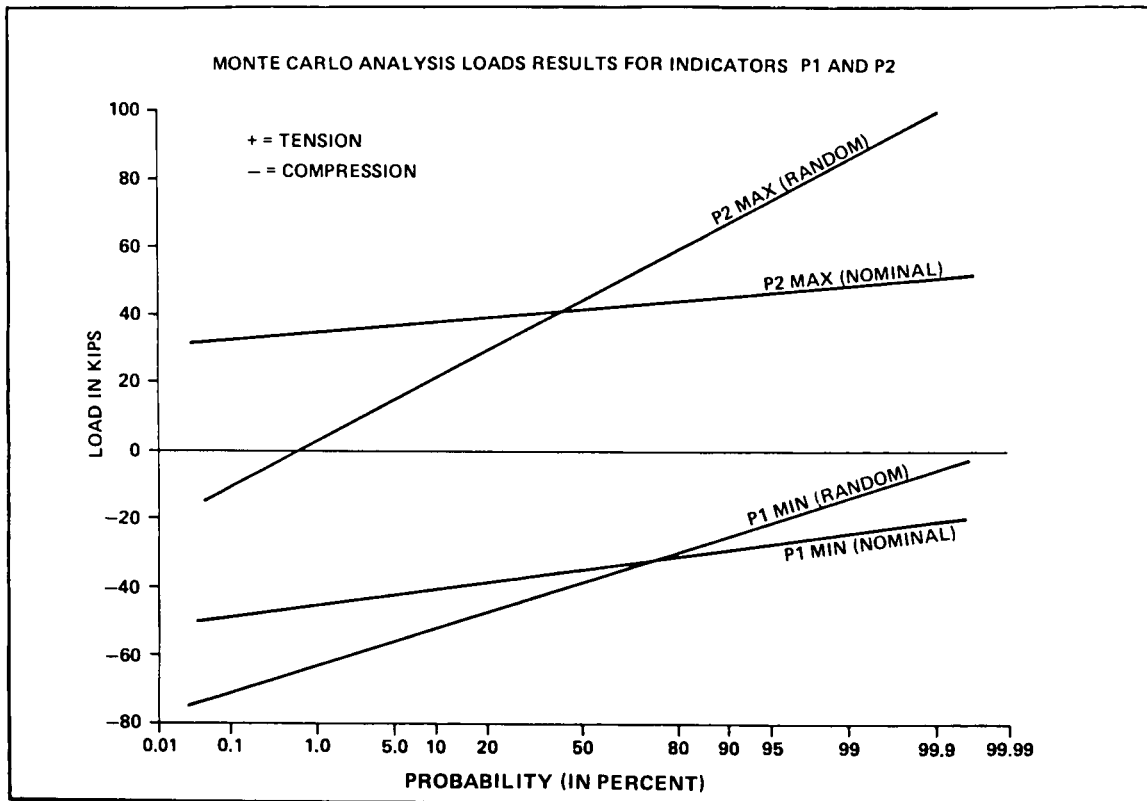


Figure 27. Monte Carlo analysis loads results.

In the case of P1 and P2, the design load was not exceeded, hence a 99.9 percent launch probability exists for this load. A more comprehensive report of all these results will be published in the future.

Since dynamic pressure,  $q$ , is a launch constraint for the first Shuttle launches, its probability of exceedance is important. Table 15 shows these values for different dynamic pressures and various ways of handling the wind statistics. Notice that there is significant difference in taking each wind sequential and a sample of 150 winds and using 600 winds and randomly selecting both winds and vehicle parameters. Also, the use of 150 winds instead of 600 appears inadequate, thus the computer time saved is not available.

TABLE 15. LAUNCH PROBABILITY FOR Q

	600	640	660	680
TOTAL MONTE CARLO -- 600 WINDS	29%	71%	85%	92%
SEQUENTIAL WINDS, MONTE CARLO PARAMETERS -- 500 WINDS	28%	73%	84%	90%
NOMINAL -- 150 WINDS	25%	78%	89%	97%
740 PSF HIGHEST Q OBSERVED IN ALL RUNS				
MAXIMUM GIMBAL DEFLECTIONS				
SSME	P	Y		
#1	4.5	3°		
#2	5.5	2°		
#3	4.5			
SRB	LEFT ACTUATOR	RIGHT ACTUATOR		
LEFT	3.0°	3°		
RIGHT	2.5°	2.75°		

Shown on the same chart is the maximum gimbal angles observed on all runs. SSME's have a 10° limit and the SRB's 5° capability. More than adequate control margins exist for the no-engine-out failure cases.

Monte Carlo analysis is an excellent tool for verifying space vehicle systems. Taking this approach more accurately simulates the system since correct time phasing takes place. Also, it removes the inherent conservatism of other approaches and therefore shows higher launch probability.

#### (4) Protuberance Loads

Protuberance loads are a critical problem during the max q flight regime. These loads, in general, derive from (1) static drag loads, (2) low frequency system dynamic responses, (3) high frequency acoustic induced responses, and (4) vortex shedding induced loads. Due to frequency separation, etc., these loads can be added algebraically. Typical examples of protuberances are the SRB to tank attach struts, ET cable trays, LOX feed-line, GH<sub>2</sub> and GOX pressurization lines, and separation motors. Since most of these are attached parallel to the vehicle center line, the question arises as to the validity of the vortex shedding inclusions. The complex vehicle configuration with open areas between each element creates complex cross flow patterns that impact the above-mentioned lines, thus the potential for vortex shedding.

Detailed aerodynamic protuberance tests were run by Rockwell to determine the static drag loads, acoustic environments, and vortex shedding environments. Using the test derived unsteady environments and analytical dynamic models of the protuberances, a detailed response analysis was run and loads generated. A reponse analysis was accomplished to determine loads using power spectral density descriptions of pressure fluctuations due to vortex shedding. A typical power spectral density plot is shown on Figure 28. Table 16 summarizes these loads.

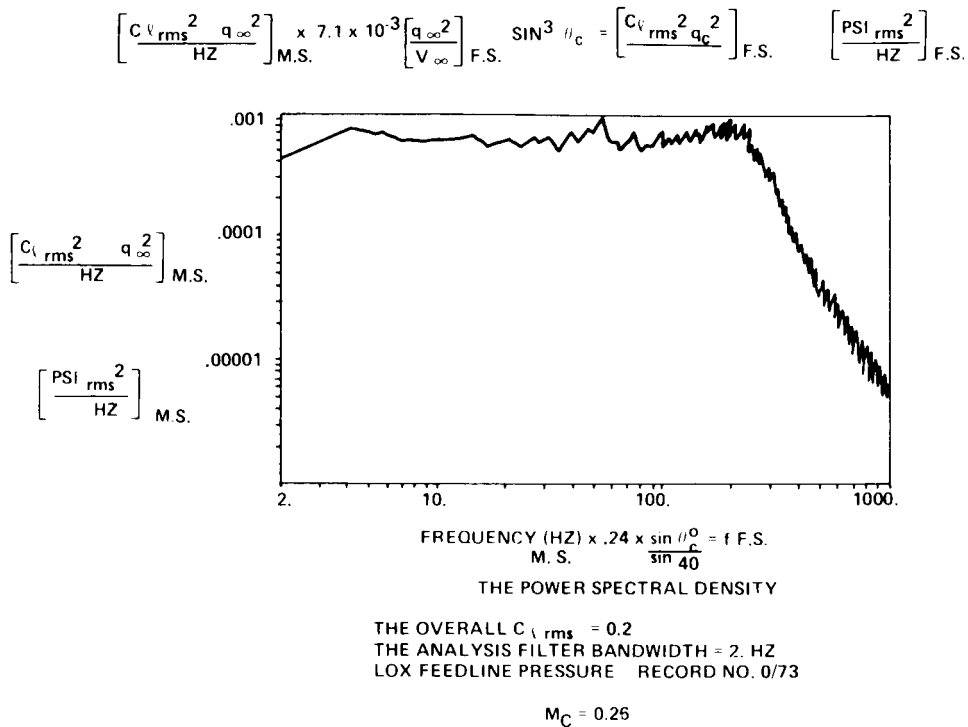


Figure 28. Vortex shedding power spectral density plot.

TABLE 16. LOAD SUMMARY

MACH NO.	RANDOM RMS LOADS (POUNDS)			PERIODIC RMS LOADS (POUNDS)		
	RADIAL	TANGENTIAL	RADIAL	RADIAL	TANGENTIAL	RADIAL
0.8	4.69	1.21	5.08	0.09	0.02	0.10
0.9	4.33	1.14	4.69	1.16	0.19	1.18
1.0	3.92	1.04	4.24	3.16	0.58	3.23
1.1	3.40	0.95	3.66	6.68	1.22	6.85
1.2	3.02	0.85	3.25	6.24	1.13	6.43
1.3	2.76	0.77	2.97	5.98	1.08	6.17
1.4	2.64	0.72	2.84	6.30	1.15	6.51
1.5	2.44	0.67	2.62	5.88	1.06	6.09



The acoustic environment did not create any loads on the LOX line due to its low frequency and large mass; therefore, it was negligible. Using the vortex induced loads, drag loads based on special tests, and the low frequency system response loads, total loads are generated. The squatcheloid and dynamic pressure derived as discussed previously using RSS'ing of vehicle parameter tolerances were used in conjunction with the test derived drag loads in making these calculations. Each protuberance was treated in this manner. Further examples are not given due to expediency; however, these loads are just as critical and important as the main body loads. The same level of involvement, environment definition, etc., are required for protuberances as is done for system loads. Many times the loads engineer tends to neglect these items in lieu of the more interesting systems loads. The message is clear. Put the same emphasis on all critical loads, placing a special emphasis on identifying very early all potential elements, protuberances, and components.

Just as important in this aspect is load due to trapped air pressure or delta air pressure across tunnels, etc. Close work between loads and environments is required to predict venting effects and design for these loads. To ensure that this is done for MSFC elements, a special venting team was formed under the direction of Dr. James Blair. This team did a detailed review of all ET and SRB potential vented compartments and their environment, thus verifying the system. The effort and data were of a very large scope. No results are therefore shown.

The max q loads analysis has demonstrated the strong interdisciplinary coupling of the Shuttle vehicle and the large sensitivity to aerodynamic data uncertainties, particularly the element to element changes. The need for highly integrated data flow and time varying simulations was demonstrated.

## 2. SRB Recovery System

The SRB case hardware design was based on launch and impacted for attrition for recovery other than the design of the recovery system related hardware itself. The recovery sequence is depicted in Figure 29 with the exception of retrieval (towing).

Load events are reentry acoustics (only driving aft skirt components), parachute deployment loads, water impact loads, and retrieval loads.

### a. Acoustic Environments

SRB reentry acoustical environments are very high and drive the design of some components, such as the APU systems. Several iterations including special test and analysis were conducted in order to define this environment. Table 17 lists the basic sequence of events that developed.

As noted in the fourth major bullet of Table 17, several large amplitude discrete spikes were found during the AEDC wind tunnel special test program. These trends had not been expected; therefore, a special two-dimensional water table test program was conducted to define the mechanism. Figure 30 depicts this test setup and results. For the

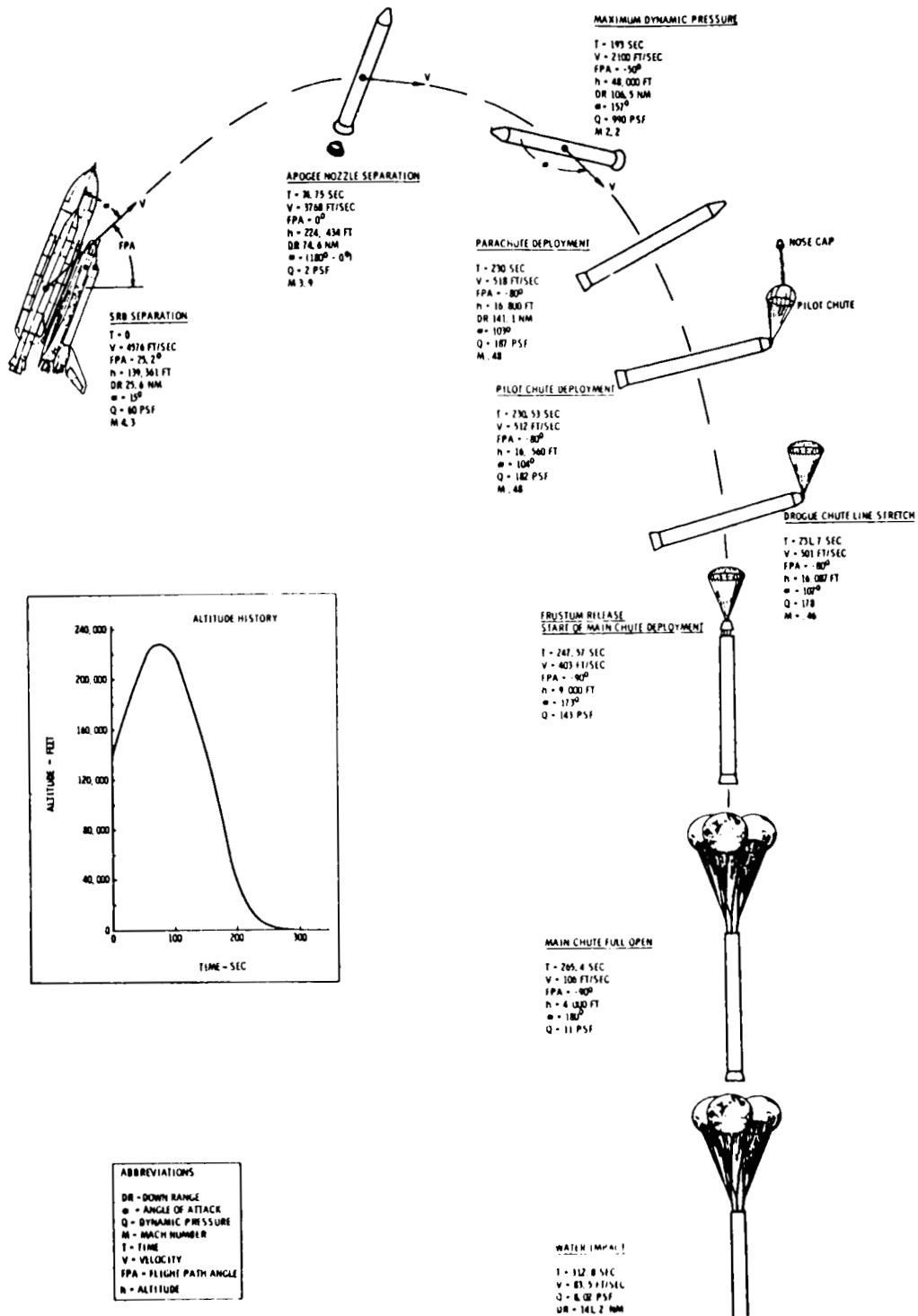


Figure 29. SRB nominal reentry profile.

TABLE 17. SRB REENTRY ACOUSTICS-FLUCTUATING PRESSURES

- ANALYTICAL PREDICTIONS BASED ON LOCALIZED FLOW CONDITIONS
- DEvised & CONDUCTED SCALE MODEL TESTS AT MSFC'S 14 x 14 INCH WIND TUNNEL WITH OLD BASELINE CONFIGURATION
  - PROMPTED REMOVAL OF EXTENDED NOZZLE SECTION
  - PROVIDED INPUTS FOR ACOUSTIC RESPONSE DESIGN/TEST CRITERIA
- VERIFIED TRENDS VIA LARGER MODEL & EXPANDED TEST CONDITIONS AT AEDC
- NOTED SEVERE ACOUSTIC DISCRETES ASSOCIATED WITH MOTOR CAVITY RESPONSE \* USE WATER TABLE TO INVESTIGATE \*
- CONSIDERED TRAJECTORY STATISTICS & ENVIRONMENTAL ZONING FOR RESPONSE CRITERIA UPDATE
- DESIGNED & TESTED VARIOUS AERO-FIX CONFIGURATIONS
  - VERIFIED ACOUSTICAL NEED FOR A FLEXIBLE HEAT SHIELD
  - ESTABLISHED BLAST SHIELD EFFECT
- PREPARING FOR FLIGHT ENVIRONMENTAL VERIFICATION TEST AT AMES WITH REVISED BASELINE & A FIX CANDIDATE

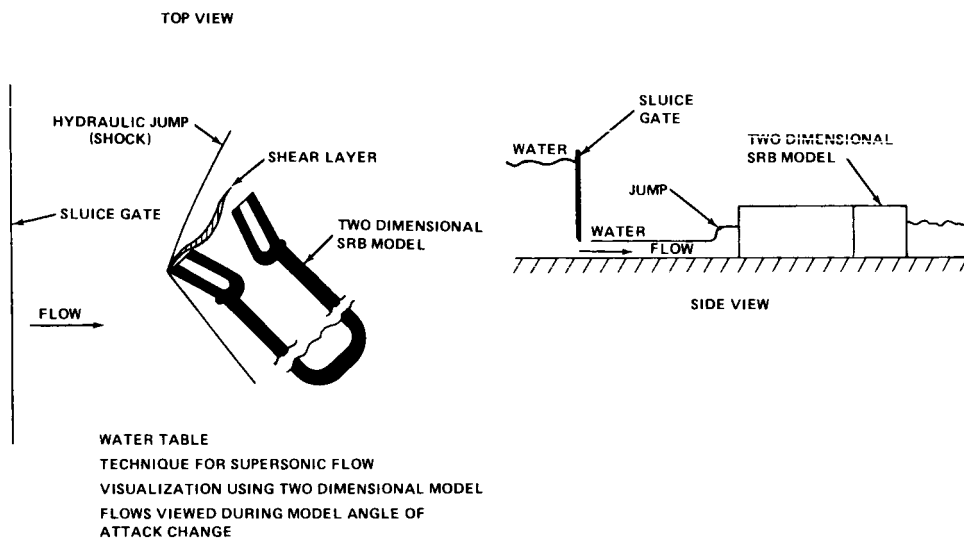


Figure 30. Test setup and results.

angles of attack expected during reentry, there are large cross flows which create a hydraulic jump (shock) and a shear layer. Carrying this information to the three-dimensional SRB during reentry and conducting analytical analysis, it was found that there existed an oscillating shear layer off the nozzle lip and the basic acoustical cavity mode of the internal motor cavity. At certain Mach numbers, these modes are in resonance. Figure 31 depicts the basic phenomenon.

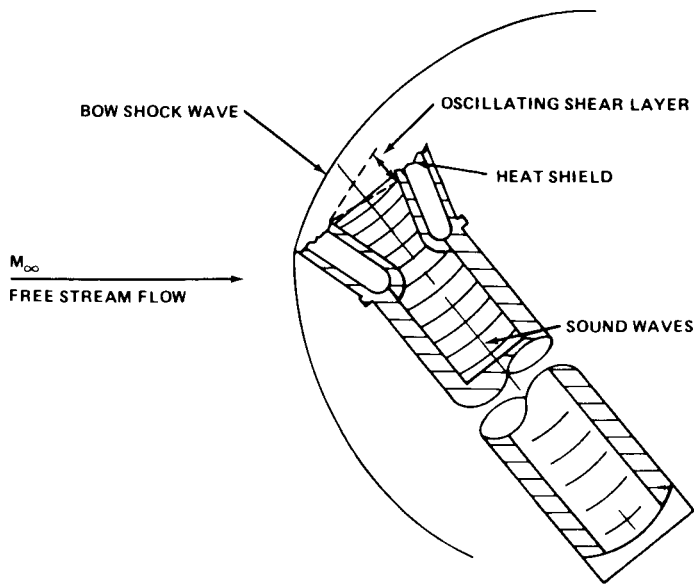


Figure 31. Resonance modes.

A plot of the longitudinal SRB cavity acoustical modes are plotted as solid lines on Figure 32. The nozzle shear layer excitation modes (sharp edge created) are illustrated as dotted lines. Notice the resonance for  $K = 3$  and the  $M = 1$  modes at a local Mach number of approximately 0.6.

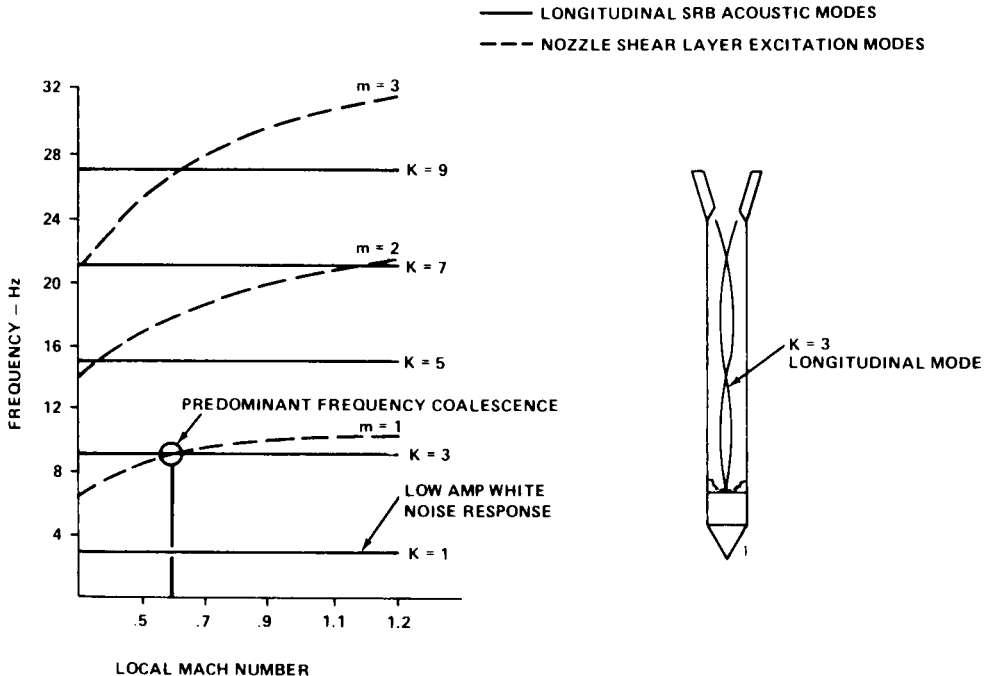


Figure 32. SRB motor frequency prediction model.

These modes were verified in MSFC's 14-inch wind tunnel and the AEDC tunnel using a larger model. At the same time, many means for reducing the environments were investigated. Figure 33 shows the environment as a function of angle of attack with and without the nozzle thermal curtain, showing that the curtain reduced the environments. This led to the preliminary requirement that the thermal curtain must survive reentry. Later studies have eliminated this requirement.

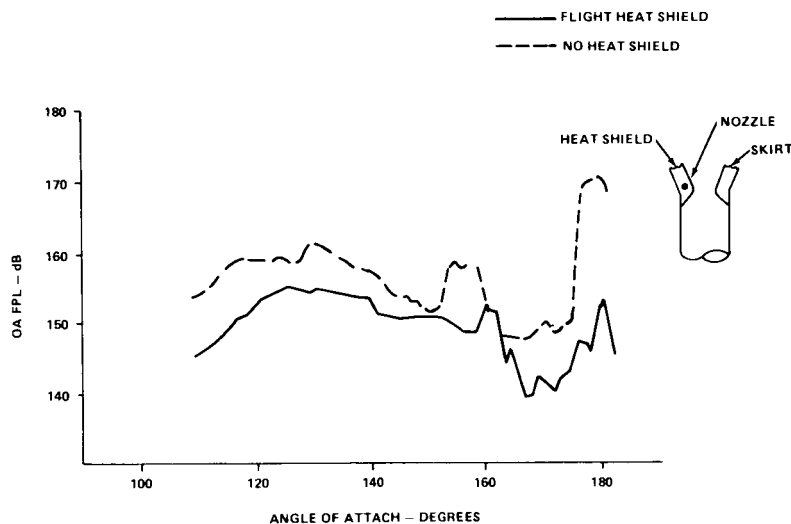


Figure 33. Environment as a function of angle of attack.

In addition to this requirement, it was decided to develop envelopes as a function of probability of the reentry conditions (angle of attack and  $q$ ) as a function of Mach number using a Monte Carlo analysis. Key parameters varied were the aerodynamic characteristics, SRB separation-induced initial conditions, and vehicle center of gravity.

Special wind tunnel tests were run for various SRB roll angle conditions to define the aerodynamic data base. The simulation developed for the trajectory response was quite detailed giving SRB response in pitch, yaw, and roll. Through this systems approach, it was possible to verify the SRB aft components design without redesign and impacts. This problem illustrates the need for the results obtained when key disciplines have good communication and work together on a problem. This same type analysis and working relations were key in developing the parachute (recovery system) and predicting water impact loads.

#### b. Recovery System

The parachute design and development for the SRB recovery system was a special program in itself. The chute size, the sequencing and timing, trajectory conditions, sensor development, and the lack of sufficient analytical approaches for predicting loads were contributing factors. These factors lead to a detailed rocket sled and drop test program to verify the system deployment characteristics and loads. Key parameters from the loads prediction side that helped drive this program were (1) chute fill time, (2) inflation characteristics, (3) dereefing sequencing, (4) snatch loads, (5) dynamic pressure, and (6) velocity.

The recovery subsystem consists of a 11.5-foot-diameter pilot parachute assembly, a 54-foot-diameter drogue parachute assembly, and three 115-foot-diameter main parachute assemblies with retention components. The subsystem is located within the nose cap and frustum of the nose assemblies of each SRB and provides the required terminal velocity and attitude for water impact of the SRB and SRB nose assembly frustum.

An altitude sensing switch activates the recovery subsystem by initiating the ejection of the SRB nose cap. The jettisoned nose cap pulls away the pilot chute pack and deploys the pilot chute. Full deployment of the pilot chute releases the drogue chute retention straps and rotates the drogue chute from its mounting on the deck of the frustum. The pilot chute then pulls the drogue chute and pack away from the SRB to deploy the chute into its first reefed position.

The reefed drogue chute starts the rotation of the SRB into an axial alignment with the relative airstream. Approximately seven seconds after drogue chute line stretch, reefing line cutters fire to allow the drogue chute to inflate to its second reefed condition. The final disreef to full open occurs 12 seconds after line stretch.

At a nominal altitude of 6,600 feet, the frustum separates from the SRB. The drogue chute pulls the frustum away from the SRB. The main chute risers are pulled out from the main chute bags, and the chutes begin to deploy. At line stretch, the main chute reefing line cutters are initiated. The main chutes open to a first stage reefed position. The first stage reefing cutters fire about ten seconds after line stretch, allowing the chutes to expand to the second stage reefed position. About 17 seconds after line stretch, the second stage cutters fire, allowing the chutes to achieve full diameter. Figure 34 depicts the sequence of events for the system.

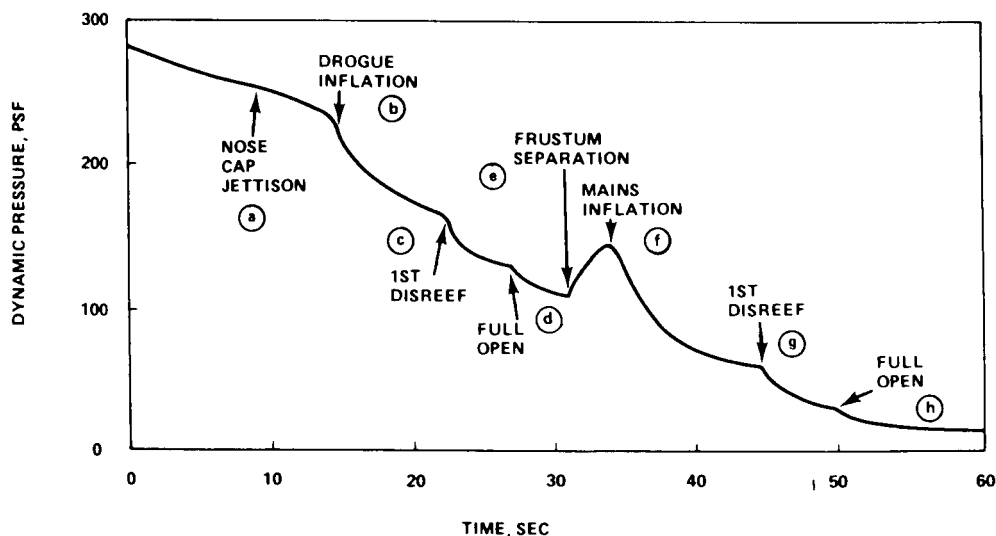


Figure 34. Sequence of events.

The basic recovery subsystem requirements which fall out of these sequences and other systems-induced environments are given in Table 18.

TABLE 18. DECELERATOR SUBSYSTEM REQUIREMENTS

O DESIGN REQUIREMENTS DRIVERS	
TAIL FIRST TERMINAL VELOCITY	85 FPS NOMINAL
BOOSTER POST SEPARATION WEIGHT	170,000 POUNDS
O DERIVED BASELINE CONDITIONS	
START DEPLOYMENT SEQUENCE (DROGUE)	15,000 TO 16,000 FT
BOOSTER ANGLE OF ATTACK	80° TO 140° (110° NOMINAL)
DYNAMIC PRESSURE	175 TO 240 PSF (200 NOMINAL)
MACH NUMBER	< 0.6
BOOSTER ROLL RATE	< 45°/SEC
PITCH/YAW RATE	< 30°/SEC

Because of the problem of simulating all these conditions in one test program, it was decided to verify the nose cone separation using a rocket sled test. Sandia conducted this rocket sled test for MSFC. Figure 35 is a schematic showing the camera and laser tracking devices used in the test.

Several parameter variations were run with adequate separation clearances being obtained. Table 19 summarizes the results obtained for the 80° deployment condition and is typical of results obtained. All results were well within the range expected.

To fully work the chute system, a drop test program was designed and implemented using a specially designed drop test vehicle which simulated the SRB forward compartment dropped from a B-52 aircraft. The SRB drop test vehicle configuration is shown in Figure 36, showing the basic weight (49,000 pounds) and the nose cone, frustum, and parachute geometry.

To develop the test program and objectives, it was necessary to identify key areas of concern and events. Figure 37 shows the details involved in the nose cone jettison and drogue chute deployment for a broadside deployment case. The nose cap pulls the pilot chute out. In this time frame, important problems are snatch loads and line sail. Next comes the pilot-bag strip. Here bag-strip behavior and forces are problems as well as snatch loads and line sail. The pilot chute performance is a critical area coupled with the drogue chute inflation to the first reefed position. Critical areas during this time are snatch loads, chute vent loadings, and nonuniform loading on the SRB frustum.

Figure 38 depicts the additional critical areas during main chute deployment. The drogue chute goes through the second disreefing and fully opens. The critical area for this sequence is chute skirt loading. At this time, the frustum releases with separation loading and bag stripping the critical areas.

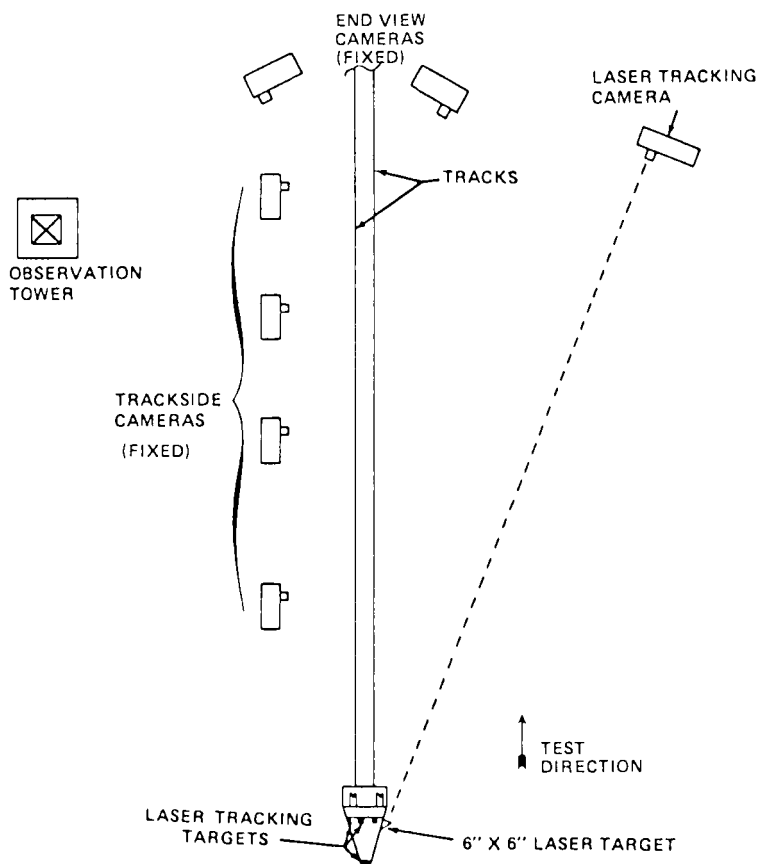


Figure 35. Sandia rocket sled test setup.

TABLE 19. DATA SUMMARY - 80° CONDITION

PARAMETER	EXPECTED RANGE	TEST RESULT	REMARKS
DYNAMIC PRESSURE (PSF)	200 ± 10	197	PEAK LEVELS
THRUSTER #1 PRESSURE (PSI)	9550 ± 1910	8700	
THRUSTER #2 THRUSTER #3	9550 ± 1910 9550 ± 1910	8800 8900	
#1 INTERNAL Δ PRESSURE (PSI)	-1.0 ± .5	-1.15	RELATIVE TO AMBIENT
#2 INTERNAL Δ PRESSURE (PSI)	-1.0 ± .5	-0.75	
SEPARATION VELOCITY (FT/SEC)	90 ± 10	85	



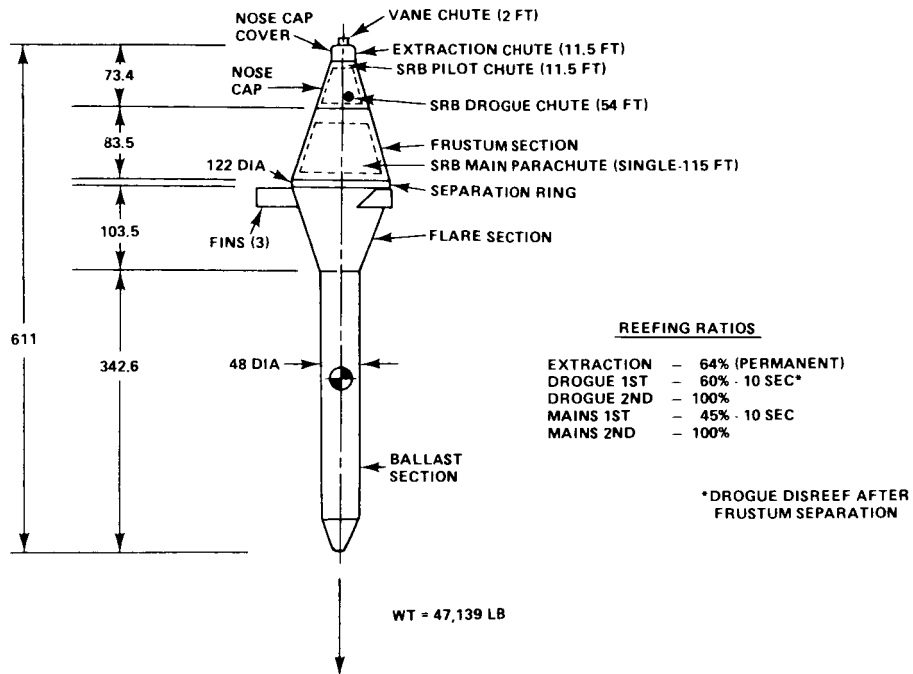


Figure 36. Drop test vehicle configurations.

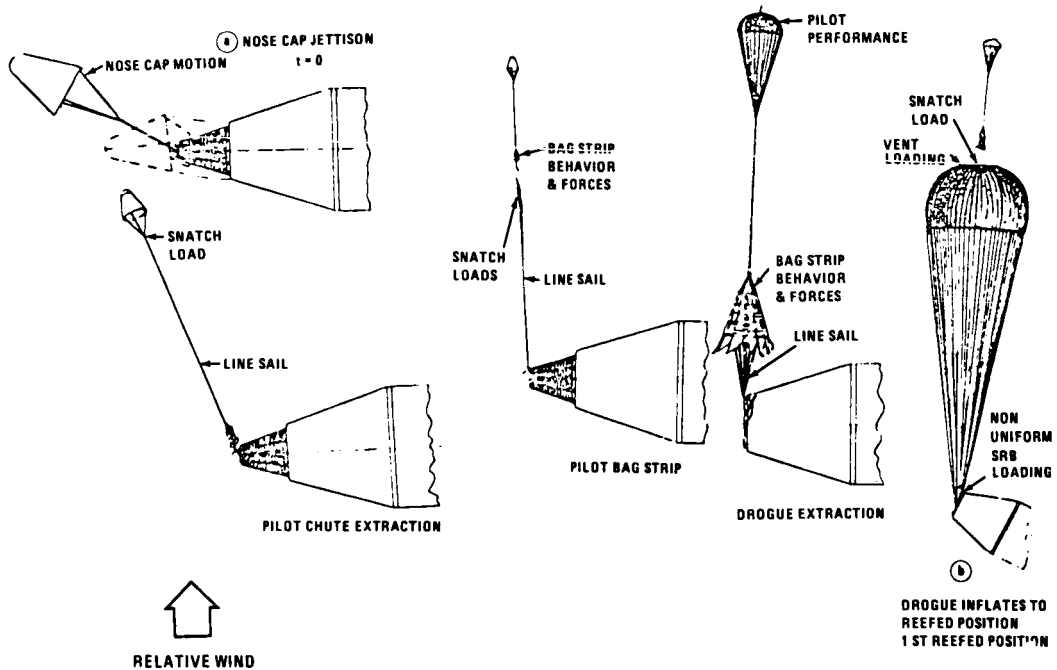


Figure 37. SRB sequence of events-broadside deployment critical areas.

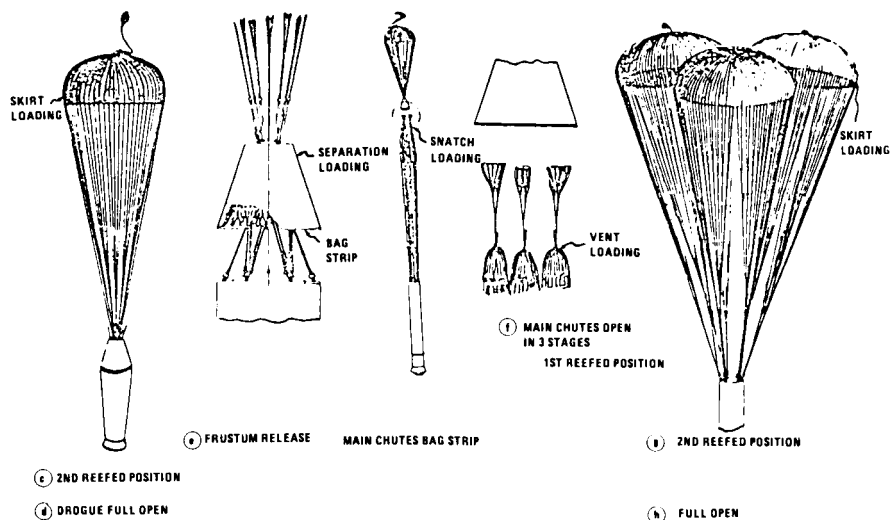


Figure 38. SRB sequence of events – deployment of mains critical areas.

These events lead to the basic design characteristics for the decelerator subsystem: (1) parachute deployment initiated by nose cap jettison, (2) broadside deployment of drogue parachute, (3) SRB stabilization with drogue chute, (4) drogue chute subjected to high loads relative to size, (5) main chute cluster extraction from hard container (frustum), (6) largest ribbon parachutes (mains) ever developed for loads of these magnitudes.

The development test philosophy formulated is summarized in Table 20.

TABLE 20. DEVELOPMENT TEST PHILOSOPHY

- A PARACHUTE DESIGN CANNOT BE ASSESSED ANALYTICALLY FOR DEPLOYMENT OR PERFORMANCE CHARACTERISTICS. A FULL SCALE PARACHUTE GROUND AND AIR TEST PROGRAM IS REQUIRED.
- THE DEVELOPMENT APPROACH STARTS AT THE COMPONENT AND SUBELEMENT GROUND TEST LEVEL AND BUILDS, IN AN ORDERLY PROGRESSION, THROUGH TO A TOTAL SYSTEMS AIR DROP TEST PROGRAM.
- IN THE CASE OF THE SRB RECOVERY SUBSYSTEM, THE DEVELOPMENT TEST PROGRAM IS COMPLICATED BY THE PAYLOAD SIZE, WEIGHT, AND DEPLOYMENT CONDITIONS.

The test program objectives arrived at are shown in Table 21. The three general areas for objectives were performance and loads, deployment process, and structural integrity.

The test plan is summarized in Table 22. Across the top is the design objective and critical area. The drop test number is shown down the side. Blocks with circles indicate the drop test where this objective was addressed.

TABLE 21. DROP TEST PROGRAM OBJECTIVES

PERFORMANCE AND LOADS

- o INFLATION CHARACTERISTICS
- o LOAD/SRB DESIGN CONDITIONS
- o PARACHUTE DRAG
- o PARACHUTE STABILITY

DEPLOYMENT PROCESS

- o DEPLOYMENT FORCES AND BEHAVIOR
- o FRUSTUM/MAIN CLUSTER EXTRACTION
- o BROADSIDE DROGUE DEPLOYMENT

PARACHUTE STRUCTURAL INTEGRITY

- o VENT AREA LOADS
- o SKIRT AREA LOADS

TABLE 22. PRIMARY TEST OBJECTIVES MATRIX

	Deployment Process		Limit Load Environment		High Q Deployment			Structural Integrity		Performance		
	Broadside	System Functional	Drogue	Single Main	Drogue	Main Cluster	Single Main	Drogue	Single Main	Drogue	Main Cluster	Single Main
Drop 1	*	●	○							●	●	
Drop 2				●								●
Drop 3					●			○				
Drop 4						●						
Drop 5								●				
Drop 6			●				●		●			
Sled Test	●											

\*Skewed deployment ( $\alpha = 50^\circ$ ) although not objective.

○ = Objective

● = Accomplished

◐ = Partial accomplishment

Figure 39 is a chart which shows how the drop test met the required conditions. The problem in devising these tests was creating the environmental conditions for each event because the total trajectory, etc., could not be generated in one drop. By creating special environments, individual tests of each key event were able to be simulated.

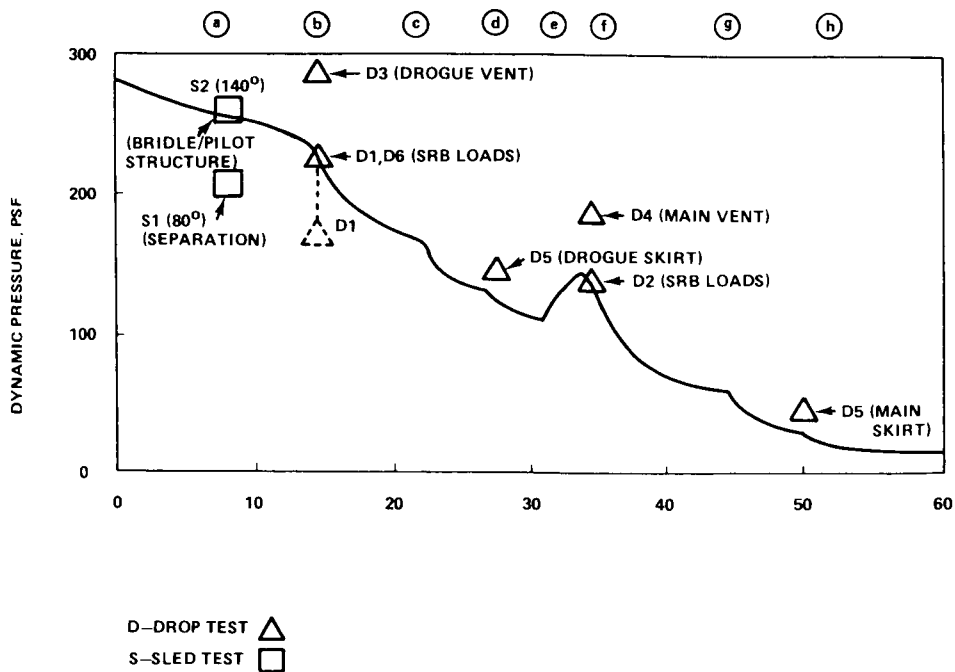


Figure 39. Test objective targets.

One special loads problem occurred during the planning and verification stages of the drop test program. This concerned the B-52 hook drop vehicle flight loads. Here, detailed aerodynamic data of the drop vehicle had to be generated and loads analysis run for the basic environments expected during flight. Also, the drop vehicle could not cause exceedances on the aircraft wing capability. Figure 40 is a typical example of the loads analysis result showing that all requirements for the aircraft wing were met.

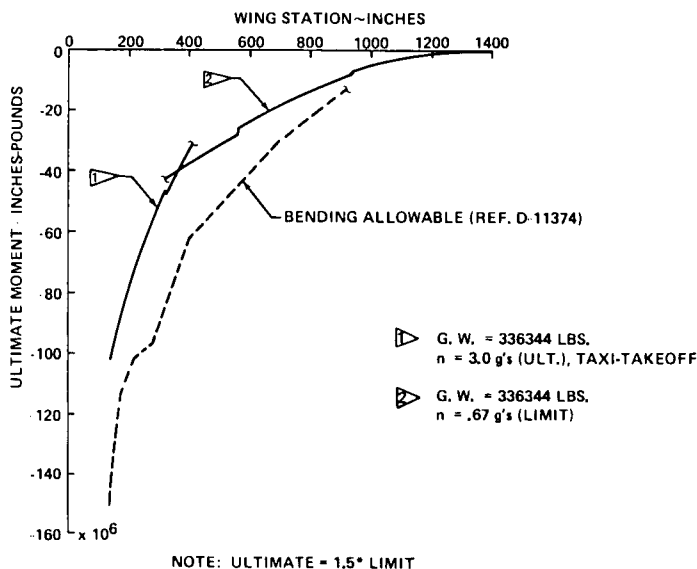


Figure 40. Ultimate wing vertical bending moment (negative) ring hand wing B-52B/DTV configuration 1.

The DTV interface design loads for the lug fittings were the only B-52 critical flight design loads; otherwise, the DTV structure was designed by the parachute induced loads. Figure 41 compares these loads.

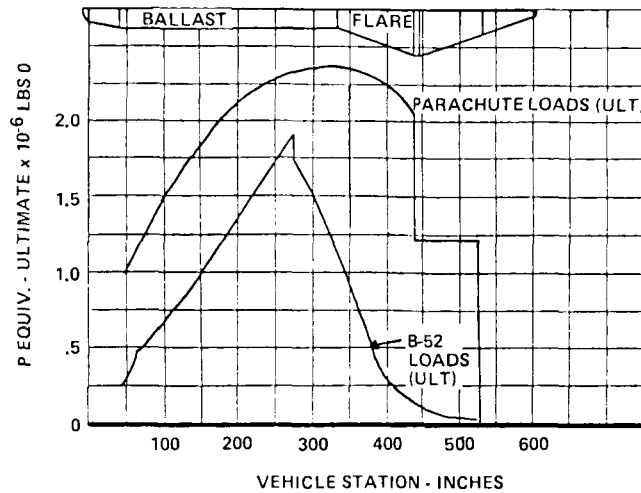


Figure 41. DTV design loads.

c. Water Impact Loads

Due to configuration complexities (i.e., not simple body), the SRB water impact loads could not be handled in the normal analytical manner. A series of drop test programs was conducted to define loads. In general, this program utilized a rigid body scale model. Elastic body responses of such subsystems as the nozzle were analytically dynamically modeled and driven using the forces measured in this scale model test program. Table 23 summarizes the total drop test program carried out by MSFC. The first test program occurred in February 1973 with the final test occurring in October 1974.

The remarks column in Table 23 summarizes what was achieved in each program. The test configuration column depicts the basic configuration. The test conditions are enveloped values determined through trajectory simulations that included sequencing, aerodynamic characteristics, environmental winds, and sea state. The same technical interplay as discussed previously was required here also.

Several events take place during water impact. It was found that some of these required pressure scaling to properly define the loads. Figure 42 gives the significant loading events and where pressure scaling was required. To satisfy the pressure scaling requirements, Navy Ordnance Laboratory and their pressure scale test facility were used.

One interesting phenomenon occurred during initial impact in the nozzle area. The nozzle was first loaded in a positive direction as the nozzle attempted to move into the water. The water subsequently filled the aft skirt, thereby creating a negative

TABLE 23. DATA BASE FOR WATER IMPACT LOADS

DIAMETER/SCALE	TEST CONFIGURATION	TEST LOCATION	TEST CONDITIONS	REMARKS
120" / 77%	<ul style="list-style-type: none"> <li>● TITAN</li> <li>● STRAIGHT SKIRT</li> <li>● CANTED NOZZLE</li> </ul>	(2-73) LONG BEACH NAVAL SHIPYARD (LBNS)	$V_v = 10 - 70$ FT/SEC $V_H = 0$ $\theta = +10^\circ - +30^\circ$	PROVIDED BASIC SCALING LAW INFORMATION
12.5" / 8%	SCALED 120"	(2-73) NAVAL ORDNANCE LABORATORY (NOL)	$V_v = 40 - 100$ FT/SEC $V_H = 0$ $\theta = 0^\circ - +30^\circ$	<ul style="list-style-type: none"> <li>● CONCURRENT WITH 120" TESTS</li> <li>● WITH &amp; WITHOUT PRESSURE SCALING</li> <li>● SHOWED PRESSURE SCALING SIGNIFICANT TO LOADS</li> </ul>
12.5" / 8%	4/11/73 SRB DESIGN	(8-73) MSFC AND NOL (9-73)	$V_v = 80 - 120$ FT/SEC $V_H = 0 - 60$ FT/SEC $\theta = 0^\circ - +30^\circ$	<ul style="list-style-type: none"> <li>● PRESSURE LOADING STRONGLY DEPENDENT ON CONFIGURATION</li> <li>● PROVIDED MEASURE OF HORIZONTAL VELOCITY EFFECTS ON LOADS</li> </ul>
12.5" / 8%	4/11/73 SRB DESIGN	(11-73) MSFC	$V_v = 80 - 120$ FT/SEC $V_H = 0$ $\theta = +5^\circ - +15^\circ$	<ul style="list-style-type: none"> <li>● INVESTIGATED LEE SIDE PRESSURES</li> </ul>
12.5" / 8%	6/6/74 SRB DESIGN	(10-74) NOL	$V_v = 80 - 100$ FT/SEC $V_H = 0 - 45$ FT/SEC $\theta = -10^\circ - +10^\circ$	<ul style="list-style-type: none"> <li>● INVESTIGATED PRESSURE SCALING, HORIZONTAL VEL. AND ENTRY ANGLE VARIATION</li> </ul>

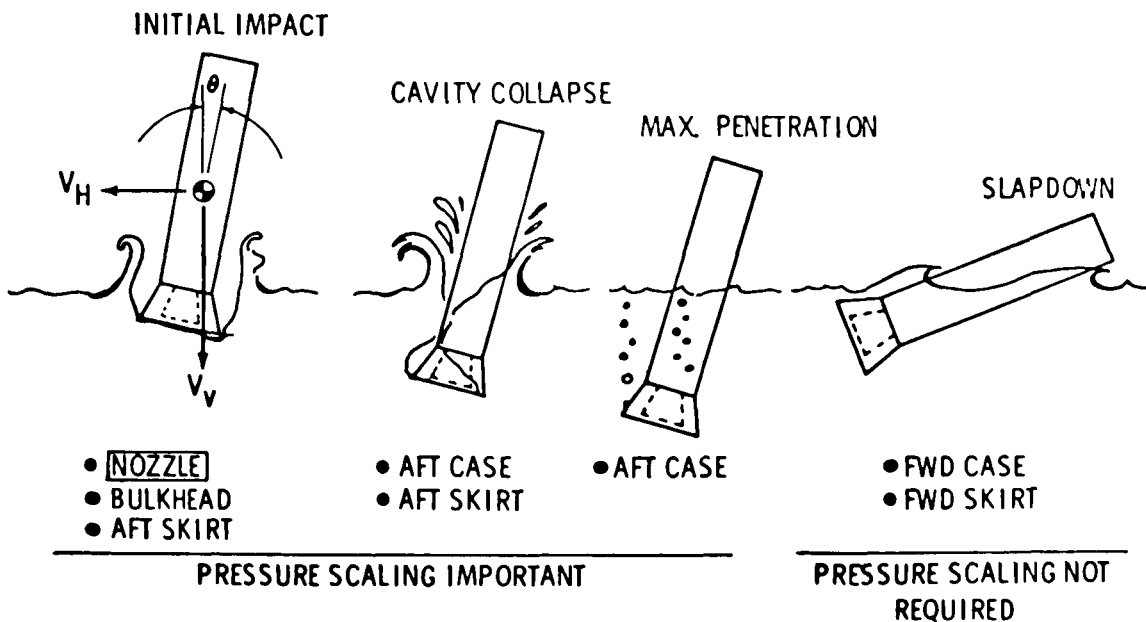


Figure 42. Significant loading events.

loading on the nozzle, the negative direction load being the peak load. Figure 43 shows this event and the loads for the nozzle, bulkhead pressure, internal skirt pressure, and internal and external nozzle pressure.

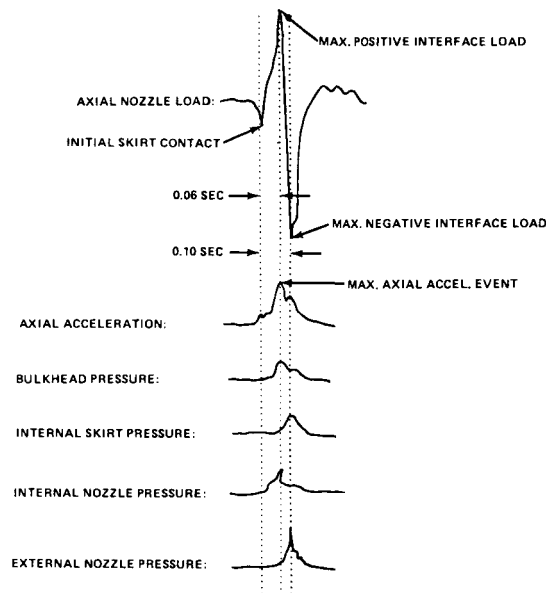


Figure 43. Typical initial impact dynamic events.

These initial impact loads can be summarized as follows:

#### Initial Impact Loads

- Three discrete loading events
- Pressure on any wetted surface defined in a time-consistent manner

(1) Max vehicle pitch acceleration event

Internal skirt and nozzle partially wetted  
Lateral g level = 7 at c.g.

(2) Max vehicle axial acceleration/max nozzle positive axial/max nozzle lateral loading event

Internal nozzle pressure and bulkhead max pressure  
Max axial g level = 21 g's

(3) Max nozzle negative axial loading event

Internal skirt and external nozzle max pressure

Cavity collapse loads can occur with either the tail trailing or leading the vehicle. The tail trailing case has low pressures and loads while the tail leading has high pressure and loads. These are summarized in graphics form in Figure 44.

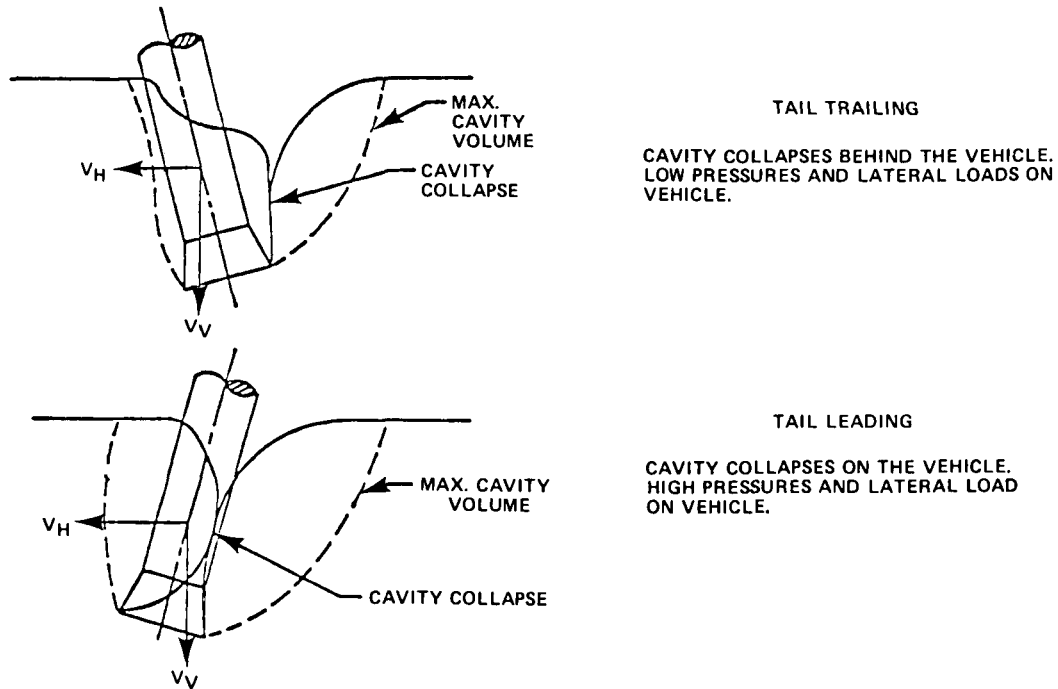


Figure 44. Cavity collapse loads.

A typical pressure distribution, longitudinally and radially, is shown in Figure 45.

As mentioned previously, the SRB nozzle loads could not be determined directly in the scale model test due to scaling problems. The nozzle system is composed of actuators, the nozzle, a series of laminated rings to allow for gimbaling the nozzle, and a snubber for response containment. Figure 46 is a schematic of this arrangement.

The loads were determined using the rigid body test data pressure time histories as forcing functions to the dynamic model. The nonlinear dynamic model was quite detailed including models for the flex bearing deflections in both rotation and translation. Figure 47 depicts this model and also gives the simulation characteristics.

Using this simulation, design loads were calculated. The total sequence is shown in Figure 48.

The actuator design assessment is shown in Figure 49. Given are both the applied-load lateral water pressure versus horizontal impact velocity and versus actuator capability.



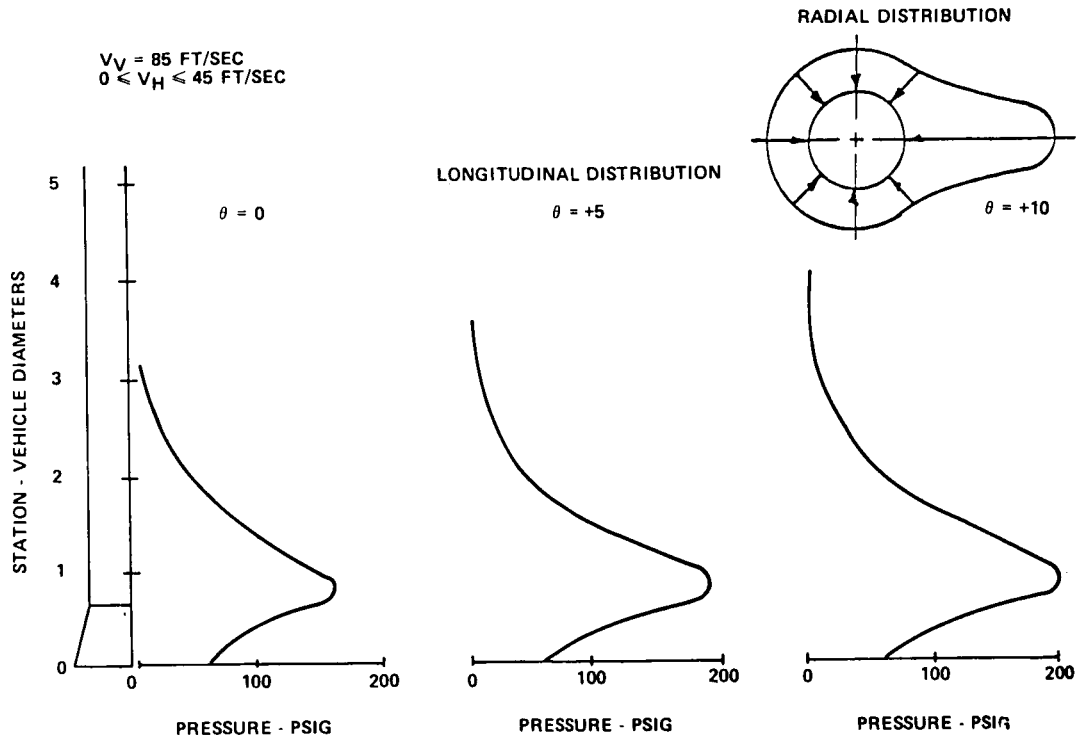


Figure 45. SRB aft skirt water impact loads.

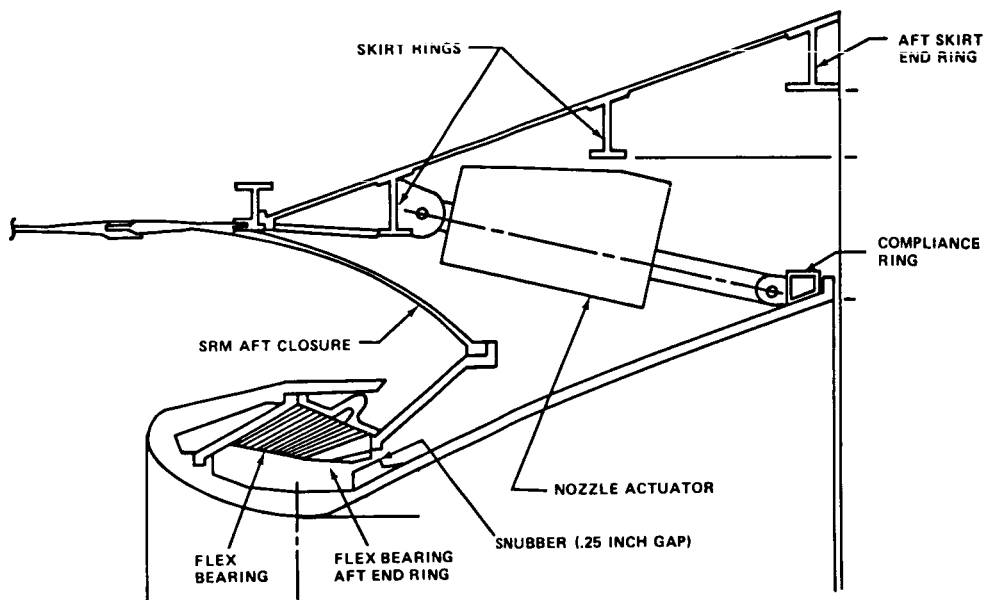
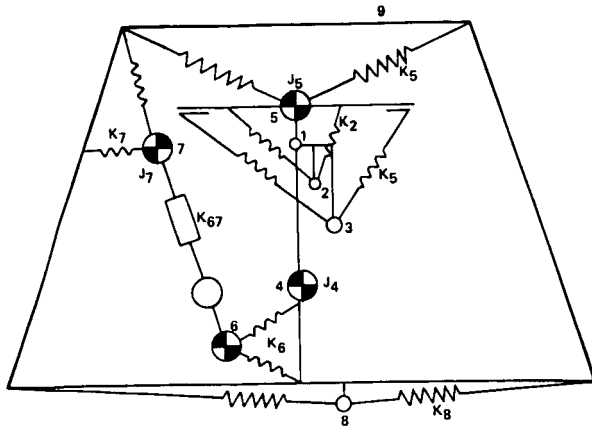


Figure 46. Nozzle configuration during water entry.



- NODES**
- 1 - NOZZLE REFERENCE
  - 2 - FLEX BEARING CENTER
  - 3 - SNUBBER CENTER
  - 4 - NOZZLE MASS CENTER
  - 5 - AFT CLOSURE
  - 6 - NOZZLE ACTUATOR CLEVIS
  - 7 - SKIRT ACTUATOR CLEVIS
  - 8 - HEAT SHIELD
  - 9 - SKIRT REFERENCE
- SIMULATION FEATURES**
- FULL 6 DIMENSIONAL MODEL
  - NONLINEAR FLEX BEARING
  - ACTUATOR BYPASS
  - SNUBBER IMPACT MODEL
  - FLEX BEARING HAS 4 RADIAL POINTS
  - HEAT SHIELD OMITTED FOR WATER IMPACT
  - MOTION DEPENDENT APPLIED LOADS
  - INERTIAL LOADS

Figure 47. Simulation description.

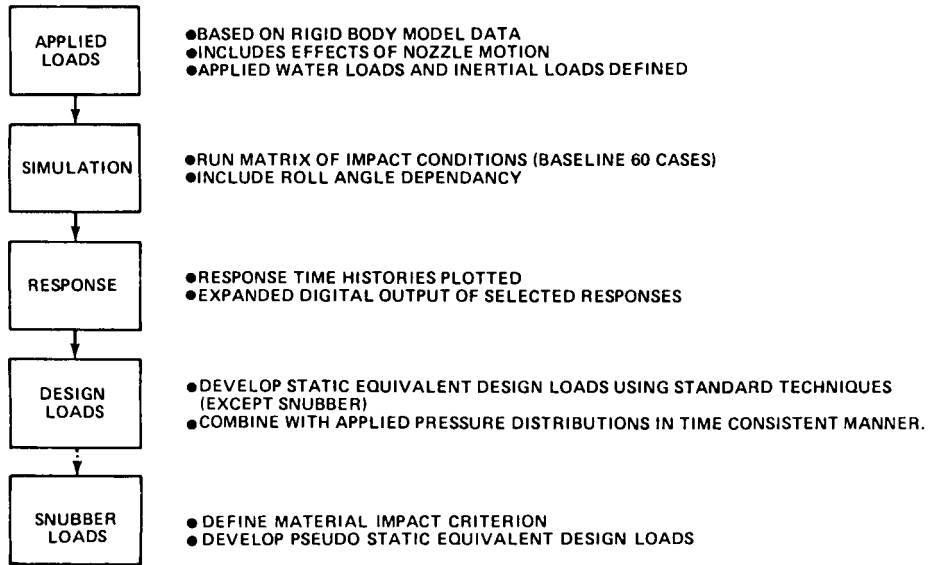


Figure 48. SRB nozzle water impact response loads status.

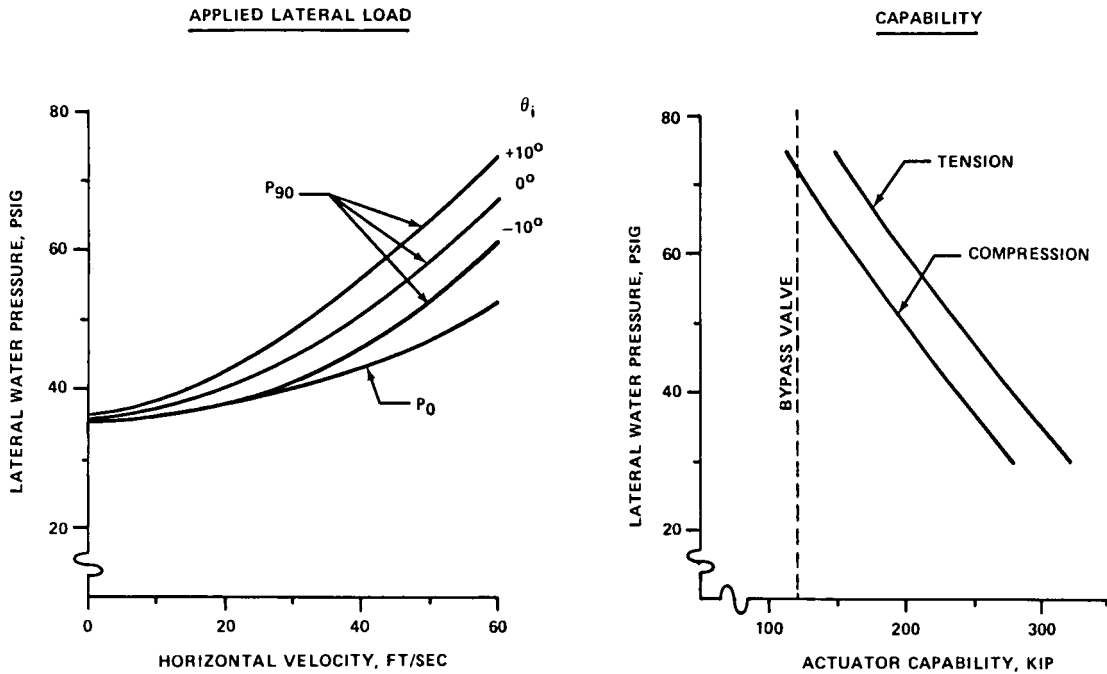


Figure 49. SRB actuator water impact characteristics.

A typical response (Fig. 50) shows the nonlinear characteristics present in the loads due to the actuator bypass valve releasing.

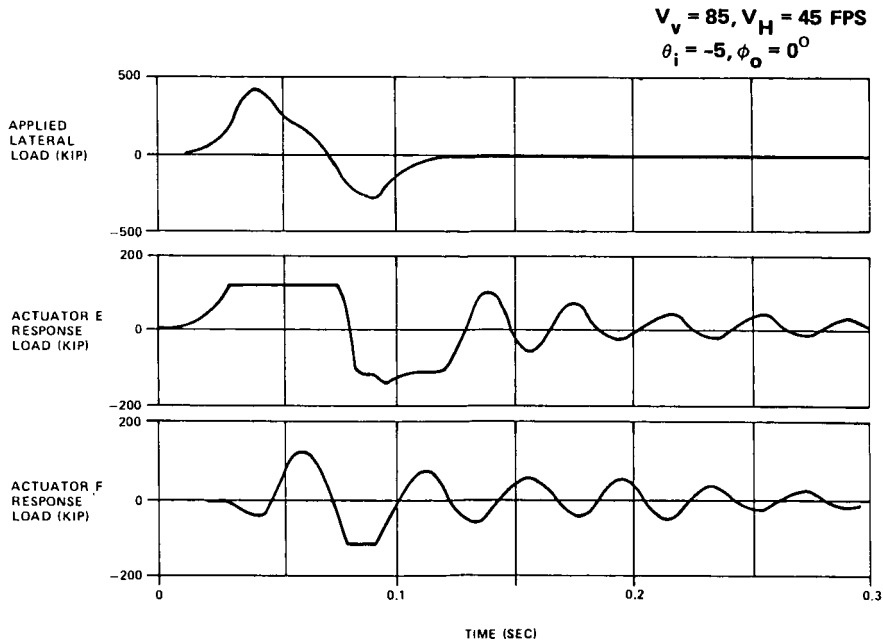


Figure 50. Typical actuator response.

Table 24 summarizes water impact loads for various elements and conditions versus vertical velocity.

TABLE 24. WATER IMPACT LOADS SUMMARY

DYNAMIC LOADING EVENT	IMPACT CONDITION ( $0 < V_H < 45$ FPS) ( $0 < \theta < 5^\circ$ )			
	$V_V = 80$ FPS	$V_V = 85$ FPS	$V_V = 90$ FPS	$V_V = 100$ FPS
I. INITIAL IMPACT				
A. MAX AXIAL ACCEL. (g's)	19	21	24	30
B. MAX NOZZLE APPLIED POSITIVE AXIAL LOAD (KIP)	700	780	860	1080
C. MAX NOZZLE APPLIED LATERAL LOAD (KIP)	540	600	640	750
D. MAX NOZZLE APPLIED BENDING MOMENT (IN LB X $10^6$ )	35	38	42	50
E. MAX BLKD PRESSURE (PSIG)	200	220	240	290
F. SKIRT INTERNAL EXIT PRESSURE (PSIG)	150	160	170	200
G. NOZZLE INT. PRESSURE (PSIG)	120	135	150	200
H. NOZZLE EXIT PRESSURE (PSIG)	140	150	160	190
II. MAX CAVITY COLLAPSE PRESSURE (PSIG)	190	198	218	260
III. MAX PENETRATION DEPTH (FT.)	57	58	59	61
IV. MAX SLAPDOWN PRESSURE (PSIG)	42	39	38	34

One final point is made. As a part of this work, it becomes necessary to work the hydroelastic modeling problem. Hydroelastic modeling is a very tough problem due to structural and fluid interaction. This effort was successful and predicted the results well. SRM water impact and parachute load work not only illustrates the requirement for system approaches, but also the need for determining loads empirically when adequate analytical tools are available, particularly for predicting complex environments. Loads engineers must be prepared to pursue the empirical course when it is dictated.

#### 4. Engine Fatigue Loads

The Shuttle Main Engine, due to lifetime requirements, has major loads design requirements, particularly in the fatigue area. These load predictions and verification are compounded by several factors: (1) very high thermal environments, (2) large static pressure loads or static loads due to centrifugal forces, (3) medium alternating loads due to fluctuating pressures and mechanically induced vibration. This means that the element is operating at or near its elastic limit due to thermal and pressure loads, thus making it very susceptible to alternating loads. Also, it is not easy to obtain the thermal and pressure environments since they are usually required in some rotating system, LOX system, or otherwise basically inaccessible. This means that one must depend on the hot firing development and verification as the means of verifying structural integrity.

Typical examples of engine elements with these critical loads areas are: (1) turbine blades, (2) valves, (3) LOX post (LOX feed posts in the injector head), (4) hydrogen coolant lines (steerhorns), (5) bearings, (6) bellows. The LOX post, the steerhorn, and turbine blades analysis are chosen as examples. Information for the others is available.

a. LOX Posts

The main injector head of the Shuttle Main Engine is composed of a hot gas manifold, primary and secondary face plates, LOX dome, and 560 LOX post or feed tubes between the LOX dome and the primary injector plate. The general layout is shown on the SSME powerhead assembly schematic, Figure 51. The pumps are included to show the source of the hot gas hydrogen that flows around the LOX post.

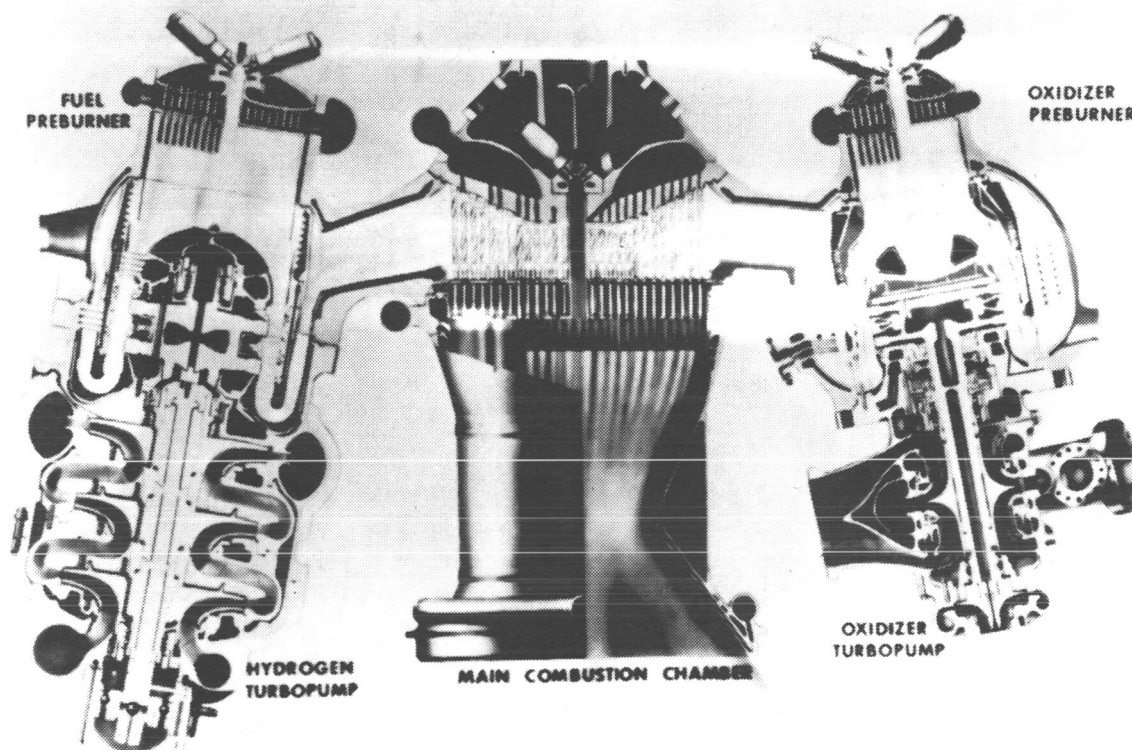


Figure 51. SSME powerhead assembly.

A typical top plane view (Fig. 52) shows the LOX post and the three transfer tubes from the hydrogen preburner and from the LOX preburner.

The flow of this high-velocity, very hot gas, impacting on the LOX post loads the post statically and dynamically. The gas then flows through the gap at the base of the post and around the tip of the injector plate where it mixes with the liquid oxygen. The liquid oxygen flows down the center of the post. This means that the thin-wall tube has a very large thermal gradient across its wall from cryogenic on the inside to 1800°R outside. Figure 53 depicts a LOX post with a two-post shield that was added as a design fix.

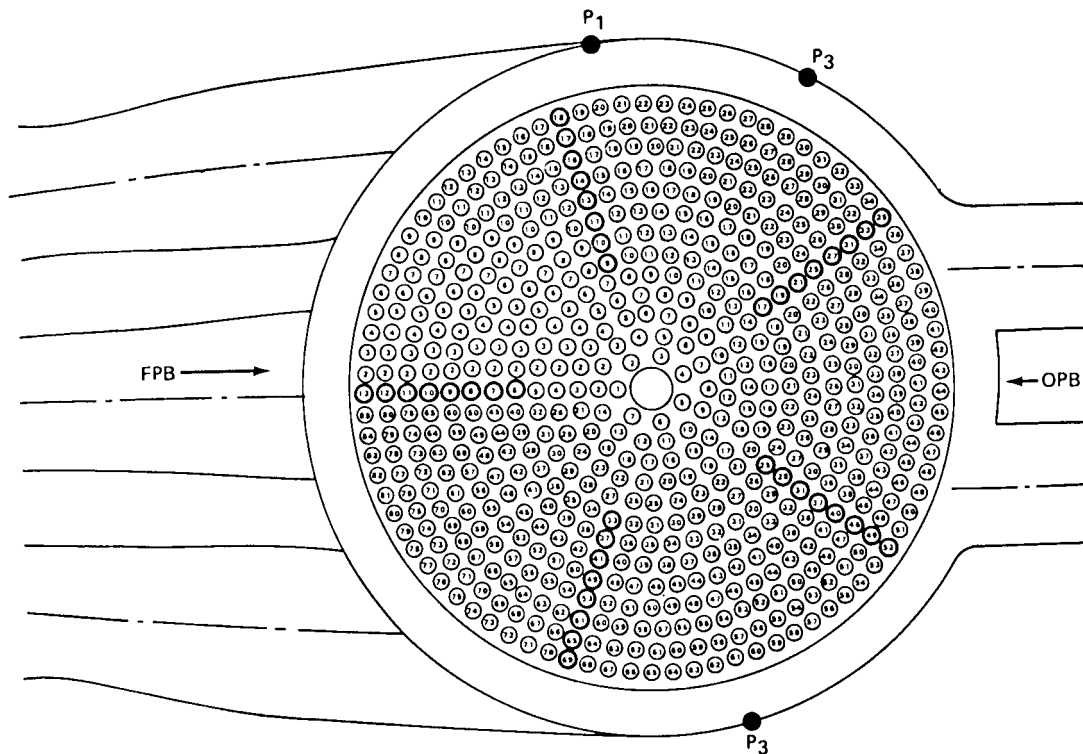


Figure 52. High-frequency pressure transducer locations in engine.

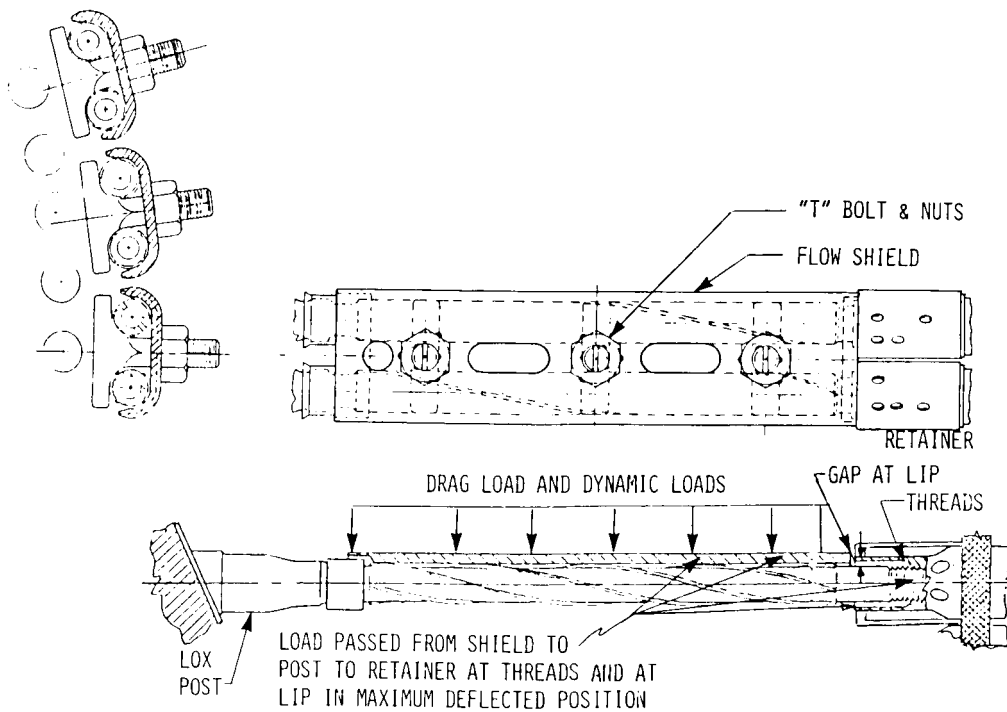


Figure 53. LOX post shield configuration.

This high flow environment, coupled with mechanical vibrations, large thermal environments, and variable dynamic characteristics, has led to a limited lifetime for LOX post and to two specific engine failures during demonstration firings.

This failure of the LOX post at the threads has been determined to result from high-cycle fatigue. The approach used to verify this failure hypothesis has been to calculate the stresses and lifetime of posts using known potential forcing functions and to compare the results with the observed failure characteristics and test results. The phenomenon occurring on the LOX post is one where the static loads arising from thermal gradients and internal flow induced pressures put the outer 3 or 4 rows of posts in tension. In addition, the steady-state flow puts a drag force on at least the first two outer row posts bending them and increasing the tension on the backside of the post. The greatest tension is in row 13 (see Figure 54). This makes the post more susceptible to high-cycle fatigue. Superimposed on the static loads is the oscillatory or alternating stress load. The potential sources for these alternating stresses are mechanical oscillations, vortex shedding, and fluctuating pressures (flow and acoustics). Figure 55 is a pictorial representation of these various forces and the direction of the alternating stresses. The first group is the static flow forces. The next line depicts the oscillatory forces. The first is classic vortex shedding, where the oscillation is  $90^\circ$  to the flow. Next is fluctuating pressures including flow and acoustics, which are omni-directional. The same is true for the mechanical vibration induced loads.

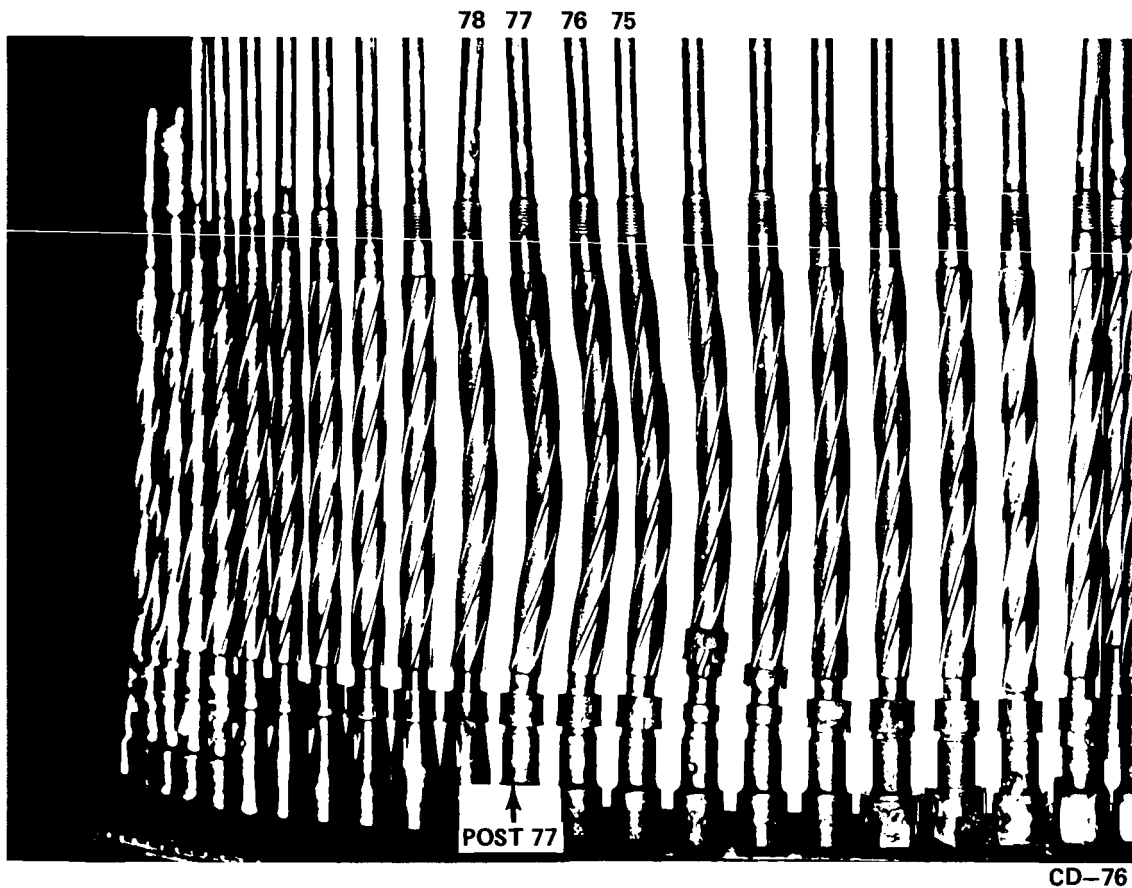


Figure 54. Maximum tension.

CD-76

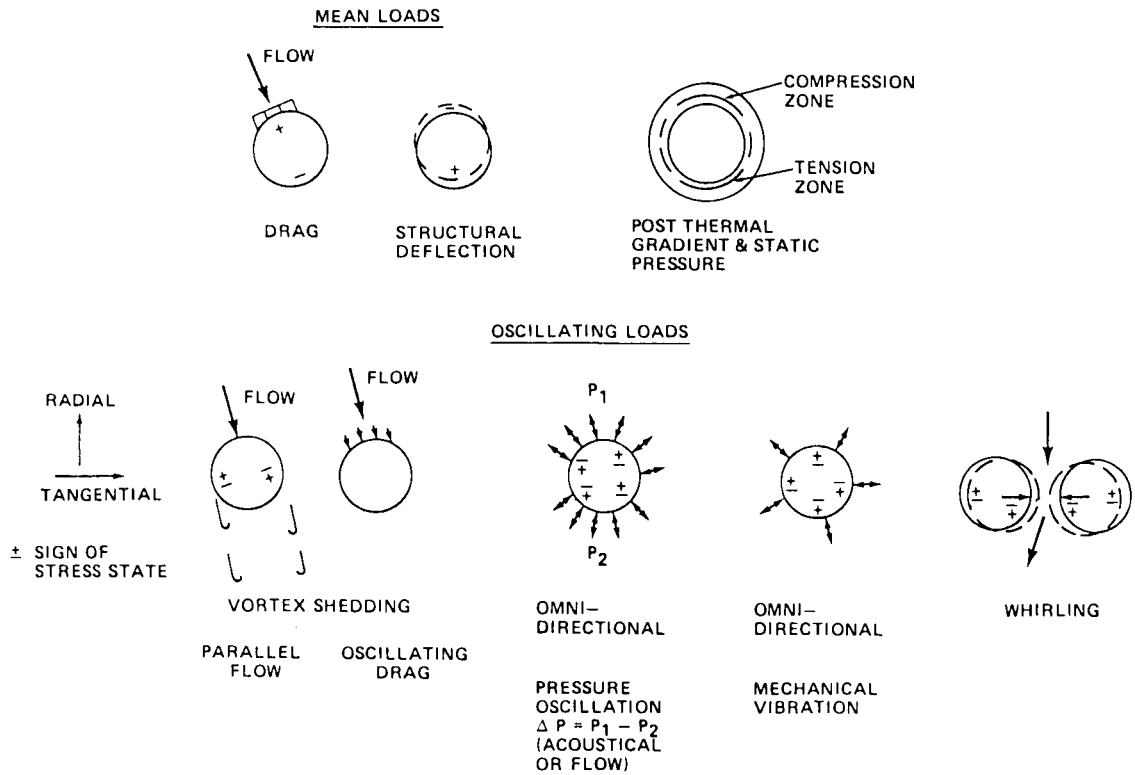


Figure 55. Force and loads characteristics on LOX posts.

Figure 56 shows the interactive flow of these potential forces. Notice that in case of vortex shedding and acoustics, there is a feedback between the force and structural dynamics as observed in the classical aeroelastic problems that can lead to unstable or increasing buildup in amplitudes.

The last sketch in Figure 55 depicts two posts oscillating towards each other due to pulsating flow between the posts. Based on known flow conditions and mechanical vibrations, all have the potential to exist in the engine. Two conditions are usually required for any one of the potentials to create a problem. First, the post must have dynamic characteristics (frequencies and high gain modes) in the frequency range of the forcing function and a forcing function amplitude and distribution level to create excessive fatigue loads.

In the first case, there are individual post modes and modes of the total injector plate LOX dome head in the range of the forcing function, 200 to 2,000 Hz. These modes have been shown both analytically and by test. There is a big uncertainty in these dynamic characteristics due to the varying boundary conditions of the post threads due to tolerances, thermal, and static forces. These have been demonstrated by both analysis and test and must be included as tolerances in all analyses. To help remove or decrease this uncertainty, a model has been developed that includes the static forces in the dynamic model which predicts these resulting boundary conditions. This has been a joint effort



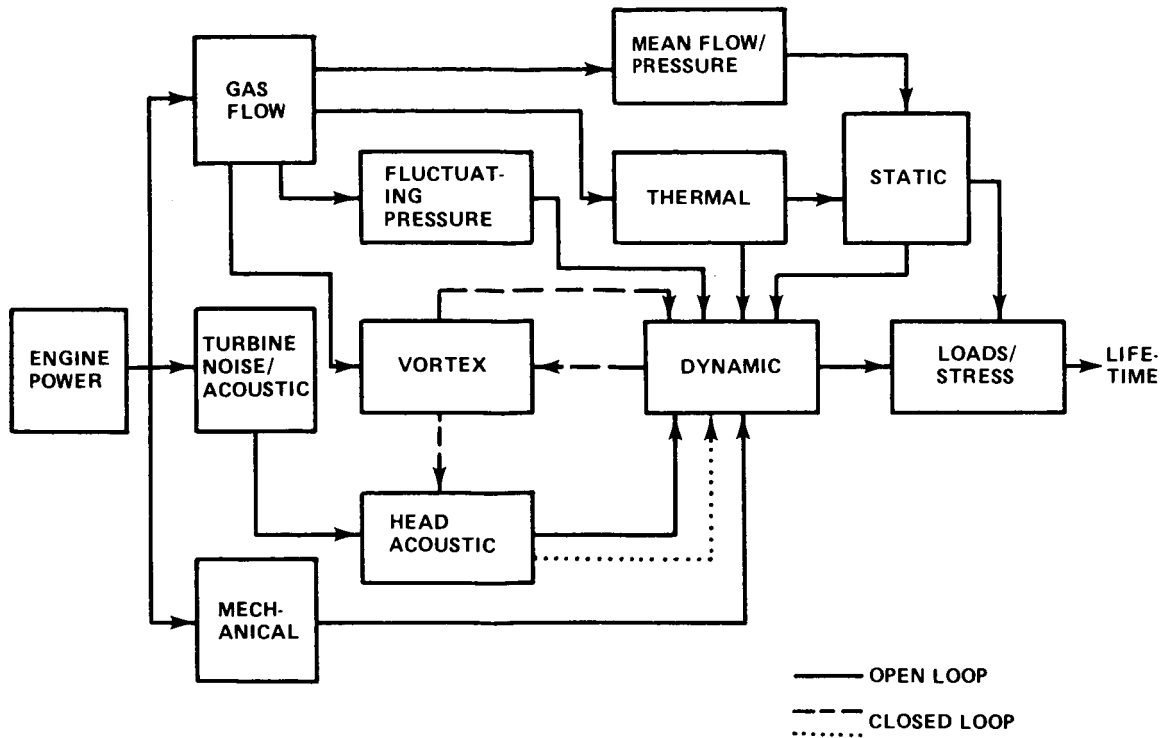


Figure 56. LOX post loads block diagram.

between stress and dynamics. Table 25 summarizes a study conducted using various boundary conditions and materials properties for mechanical random excitation and vortex shedding. Various conditions were assumed for the post threads and attachment nuts indicated as fixed, pinned, pinned-pinned, etc. Stress is shown for four positions and used to indicate stress levels.

Due to the complexity of the environment prediction, demonstrated life-time from single engine firings must be combined with analytical data to arrive at lifetime predictions. Figure 57 is a plot of the alternating stress capability versus number of cycles. This curve has taken into account the static stress loads and temperature effects. Two empirical data conditions have been assumed: (1) the failure time observed on one engine test of 750 seconds, and (2) the 5,000 seconds no-failure case demonstrated for shielded posts. The first block is the mechanically induced alternating stress level of the total head mode of 250 Hz for 750 seconds operation. Although significant stress levels occur, there is ample margin. The second bar is the alternating stress for single post mode (750 seconds) showing the combined stress induced by mechanical (cross hatched) and fluctuating pressure of 1 psi (assumed effective distribution). The uncertainty in the mechanical model is indicated. The analysis conducted would predict high cycle fatigue failure in the 750 seconds time using mechanical and fluctuating pressure forcing function ranges based on best estimates. The last bar is the two-post flow shield predicted alternating stresses for mechanically induced oscillations. Again, the model uncertainties are indicated. Since no failures have occurred on the shielded post, the potentially indicated failure has not occurred; however,

TABLE 25. STRESS x 10<sup>3</sup>

		STRESS (KSI)							
MODEL	EXCITATION LOADING	MODE	FREQ. (HZ)	σA	σB	σC	σD		
ELASTIC PIN PIN	PULSATING JET	1	1815	108	28	31	104	} IN RESONANCE	
		2	2956	4	8	8	17		
		3	5450	12	7	4	16		
	OSCILLATORY JET	1	1815	90	23	25	86		} IN RESONANCE
		2	2556	3	9	6	11		
		3	5450	3	2	1	3		
ELASTIC PIN PIN	ACOUSTICS #1	1	1815	300	78	85	290	} IN RESONANCE	
		2	2956	9	17	18	37		
		3	5450	5	3	2	7		
	SYSTEM			28	8	9	28		2,000 Hz
ELASTIC PIN	ACOUSTICS #2	1	726	61	95	104	330	} IN RESONANCE	
		2	1817	302	78	87	294		
		3	4455	8	13	13	25		
		4	5856	2	2	2	6		
	SYSTEM	-	---	28	7½	8	28		2,000 Hz
ELASTIC PIN PIN	ACOUSTICS #2	1	1815	32	8	9	31	} IN RESONANCE	
		2	2956	1	2	2	4		
		3	5450	2	1	6	2		
	SYSTEM	-	---	3	1	1	3		2,000 Hz
HEAD MODE	MECHANICAL	1	456	6	5	6	1	SPECTRUM	
			209	3.4	1.0	7.2	0		
	NEW THREAD			238	2.0	0.6	4.0		0

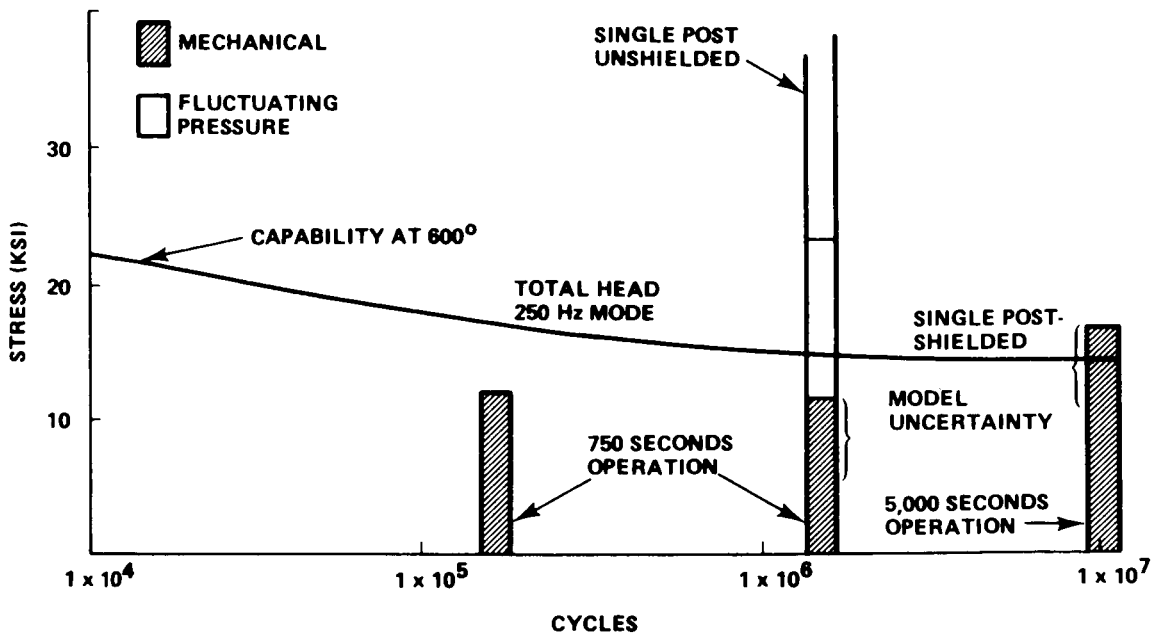


Figure 57. Alternating stress versus lifetime.

The inner row 12 which sits behind the shield post did fail after an equivalent lifetime at rated power level of 20,000 seconds. The conclusion is drawn that the shields solve the problem for first Shuttle flights at rated engine power level.

One point should be made. Since the lifetime curve is so flat, very small changes put the stresses under the endurance limit in a potential failure mode. This is a particular concern for any system with lifetime limits since small changes in system responses can drastically reduce life. This means that there must be a constant guard to ensure that system changes made for performance, etc., do not create loads problems.

b. Turbine Blade

The high-pressure fuel pump turbine blades loads and lifetime are another example of the same type problem discussed for the LOX post. Figure 58 shows a turbine blade. Arrows indicate where failures have occurred.

**HPFTP  
1st STAGE  
BLADE CRACKING**

AIRFOIL LEADING EDGE  
TRANSVERSE CRACKS

SHANK LEADING EDGE  
TRANSVERSE CRACKS

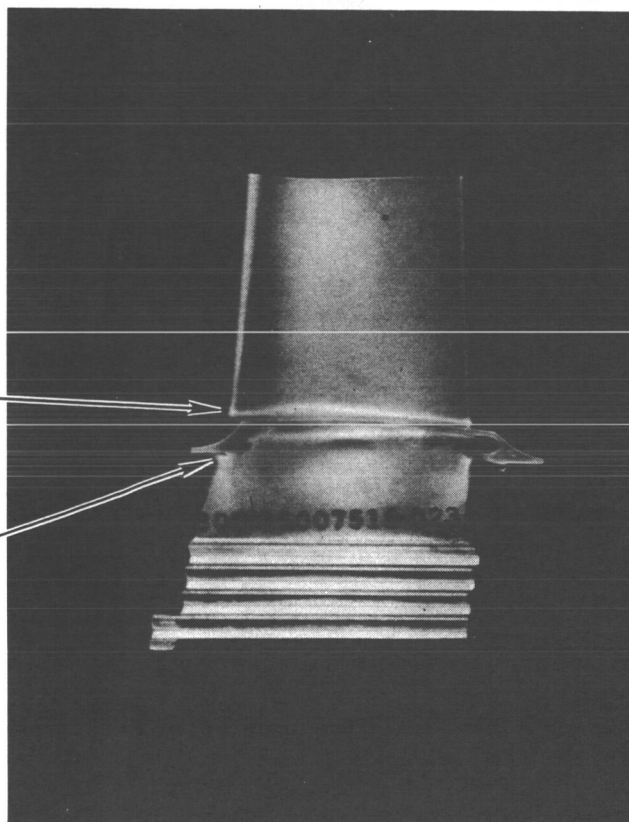


Figure 58. HPFTP 1st stage blade cracking.

The major problems in conducting this analysis are the environment definition, dynamic modeling, and static stress definition. The environment definition is complex

from both the thermal and fluctuating pressure standpoints. The blades are near the preburner and use the hot preburner gas as the source of its power (flow forces). These environments are not uniform due to baffle posts, struts, etc., and the blade geometry. Fluctuating pressures have the same problem plus the clear introduction of harmonics due to the struts and the multi-blade passages. These forces were obtained in a special air rig and whirlygig test. The dynamic model is complicated because of the basic geometry, hot surface, boundary conditions at the wheel, and special design dampers. Stress is composed of the static centrifugal force induced stress, the average thermal stress, the cyclic thermal stress, and the fluctuating pressure-induced stress.

The basic wheel blade strut configuration consists of 63 blades, 41 nozzles, and 13 struts upstream, each of which is in front of a nozzle cone. Significant factors in the alternating loads (stress) are (1) turning of strut wakes with blade lower modes, (2) multi-blade relative motion of adjacent blades, (3) dampers coefficients, lockup, (4) changes through engine operating range.

A detailed finite element model was generated of the blade. A typical model was typical stress values for one forcing function are shown on the side of the grid, Figure 59.

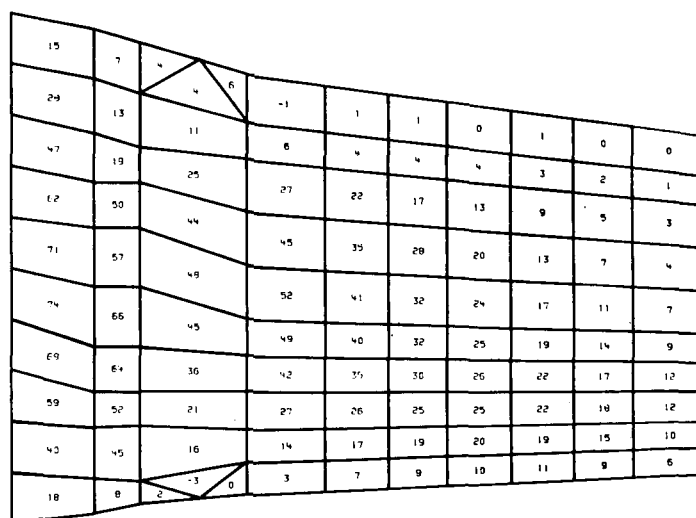


Figure 59. View of blade finite element grid with stress for a response case.

To accomplish the detailed alternating stress analysis required the detailed definition of the forcing function. Figure 60 depicts the stationary nozzle, the upstream strut, and the moving blades. Flow direction is indicated by arrows.

The resulting aerodynamic interaction can be clearly seen. The resulting aerodynamic forcing function acting on the blades is shown in Figure 61. Notice the harmonics and their corresponding relative amplitude shown at the bottom of the figure.

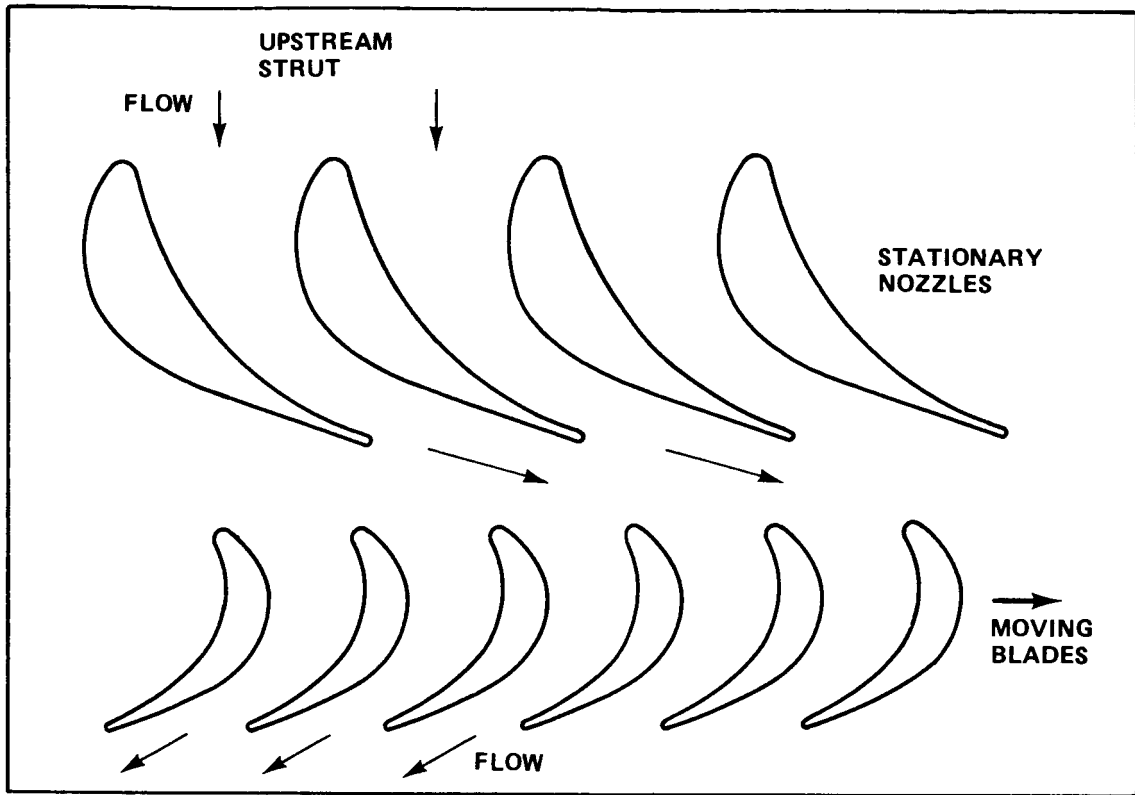


Figure 60. Aerodynamic interaction of strut/nozzle/blade configuration.

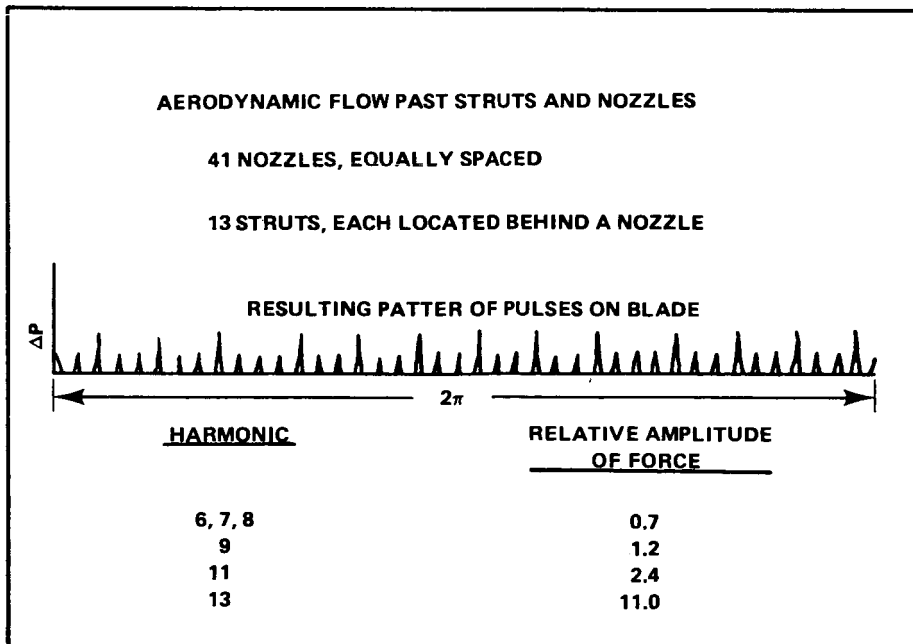


Figure 61. Aerodynamic flow past struts and nozzles.

Figure 62 shows the relative harmonic amplitude versus harmonic number  $n$ , where  $n$  is the shaft rotation frequency.

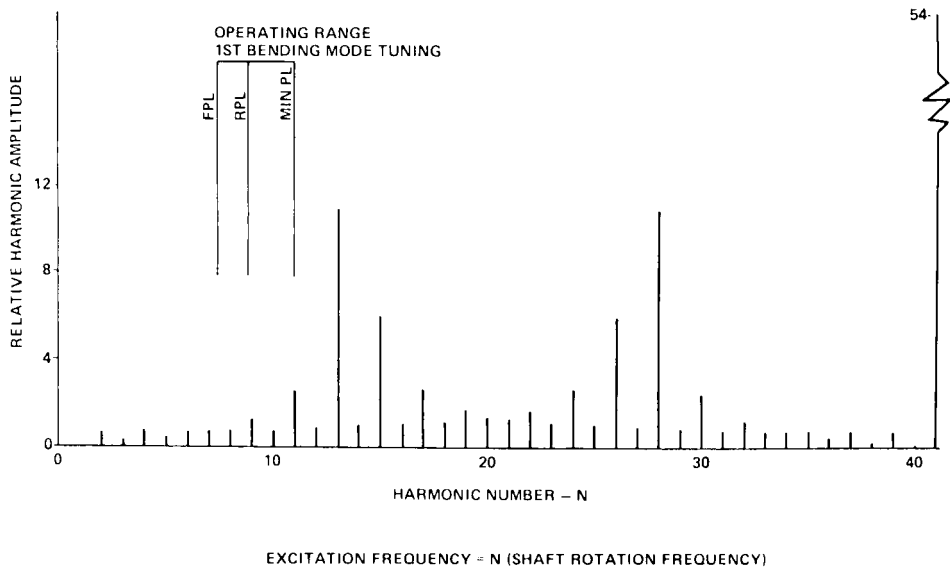


Figure 62. Harmonic amplitude vs. harmonic number.

Figure 63 gives the relative amplitude versus harmonic number for a 14-strut case, which was studied as an alternate.

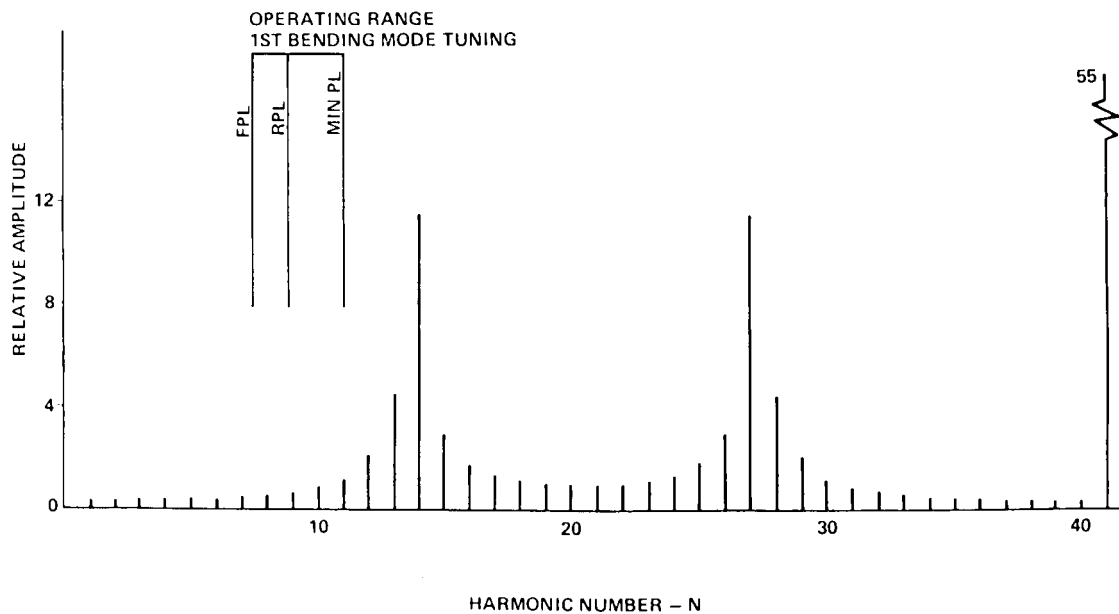


Figure 63. Relative amplitude vs. harmonic number, 14-strut case.

Changing numbers of struts greatly reduces the stress amplitudes through detuning. Changing the number of struts is a means, therefore, of reducing the alternating stresses.

Additional analysis was conducted to determine the effects of dampers on alternating stresses. There is a small decrease in alternating stress if dampers are used; however, if the dampers lock up, the alternating stress increases by a factor of five.

<u>Condition</u>	<u>Alternating Stress Blade Leading Edge (Ksi)</u>
No dampers	9.5
Operational dampers	9.1
Locked dampers	50

No stress concentrations were considered. Worst-on-worst model tuning was considered.

Combining steady-state stresses and plotting alternating stress against blade temperature shows the basic blade lifetime problem (Fig. 64). Plotted are three conditions or assumptions. Curve 1 is for rated engine power level (RPL) assuming 5,000 seconds of life. Curve 2 is full or maximum engine power level (FPL) and 5,000 seconds of life, while curve 3 is the same power level assuming 2,500 seconds of life. The mean stress for RPL is 46 Ksi, and for FPL, it is 55 Ksi. The blade operating temperature is in the 1,600 to 1,700 degree range showing the low allowable alternating stress. The message of this analysis is that accurate models and environments are mandatory requirement for loads generation when dealing with high-performance rotary dynamics machining.

One source of alternating stress is nearly impossible to quantify analytically, blade tip rubbing against the seal. Presently, the final loads verification of the blades must depend on hot engine firings. Work needs to be accomplished in this area.

#### c. Engine Side Loads, Nozzle and Steerhorn

The Shuttle Main Engine nozzle has three engine downcomer coolant lines that take hydrogen from the main fuel valve to the aft nozzle manifold. The aft nozzle manifold feeds the coolant tubes which in essence is the engine nozzle. Two of these coolant lines have failed during hot engine firings due to low cycle fatigue. Figure 65 gives the basic configuration, showing the downcomer line (steerhorn).

The loads on the line nozzle system arise due to firing of a high-expansion-ratio nozzle under ground atmospheric conditions. The plume does not fill the nozzle until the internal pressure is greater than atmospheric. Also, the nozzle plume flow velocity increase passes through a region where a Mach disc or cone exits the nozzle. Two distinct

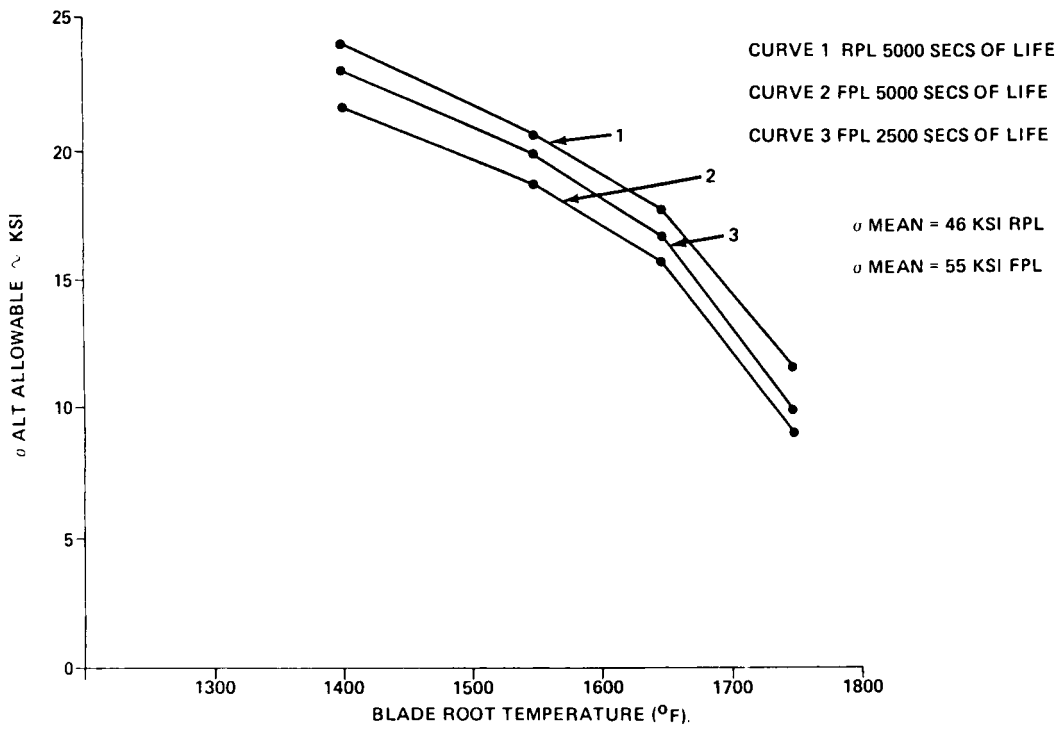


Figure 64. Alternating stress versus blade root temperature allowable.

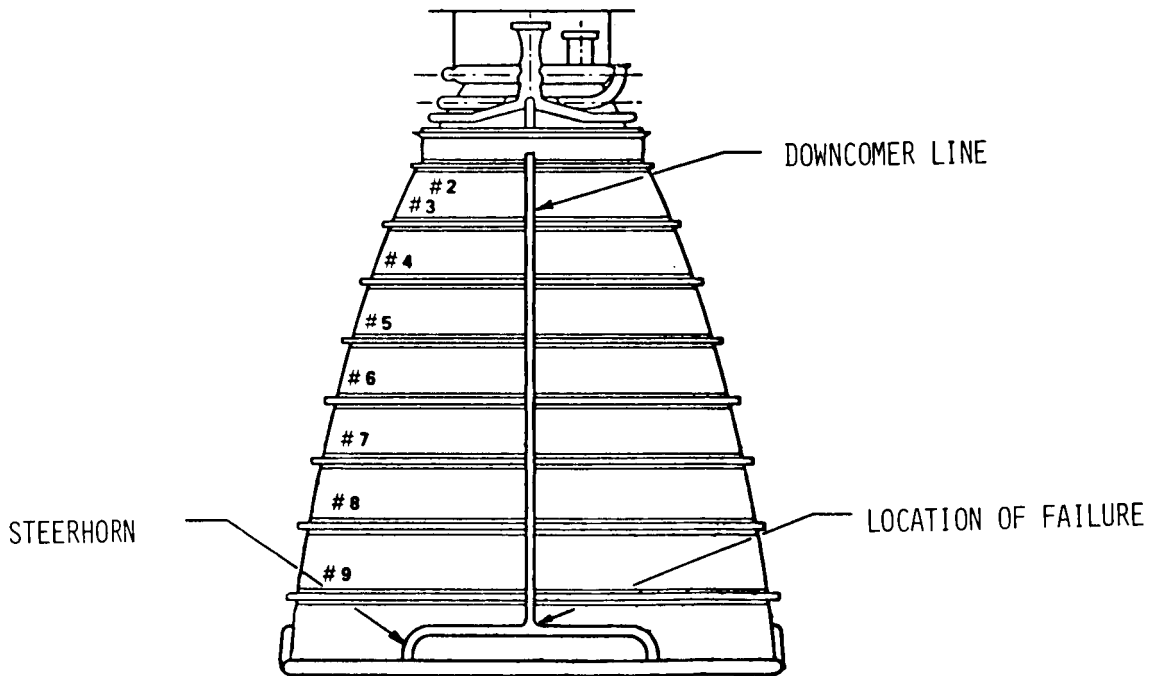


Figure 65. Description of nozzle system.



phenomena occur during this thrust buildup phase. The first occurs around 600 to 700 psia chamber pressure. In this case, the plume is basically cylindrical in nature and is directionally unstable, moving around radially within the nozzle. The loads induced by this case, in general, drive the actuator design. The second occurs around 1,200 psia where the Mach cone leaves or enters the nozzle, creating high local shock loads. Figure 66 shows a typical thrust buildup and shutdown curve and stress response measured on the nozzle steerhorn. The side loads response is clearly shown in this figure. The large strain amplitude occurs due to the excitation of the  $n = 0$  (expansion mode) and the  $n = 6$  shell mode. Notice that the response is very sharp and around 250 Hz. See the insert blow-up of the response.

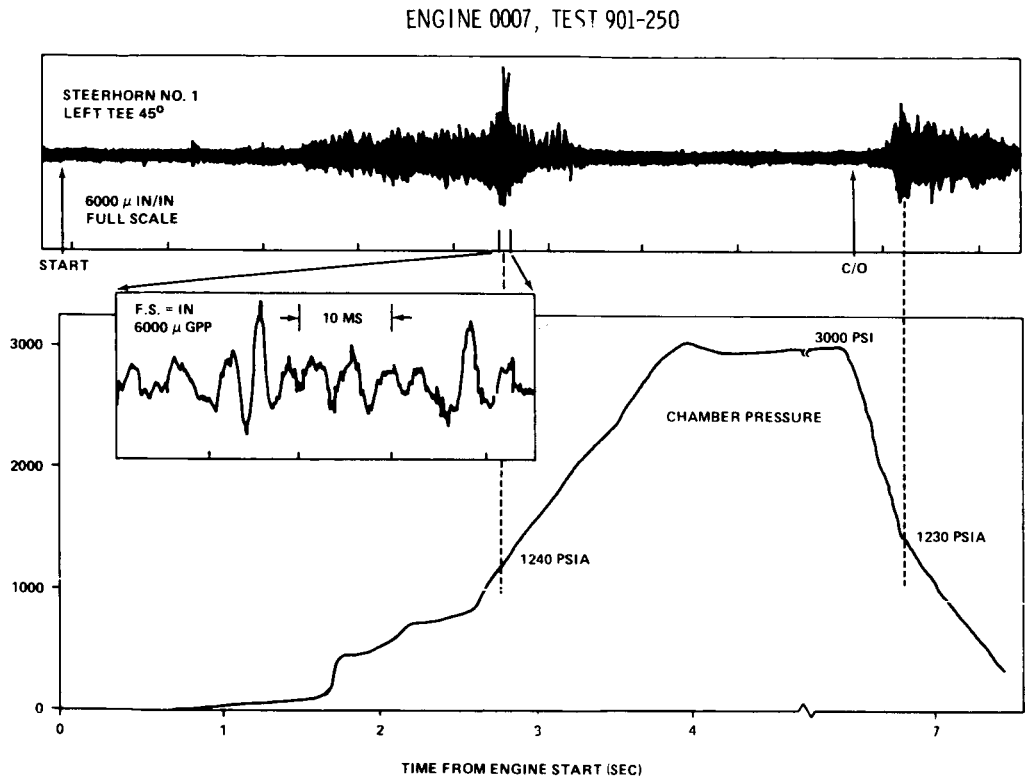


Figure 66. Steerhorn strains in transient operation.

Figure 67 depicts the  $n = 6$  shell mode on the right-hand side. The left-hand side of the figure shows the shell mode frequencies as a function of  $n$ -number. At the bottom of the figure is a spectrum of the measured acceleration of the engine nozzle aft manifold showing presence of all  $n$  modes but by far the larger peak occurring for the  $n = 0$  and  $n = 6$  modes.

The presence of this large load at the discrete frequency of 250 Hz, which the steerhorn was designed for, created many engine design and program problems, particularly the development firing program. Two things had to be accomplished: (1) fix the under-designed steerhorn so that firings could continue and (2) redesign the steerhorn for operational flights. Since initially an internal nozzle pressure forcing function was not available,

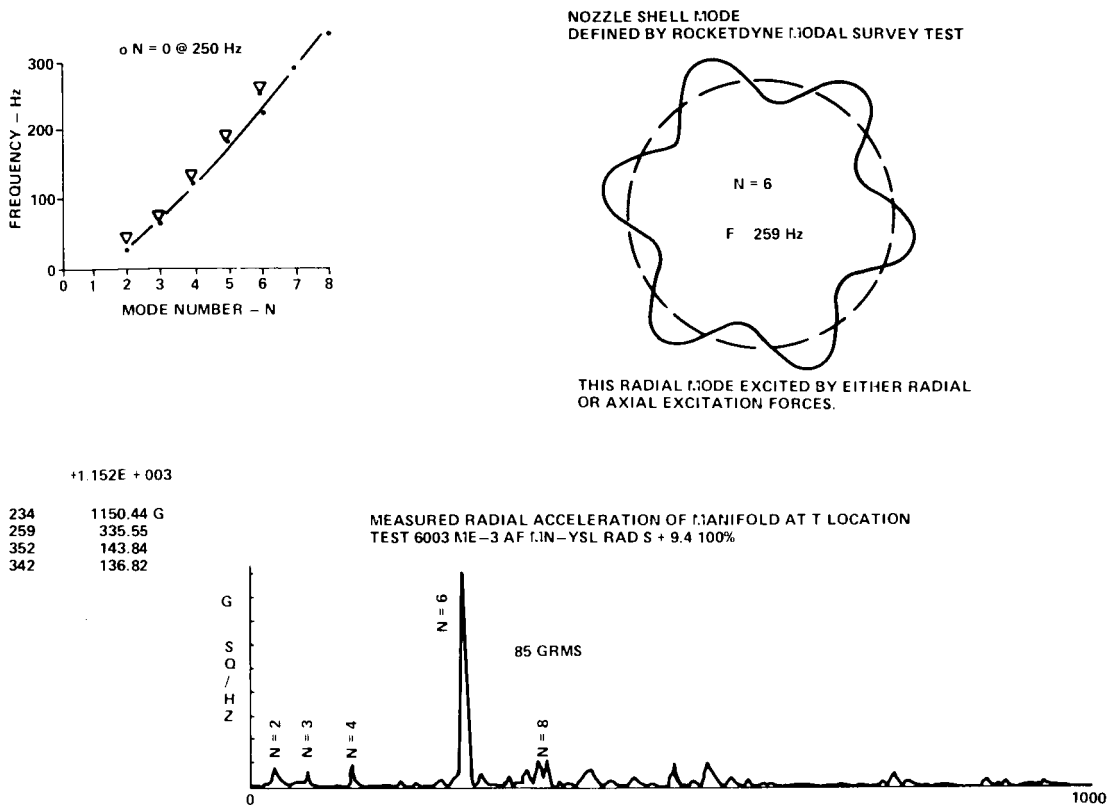


Figure 67. Nozzle shell mode defined by Rocketdyne modal survey test.

it was decided to take the hot-firing measured accelerations at the aft manifold and use these to base drive a dynamic model of the steerhorn. This is acceptable since the steerhorn mass and stiffness are very small compared to those of the nozzle, hence would not change the nozzle aft manifold response. The first major result that is obvious is that just thickening the tube does not help the problem. The increased mass offsets the increased stiffness so the frequency stays the same. The nozzle-induced driving force is not changed, hence the increased mass increases the steerhorn loads proportional to the mass increase. Using this approach, a sensitivity and redesign matrix was pursued.

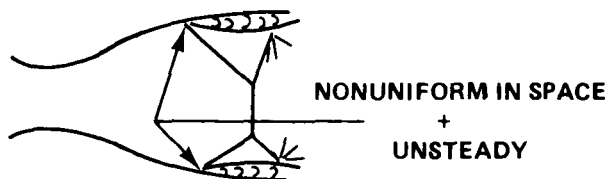
The main results were that the horizontal run of the steerhorn must be fixed to the nozzle stiffness ring to reduce loads. This means that a steam loop had to be incorporated above the hatband to take out thermal induced expansion loads. The other main result was that the T area could be nickel plated and get adequate life for developmental engine firings and first Shuttle flights.

In addition to detailed analytical modeling of steerhorn and engine nozzle, two test programs were reinstated to finalize these loads: (1) scale model engine cold flow test, and (2) full-scale flight nozzle dynamic tests. The cold-flow model test varied the flow rate, etc., to determine the forcing function. A full set of pressure gauges were mounted so that the force distribution could be determined. Figure 68 is the test configuration including pressure measurements.

**PHENOMENON:** SHOCK WAVE OSCILLATIONS ASSOCIATED WITH TEEPEES/  
MACH DISC

**ANALYSIS**  
+  
**OBSERVATIONS:** MOVIES INDICATE THAT THE SEPARATED FLOW TEEPEES ARE  
ABOVE THE SECOND RING FRAME AT FAILURE TIME WITH  
THE TEEPEES GROWING AND CHANGING SPATIALLY  
CONSERVATIVE ESTIMATE OF ENVIRONMENT SHOWED POTENTIAL.

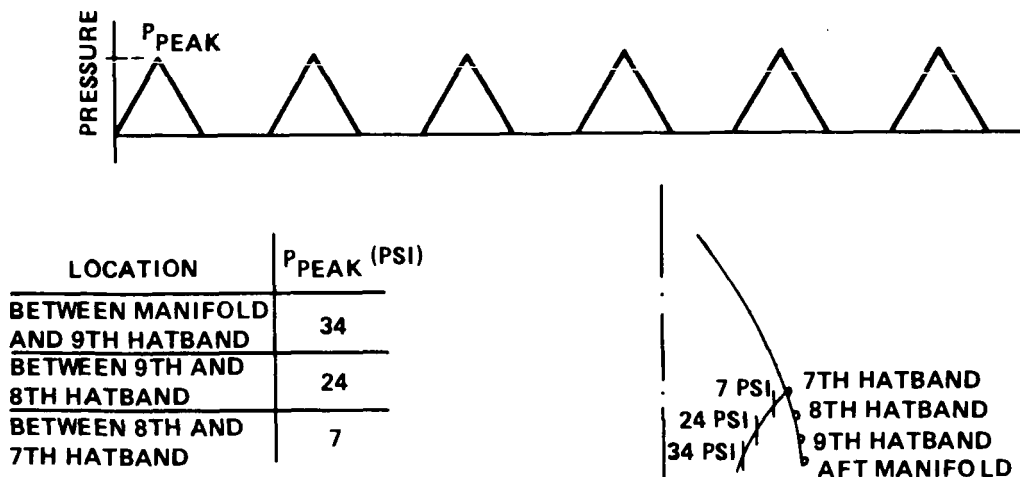
**MECHANISM:**



- TESTS:**
1. INSTRUMENT SSME HOT FIRING CONFIGURATION TO OBTAIN: AMPLITUDE, FREQUENCY, SPATIAL DIST., SENSITIVE PARAMETERS.
  2. CONDUCT MODEL TESTS TO OBTAIN: SENSITIVE PARAMETERS, AERO FIX, LOAD DEFINITION, ETC'

Figure 68. Test configuration.

The results scaled to full scale are shown in Figure 68 and Figure 69. Figure 68 gives a description of basic phenomena and Figure 69 the results.



PRESSURE DISTRIBUTION IS UNIFORM CIRCUMFERENTIALLY

Figure 69. Nozzle model pressure pulses.

Taking these test-derived forcing functions, a dynamic response analysis was run for both the original design and the redesigned steerhorn configurations (steam loop). Good agreement with hot-firing data was obtained. Table 26 shows these results for the

TABLE 26. COMPARISONS OF STEERHORN PEAK STRESSES

CONFIGURATIONS	PEAK STRESS DUE TO 6-150 HZ PRESSURE PULSES (KSI)			PEAK STRESS DUE TO 902-162 INPUT ADJUSTED BY STATISTICS (KSI)		
	TEE	MANIFOLD	BRACKET	TEE	MANIFOLD	BRACKET
080 BASELINE ON NOZZLE	172	114		180	168	
049 ON NOZZLE	201	151		200	185	
REDESIGN ON NOZZLE	32	62	104	130	115	104

original 0.049-inch-thickness nozzle steerhorn, the 0.080-inch-first-flight nozzle steerhorn, and the redesigned nozzle steerhorn. The reduction in loads is approximately 40 percent for the redesigned case. Table 27 is a summary of stresses measured in hot-firing data for the nonsteam loop configuration. Comparing the 3-sigma stress measured to the calculated stress using the scale model derived 3-sigma forcing functions shows the excellent agreement alluded to earlier. Shown on this chart is a column of the effects of hot-firing statistics.

TABLE 27. HOT-FIRING DATA SUMMARY

DATA BASE	STRAIN AT T LOG DISTRIBUTION*				
	STAND	START		CUTOFF	
		MEAN	3 $\sigma$	MEAN	3 $\sigma$
A1 (14 TESTS)	3,262	10,537	5,033	15,642	
A2 (20 TESTS)	3,876	16,503	1,636	6,529	
MPT (3 TESTS, 7 ENGINES)	6,270	20,685	4,916	12,088	
MPT & A1	4,064	18,469	4,983	13,552	
COMBINED ALL STANDS (41 TESTS)	3,954	17,084	2,722	21,528	
COMBINED ALL STANDS ALL MEASUREMENTS ALL EVENTS 41 TESTS		19,053			

\*CONTAINS NO EXTRAPOLATED DATA.

Steerhorn and nozzle response data have been measured on more than 50 hot firings. Table 28 summarizes these data. These data are shown for the three single-engine test firing stands and for the three engine cluster firings (MPT). Test stand A-2 has a simulation altitude (reduced pressure) showing different characteristics from the other stands. The dynamic model used in this analysis was verified in a full-scale dynamic test. Analytical modes had good agreement with test modes. Based on this analytical work and the statistics of the hot-firing data allows for a lifetime prediction of the development firing program using any given configuration. These are in terms of number of engine firings.

TABLE 28. STEERHORN LIFETIME

<u>CONFIGURATION</u>	<u>NUMBER OF FIRINGS</u>
049	55
080	102
Redesign (steam loop)	1,100

#### 4. Conclusions

Three examples have been given for loads analysis that cut across both ultimate loads and fatigue. Much of the Shuttle hardware must meet both requirements. For example, the SRB's are to be recovered and reused, thus fatigue data were generated for the SRB. It turned out that the ultimate load was the design driver, which is the opposite from the examples used here. In any case, the loads engineer must be aware of both requirements and be able to handle both sets of analysis.

## SECTION II. PAYLOAD LOADS

### A. Space Telescope

The Space Telescope is a very complex dynamic system designed to survive launch, 5 years stay time in orbit, and then Shuttle landing. After refurbishing, the sequence is repeated. The structure shape, etc., is derived by the optical considerations during operations, while the design loads are generally launch derived. The complex system is shown in Figure 70, an exploded view for the operational configuration.

The solar arrays would not be deployed during the launch configuration. As can be seen from the figure, the telescope consists of the outer shell (Support System Module (SSM)) and the inter scope (Optical Telescope Assembly (OTA)) containing the mirrors and scientific instruments. The OTA pivots within the SSM to get the high pointing accuracy required during operations. This multi-body systems cradles in another multi-body system for launch, then gives rise to dynamic coupling and loads problems. In addition, there is a

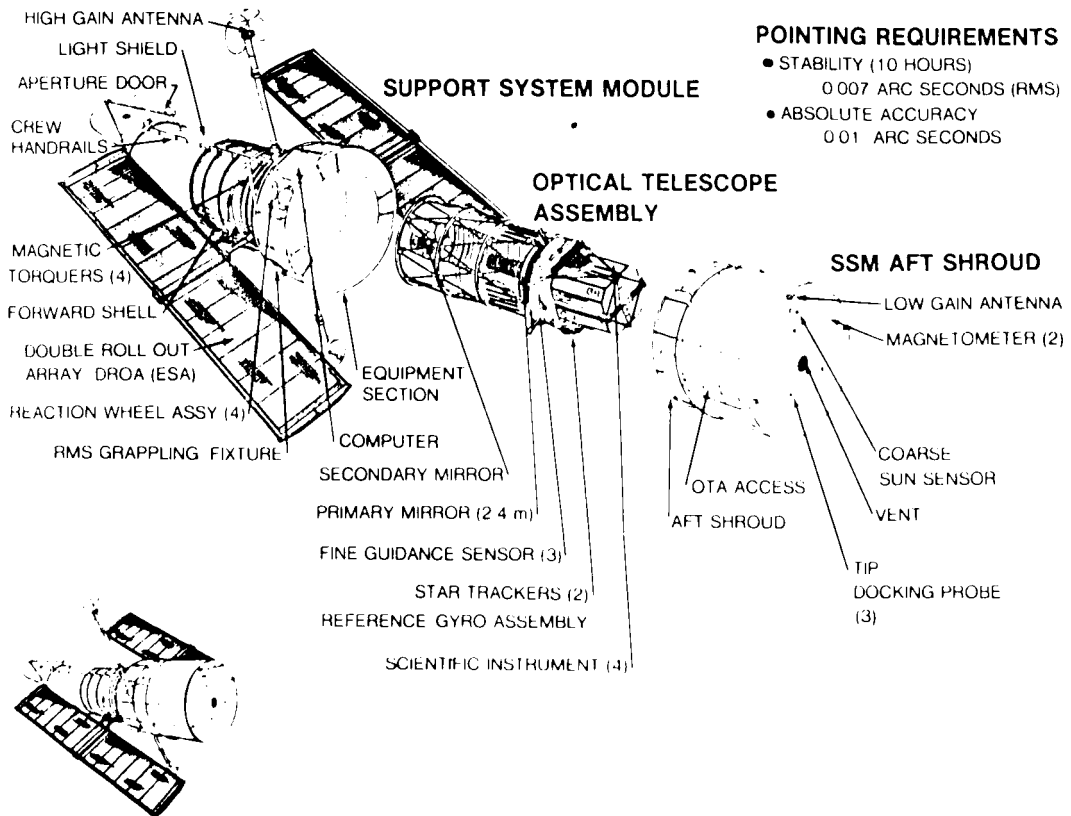


Figure 70. Space telescope.

17 Hz minimum frequency constraint placed on the OTA to detune the structure from the control systems during operations. In the launch and landing configurations, this constraint leads to a 12-Hz payload-systems mode which tunes somewhat with the Shuttle system forcing functions.

Criteria for Space Telescope loads fall into two categories: (1) Shuttle systems, and (2) Space Telescope peculiar. Shuttle systems criteria are the same as shown earlier under Shuttle systems loads. The Rockwell Shuttle Payload Integration and Development Project Office (SPIDPO) at JSC provided to the Space Telescope project the external forcing functions, derived as discussed previously, for both liftoff and landing. Since the landing criteria were not discussed in the Shuttle system, some general discussion is warranted here. The Orbiter landing loads forcing function is based upon air worthiness standards for transport category airplanes, FAA regulation 25. These criteria state that the sink speed,  $V_s$ , is:

$$V_s = 10 \text{ fps, limit sink speed at the design landing weight.}$$

$$V_s = 6 \text{ fps, limit sink speed at the design takeoff weight.}$$

Transforming these criteria to the Orbiter for returnable payloads (payload weight, 32,000 pounds) gives:

$$V_s = 9.6 \text{ fps with no cross wind.}$$

$$V_s = 6.0 \text{ fps with 20-knot cross wind.}$$

Orbiter sink speed for nonreturnable payloads (payload weights, 32,000 pounds) (abort condition) is:

$$V_s = 6.0 \text{ fps.}$$

The Space Telescope design criteria are in two general areas: (1) external load and (2) safety factors. The Space Shuttle project made the decision early to use a no structural test program and a factor of 3 on an ultimate loads with a 1.4 on yield. External loads during the early design phase were to be of a max/min variety instead of time consistent. Also, it was decided to use an uncertainty factor on the external loads to cover changes in the Shuttle system forcing functions and the Space Telescope dynamic model. This factor varies from 1.4 to 2.8 depending on the load station or hardware. Additional conservatism was introduced into the loads through the use of max/min loads instead of time-consistent loads.

Much of the critical Space Telescope design loads are strongly influenced, if not determined, by the acoustic-driven responses, particularly during the liftoff event. These loads are derived using the 97.5 percent envelop of payload bay acoustic criteria zoned to the appropriate component or element criteria and structural response at each element. The element response in g's is then calculated using Miles formula or more detailed models and harmonic analysis techniques. These peak loads are added directly to the low frequency loads. Figures 71 and 72 are examples of the loads for the primary and secondary mirrors for two landing conditions and liftoff. Two different loads analyses are shown side by side. The second loads analysis does not have the uncertainty factors applied although the first does. Notice that for the liftoff loads, a high percentage of the loads are due to acoustic-induced loads.

As stated previously, MSFC has conducted independent loads analysis for the Space Telescope. One analysis used the Rockwell-derived forcing functions applied to the free-free Shuttle model including the ST.

The analysis flow diagram is depicted in Figure 73. As indicated by this figure, the in-house analysis constitutes a completely independent verification except for the SSM and OTA models which are provided by their respective contractors. The pertinent coordinate systems are shown in Figure 74. The description of the interface forces calculated in the analysis is shown in Figure 75. The maximum and minimum values of accelerations and interface loads for some elements are provided in Tables 29 and 30.

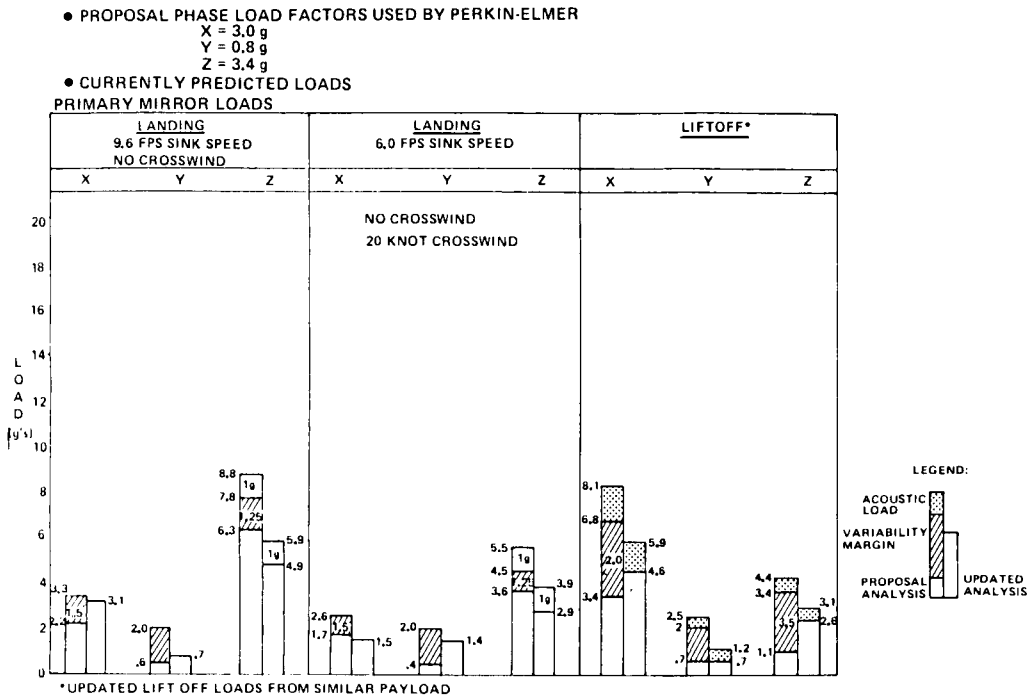


Figure 71. Primary mirror loads.

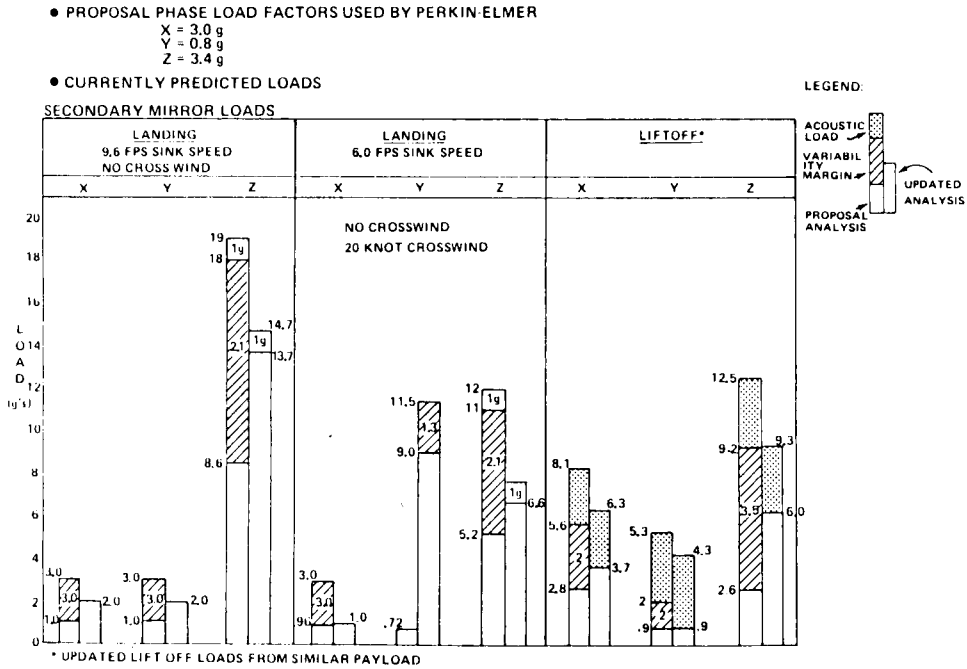


Figure 72. Secondary mirror loads.



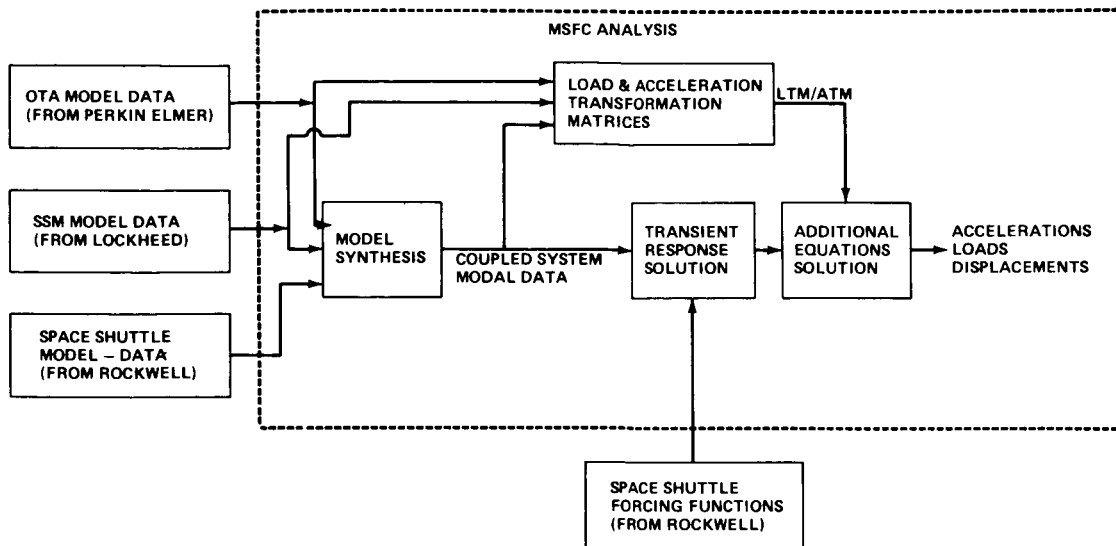


Figure 73. Analysis flow diagram.

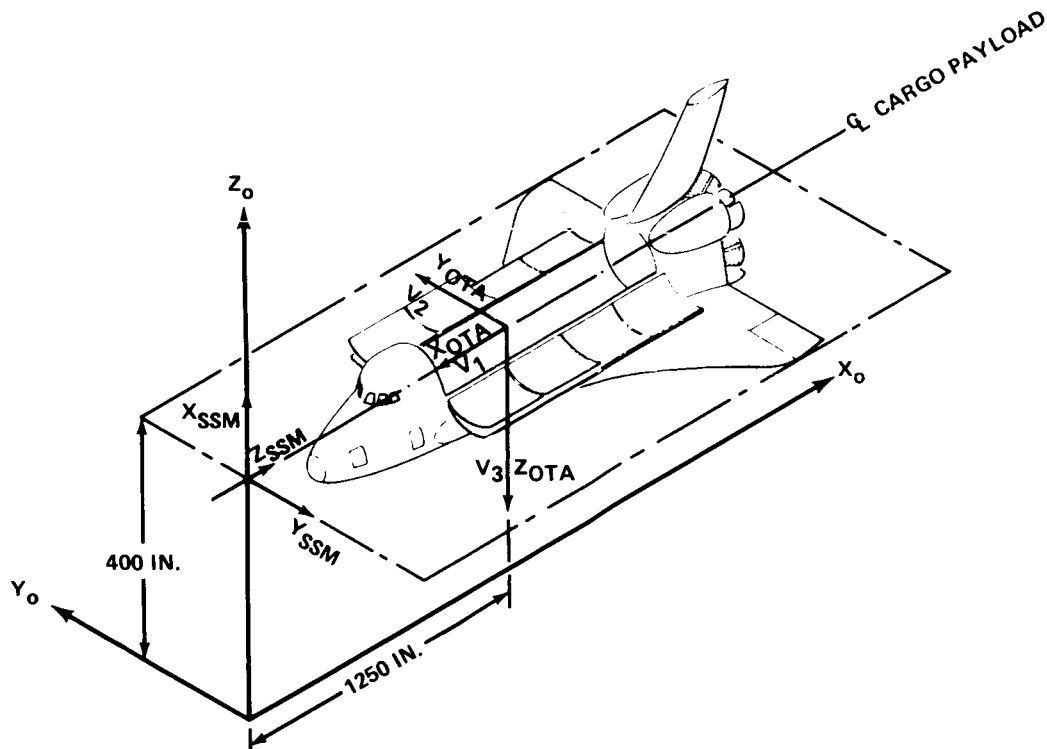
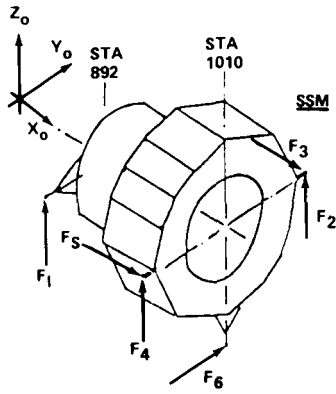


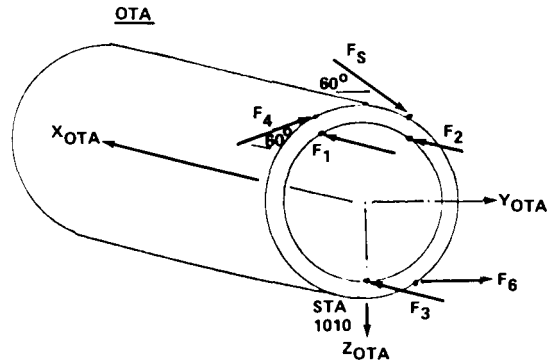
Figure 74. Space telescope coordinate systems.

**SSM/ORBITER INTERFACE FORCES**



FORCE	ORBITER DIR.
F <sub>1</sub>	Z
F <sub>2</sub>	Z
F <sub>3</sub>	X
F <sub>4</sub>	Z
F <sub>5</sub>	X
F <sub>6</sub>	Y

**OTA/SSM INTERFACE FORCES**



FORCE	OTA DIR.
F <sub>1</sub>	X
F <sub>2</sub>	X
F <sub>3</sub>	X
F <sub>4</sub>	C
F <sub>5</sub>	C
F <sub>6</sub>	Y

C = CIRCUMFERENTIAL @ 60°

Figure 75. Interface forces.

TABLE 29. COMPARISON OF RESULTS MAXIMUM AND MINIMUM ACCELERATIONS (GEES) IN THE OTA LIFT OFF FORCING FUNCTION CASE LP604

Item	Joint(s)	OTA DIR	Maximum Value	Minimum Value
Primary Mirror CG.	3201	X	1.55	-1.78
		Y	0.41	-0.46
		Z	2.15	-5.02
Secondary Mirror CG.	1500	X	1.47	-1.71
		Y	2.26	-2.16
		Z	12.75	-13.90
Focal Plane (Average of 4 pts.)	3619 3172	X	1.62	-1.88
		Y	0.40	-0.47
Forward End of Main Baffle (Average of 16 pts.)	2601 2613	X	1.48	-1.70
		Y	1.43	-1.49
		Z	8.32	-9.52
Axial S.L. Latch	3110	X	1.64	-1.94
		Y	0.29	-0.23
		Z	4.26	-4.35
WIPC CG.	3188	X	2.95	-3.84
		Y	0.34	-0.32
		Z	1.63	-5.40
Axial S.L. CG.	3181	X	1.67	-1.88
		Y	0.29	-0.31
		Z	2.53	-4.24
Fine Guidance Sensor CG	3185	X	1.65	-1.79
		Y	0.53	-0.60
		Z	1.40	-4.95
SSM OTA Interface	5103 5102 5101 5213 5212 5211	X	1.83	1.82
		X	1.82	-1.92
		X	2.74	-2.54
		C	3.91	-1.35
		C	1.40	-4.10
		Y	0.52	0.56

TABLE 30. COMPARISON OF RESULTS MAXIMUM AND MINIMUM ACCELERATIONS (GEES) IN THE OTA LANDING FORCING FUNCTION CASE LM35128 (SYMMETRICAL LANDING VS = 9.6 FPS)

Item	Joint(s)	OTA DIR	Maximum Value	Minimum Value
Primary Mirror CG.	3201	X	3.46	-0.68
		Y	1.12	-1.09
		Z	1.87	-1.57
Secondary Mirror CG.	1500	X	3.43	-0.64
		Y	2.07	-1.79
		Z	2.60	-2.98
Focal Plane (Average of 4 pts.)	3619 3172	X	3.49	-0.72
		Y	1.06	-1.32
Forward End of Main Baffle (Average of 16 pts.)	2601 2616	X	3.42	-0.63
		Y	1.92	-1.52
		Z	2.31	-2.52
Axial S.L. Latch	3110	X	3.50	-0.73
		Y	1.06	-1.51
		Z	3.48	-3.46
WIPC CG.	3188	X	3.87	-0.92
		Y	1.44	-1.58
		Z	2.45	-2.15
Axial S.L. CG.	3181	X	3.48	-0.76
		Y	1.06	-1.45
		Z	3.02	-2.65
Fine Guidance Sensor CG	3185	X	3.49	-0.91
		Y	1.07	-1.38
		Z	2.41	-2.12
SSM OTA Interface	5103 5102 5101 5213 5212 5211	X	3.46	-0.75
		X	3.43	-0.67
		X	3.74	-0.43
		C	1.63	-1.86
		C	2.08	-1.69
		Y	0.88	-0.98

Liftoff is currently the primary design driver for most ST structure.

The second study conducted by MSFC, briefly discussed under Shuttle Liftoff loads, dealt with whether it was adequate to approximate the liftoff model using one SRB MLP attach point or whether models of the four actual attach points per SRB were required. The model of the individual footpads assumed that the lateral force goes to zero (no constraint) where there is zero longitudinal force (acceleration minus gravity equal zero). This allows each footpad to be released individually. In the other case, the centerline of the SRB is assumed to be unconstrained when the net longitudinal force is zero. In this case, Rockwell does the analysis in two steps: (1) runs the system in a cantilevered condition until the zero force point is reached, and (2) forms the total system forcing function by ramping the remaining cantilever interface loads at zero. This study was conducted because of significant changes in the primary and secondary mirror design loads computed for the CDR loads cycle. Table 31 shows the design values and the three analysis cycle values. Notice the large increases particularly in the z-direction for the CDR load cycle, 6.7 versus 12.9 g's for the secondary mirror.

TABLE 31. DESIGN VALUES AND ANALYSIS CYCLE VALUES

COMPONENT	DIR.	MAXIMUM ACCELERATION (G's) LIFTOFF LOADS			
		DESIGN VALUE	P.L.C.	I.L.C.	C.D.R.
PRIMARY MIRROR	X	3.7	3.1	3.5	4.5
	Y	2.4	1.1	1.2	0.9
	Z	3.7	2.6	2.0	3.2
SECONDARY MIRROR	X	3.8	3.1	3.4	4.5
	Y	3.5	2.3	2.6	2.3
	Z	6.7	5.0	3.3	12.9

P.L.C. = PRELIMINARY LOAD CYCLE, USED 5.4 SHUTTLE DATA  
I.L.C. = INTERMEDIATE LOAD CYCLE, USED 5.7 SHUTTLE DATA  
C.D.R. = CRITICAL DESIGN REVIEW LOAD CYCLE, USED 5.8 SHUTTLE DATA

Several avenues were explored as explanation of these changes. The first investigation centered on the change in the ST model by rerunning the loads, changing only the ST model. No change in trends was observed, thus removing the ST model as the reason for the increased loads. Next, the modal contributions were investigated showing that the modes of frequencies between 13.0 and 14.0 Hz were the big contributors. Then the forcing functions were evaluated to determine what was causing the increase. The observed response was almost completely due to the launch release forces,  $M_y$  forcing function being the primary driver. A small glitch was found in the SRB forcing function, namely, the internal pressure

versus time. Smoothing out this glitch reduced the Z loads. This large load sensitivity to a small transient in SRB pressure was not intuitively realistic. It seems that rather the analytical procedure (described above) could be the cause of the problem by generating an unrealistic forcing function that tuned with the modes.

A comparative analysis of the two models was run to determine if there is a requirement to use the four-point release model in deriving liftoff forcing functions for payloads analysis. The multi-point program has the following features:

Features:

- Multiple boundary changes associated with liftoff of the SRB footpads are analyzed using a stiffness coupling method.
- Axial loads at the launch vehicle/stand attach points are monitored.
- When the holddown bolt has released (time dependent only) and the support point goes into tension, the stand stiffness representation is changed by collapsing out the corresponding stand coordinates.

The equations of motion, when vehicle is completely attached to stand (neglecting damping and applied forces), can be written as:

$$\begin{bmatrix} \underline{M} & \underline{O} \\ \underline{O} & \underline{O} \end{bmatrix} \begin{Bmatrix} \underline{\dot{h}} \\ \underline{\delta}_o \end{Bmatrix} + \begin{bmatrix} \underline{K}_{11} & \underline{K}_{12} \\ \underline{K}_{21} & \underline{K}_{22} + \underline{K}_S \end{bmatrix} \begin{Bmatrix} \underline{\ddot{h}} \\ \underline{\ddot{\delta}}_o \end{Bmatrix} = \{0\} \quad (1)$$

It is assumed that the vehicle/stand interface points are massless

where

- $\{h\}$  = Free-free vehicle coordinates
- $\{\delta_o\}$  = Stand/vehicle attach point coordinates (X, Y, Z only)
- $K_S$  = Stand stiffness matrix.

Equation (1) can be written as

$$\begin{aligned} [M] \{ \ddot{h} \} + [K_{11} - K_{12}K_{22}^{-1} K_{21}] \{ h \} \\ - [K_{12}(K_{22} + K_S)^{-1} K_{21} - K_{12} K_{22}^{-1} K_{21}] \{ h \} = \{0\} \end{aligned} \quad (2)$$

by using the lower part of (1) to eliminate  $\{\delta_o\}$ .

The first part of Eq (2) is the free-free equations of motion for the launch vehicle for which modes and frequencies are available. Then, incorporating the transformation between discrete and modal coordinates.

$$\{h\} = [\phi]\{q\} \quad (3)$$

by also including damping and applied forces, equation (2) becomes:

$$\begin{aligned} \left\{ \ddot{q} \right\} + [2 \xi \omega] \left\{ \dot{q} \right\} + \left[ \omega^2 \right] + [\phi]^T [K_{12}] \left[ K_{22}^{-1} - (K_{22} + K_S)^{-1} \right] \\ [K_{21}] [\phi] \left\{ q \right\} = [\phi]^T \left\{ F(t) \right\} \end{aligned} \quad (4)$$

Equation (4) is solved using a Runge-Kutta integration procedure.

When one of the attach points has gone into tension and the corresponding hold-down bolt has released, the stand stiffness matrix,  $K_S$ , is modified and a new generalized stiffness in (4) is calculated. This continues until all attach points have lifted off, at which time  $K_S = 0$  and equation (4) becomes

$$\left\{ \ddot{q} \right\} + [2 \xi \omega] \left\{ \dot{q} \right\} + \left[ \omega^2 \right] \left\{ q \right\} = [\phi]^T \left\{ F(t) \right\} \quad (5)$$

The approach should yield, in general, a conservative estimate for liftoff loads since the lateral (Y, Z) constraints at the footpads are relieved instantaneously.

A comparison between this approach and the single-point assumption used by Rockwell is shown in Table 32. Three cases are shown: (1) the single-point release using Rockwell forcing functions derived for an incompatible model relative to the one MSFC used, (2) the multipoint liftoff forcing functions induced loads, and (3) MSFC-developed single-point release forcing function model using Rockwell's procedure and a compatible dynamic model. Notice the big reductions, particularly in the Z-loads.

Typical footpad forces time traces for the SRB (right) are shown in Figure 76. Notice how the force builds, then releases and goes to zero.

Figure 77 shows the net section load as would be acting on the launch pad. Shown are both the forces and moments. Notice the transits and releases to zero.

Comparing these forces and moments in a qualitative way for the single and multipoint release shows the following:

TABLE 32. MULTIPOINT LIFTOFF LOADS

● SUMMARY OF RESULTS										
ITEM	D <sub>1R</sub>	ACCELERATIONS (G'S)								
		L0725	L4P725	L1P725	L0733	L4P733	L1P733	L0736	L4P736	L1P736
PRIMARY MIRROR C.G.	V <sub>1</sub>	3.97	4.01		3.63	3.12		2.70	2.42	
	V <sub>2</sub>	-.73	-.88		-.79	.69		-.62	-.48	
	V <sub>3</sub>	2.46	2.61		-2.48	-1.87		2.01	1.44	
SECONDARY MIRROR C.G.	V <sub>1</sub>	3.91	3.96		3.59	3.08		2.69	2.40	
	V <sub>2</sub>	-1.66	1.63		-1.92	1.62		-1.56	-1.53	
	V <sub>3</sub>	8.82	7.20		10.16	5.73		-6.62	3.83	
CABIN LUMPED MASS NODE 6	X		-2.69			-2.21			-2.16	
	Y		-.36			.46			-.21	
	Z		1.99			1.46			-.83	
+Y OMS POD C.G. NODE 60	X		-3.59			-2.87			-2.37	
	Y		-1.41			-.99			.47	
	Z		-1.71			1.30			-.60	
-Y OMS PAD C.G. NODE 560	X		-3.47			-2.67			-2.34	
	Y		1.61			-1.01			.47	
	Z		-1.63			-1.07			.62	

NOTES:

- (1) CASES L0725, L0733, L0736 - SINGLE POINT RELEASE FORCING FUNCTIONS DEVELOPED BY RI FOR INCOMPATIBLE MODEL, 1% DAMPING, 353 MODES (MAX FREQ = 37 Hz)
- (2) CASES L4P725, L4P733, L4P736 - MULTIPOINT LIFTOFF FORCING FUNCTIONS, OVER (NO GUST, NO OVERPRESSURE), 1% DAMPING, 140 MODES (MAX FREQ = 17.4 Hz)
- (3) CASES L1P725, L1P733, L1P736 - SINGLE POINT RELEASE FORCING FUNCTIONS DEVELOPED BY MSFC USING COMPATIBLE MODEL, 1% DAMPING, 140 MODES (MAX FREQ = 17.4 Hz)

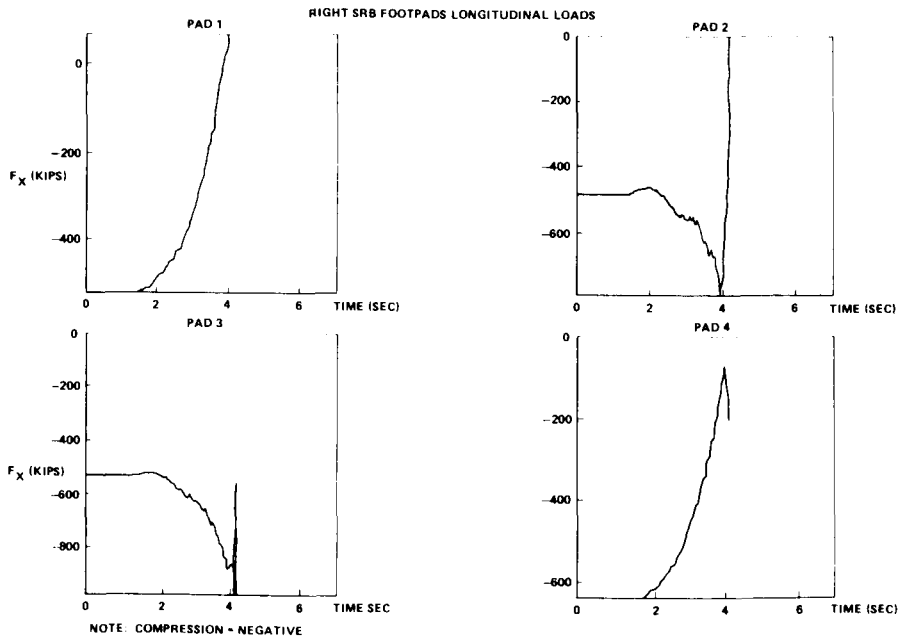


Figure 76. Footpad forces time traces.

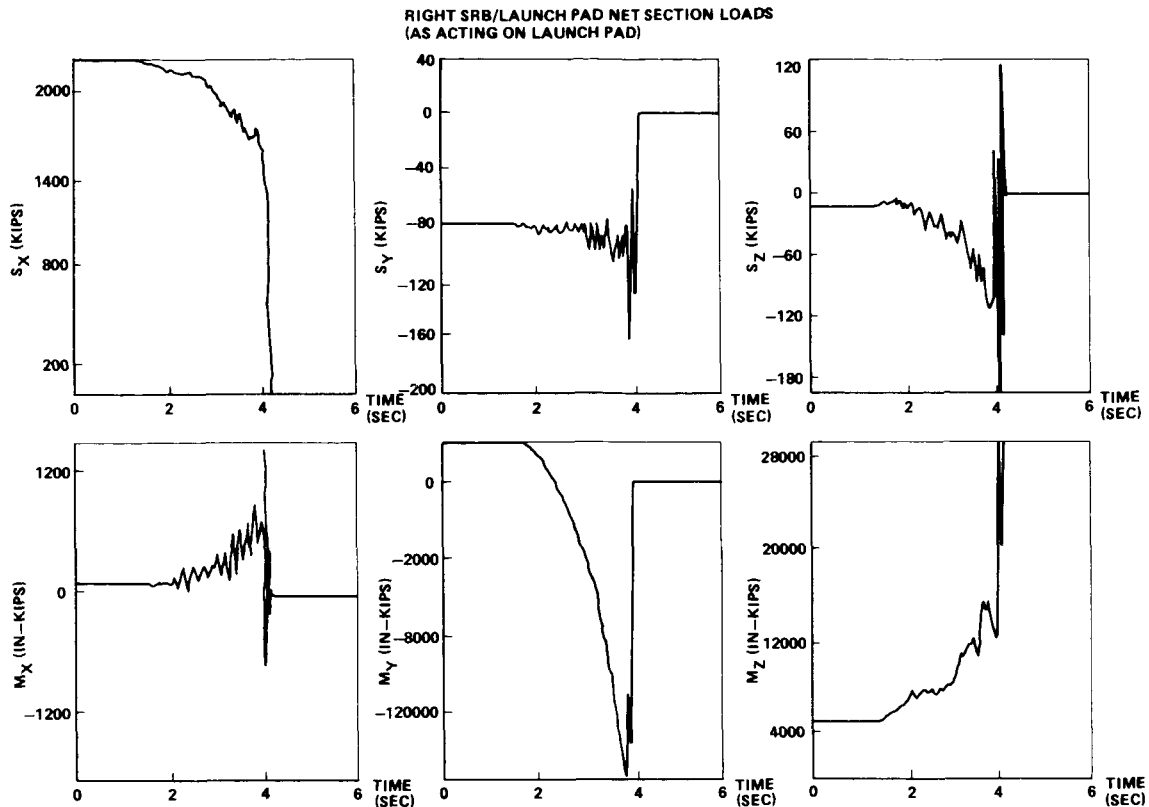


Figure 77. Net section load.

- S<sub>X</sub> Very close both in transient content and decay time
  - S<sub>Y</sub> Significantly different, four point release - Has more high frequency content during release phase
  - S<sub>Z</sub> Significantly different, four point release - Has more high frequency content during release phase
  - M<sub>X</sub> Significantly different, four point release - Has more high frequency content during release phase
  - M<sub>Y</sub>\* Overall shape close, but single point release has more high frequency during release phase.
  - M<sub>Z</sub> Overall shape close, but different transient character during release phase.
- \*Primary driver for space telescope V<sub>3</sub>, (Z), accelerations

The resulting secondary mirror responses for the two approaches are shown in Figures 78 and 79. Notice both the amplitude change and the more pure excitation in the single point versus more random in the multipoint.

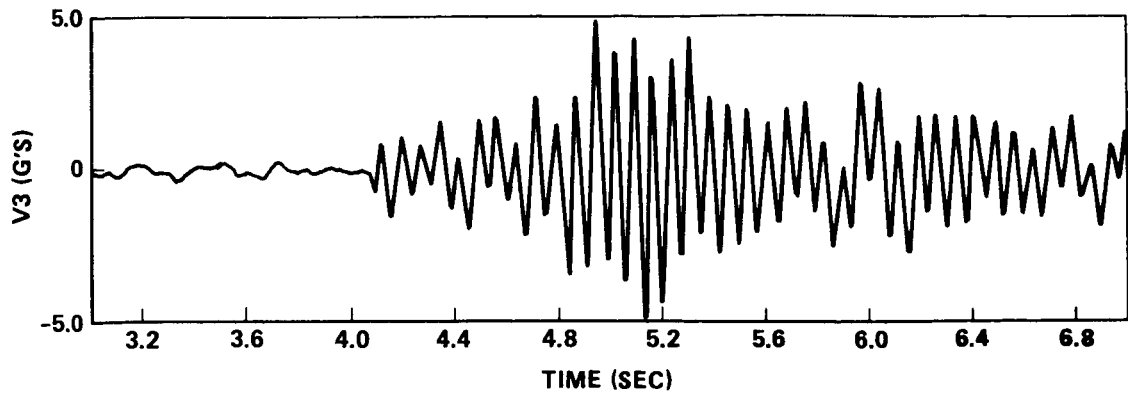


Figure 78. Multi-point release.

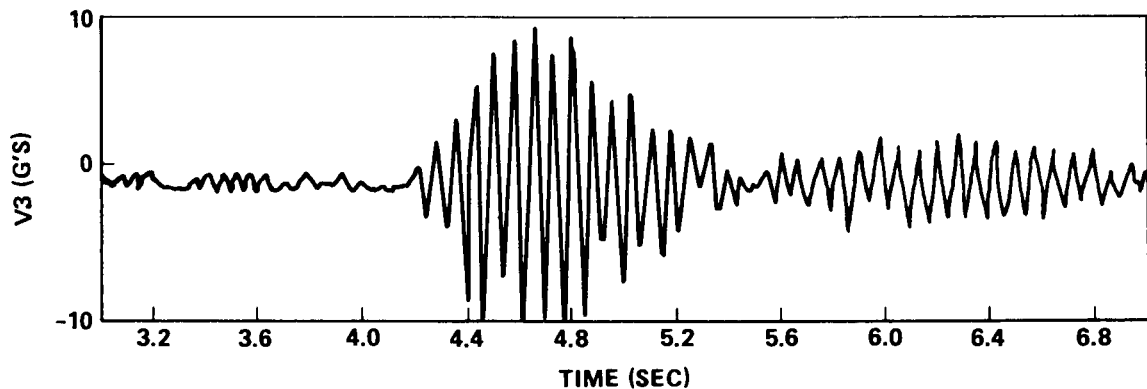


Figure 79. Single-point release.

In conclusion, the single-point release approach gives transient characteristics in the release forcing functions which are erroneous and can result in erroneous loads for components and payloads with resonances in frequency range 8-20 Hz.

Conversely, the frequency content of the four-point release, although more correct, can tune and increase loads for systems designed using single-point release-derived loads. This means that sensitivity analysis worst-on-worst combination approach can be very misleading, thus lead to wrong design load forcing function cases.

This experience clearly indicates the requirement for modeling accuracies compatible with environments, mission, etc., for deriving design loads.

## B. Spacelab

The Spacelab presents unique problems for the loads analysts, due to its many configuration potentials and reuse concept. It consists of a module that can be either the short or long version and can accommodate experiment pallets from one to three. A sketch of the



long module is shown in Figure 80. The module sidewalls have single and double experiment racks illustrated on the back part of the view. Viewing ports and an airlock are available for the astronauts to view and have access to the pallets as well as enter the Orbiter cargo bay. The module is connected to the Orbiter crew cabin with a transfer tunnel.

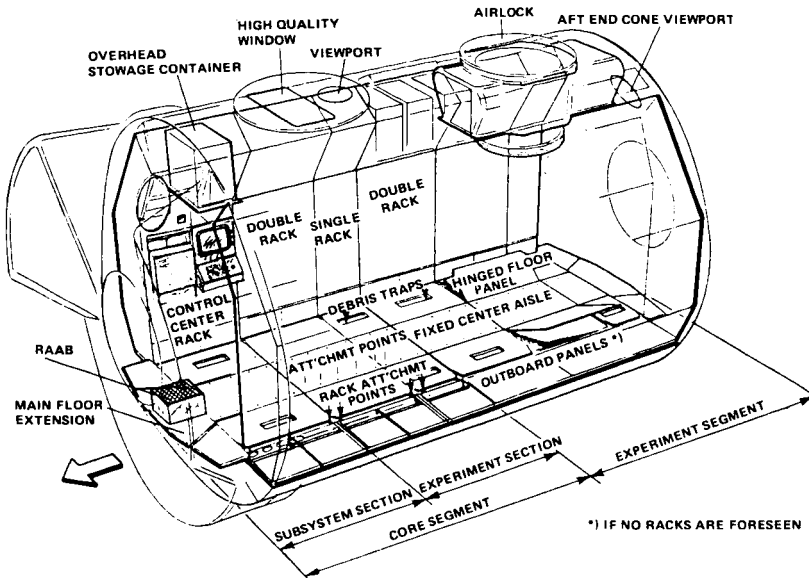


Figure 80. Spacelab long module.

The pallets are open to the bay and the outside when the cargo bay is open. They serve as mounting platforms for various experiments, particularly like the point mounts and variable viewing experiments or experiments that require exposure to space environments. Figure 81 shows a pallet frame and some typical experiment hardpoints and the orbiter keel fitting.

Various combinations of modules and pallets, or pallets, can be used in the Shuttle to make up a set of experiments for a mission. Figure 82 shows some of the various combinations. The asterisks are the configuration used in loads analysis.

Spacelab is a reusable element that must handle many experiment combinations, thus have variable dynamic characteristics. This created problems in what payload configuration to select for design loads analysis. Obviously, what is needed is an envelope case. The problem is how to handle the variable dynamic characteristics to achieve the envelope case. Early in the program, MSFC decided to place minimum frequency constraints on all experiments mounted in the Spacelab. These were chosen to be a factor of 1.4 above the maximum forcing function frequency during liftoff and landing for all mounted to primary structures. This led to a 25 Hz minimum. All secondary mounted experiments would have a minimum frequency of 35 Hz. This allowed for very simple math models of the experiment.

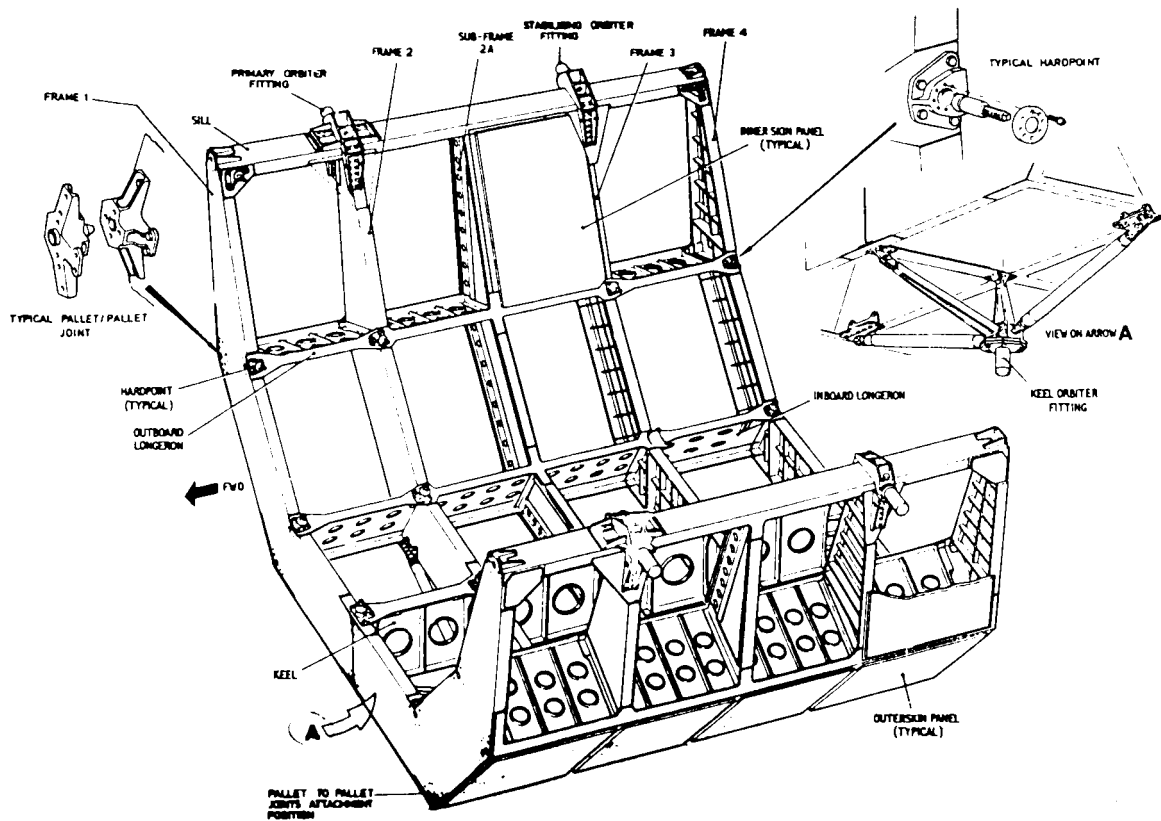
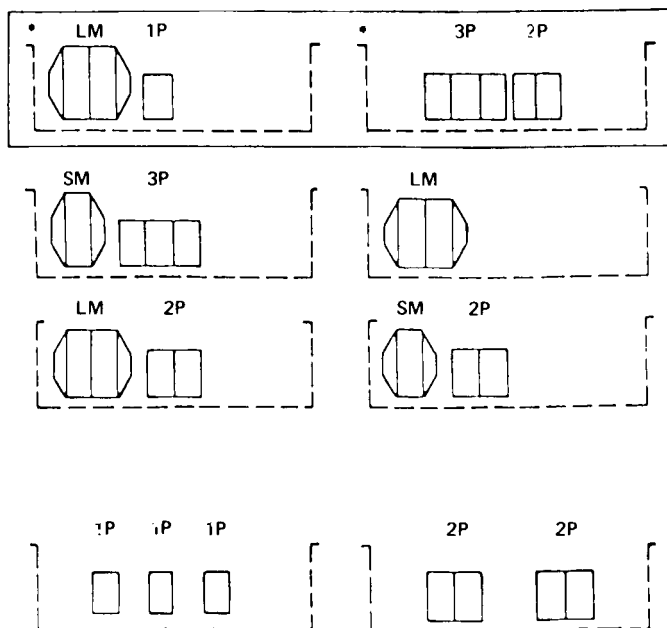


Figure 81. Pallet segment.



\*TWO CONFIGURATION USED IN COUPLED LOADS ANALYSIS

Figure 82. Design baseline configurations.

JSC, MSFC, Rockwell, and ESA (European Space Agency) decided to develop a generic payload contingency with the total mass being maximum assigned to Spacelab. For example, these generic experiments were mounted on tripods on the pallet. Figure 83 shows one configuration where the experiments were mounted on the sidewall. Other mounting configurations were chosen for design loads but are not shown.

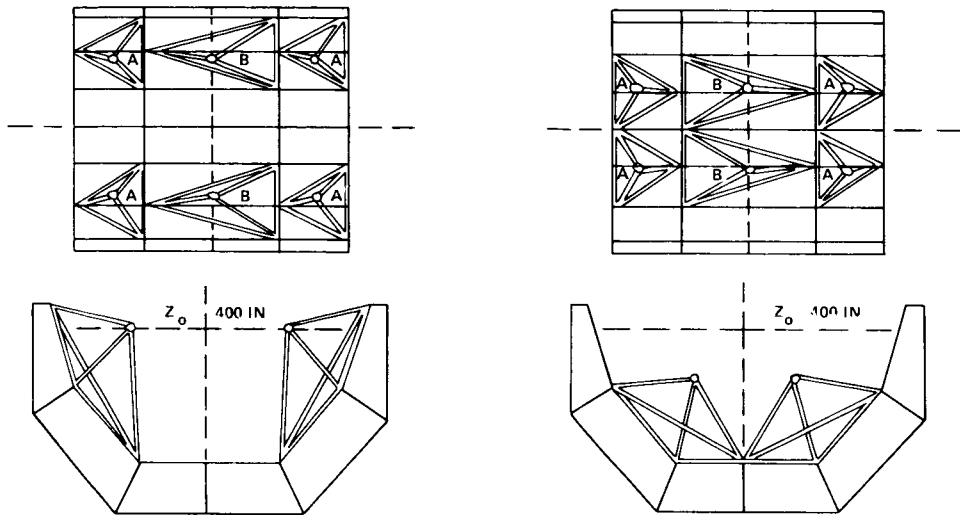


Figure 83. Sidewall mounted payloads for 5.7/5.8 triple pallet.

The module racks were mass loaded in the same generic manner. Figure 84 shows typical node points of the racks in the math model.

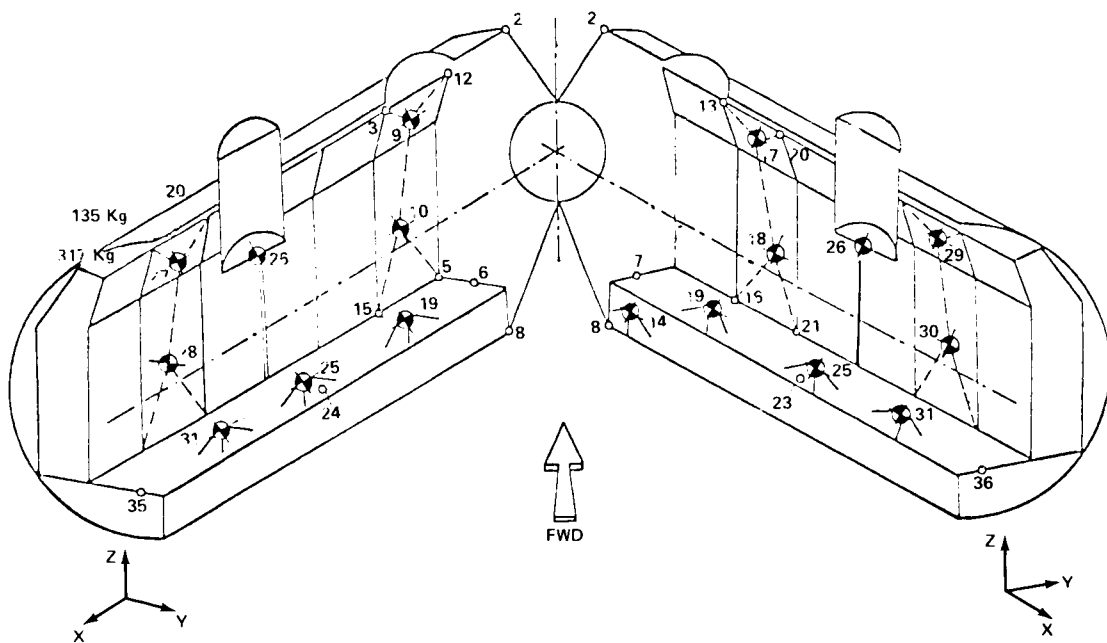


Figure 84. Location of nodal points for 89 DOF math model (internal).

These generic payload models coupled with models of the basic Spacelab structure were provided to NASA by the Europeans. Rockwell then coupled these Spacelab generic dynamic models to the Shuttle dynamic model and calculated the design node point accelerations. Due to changes in the Shuttle system forcing functions, several different sets of loads have been run. The Europeans took these time-consistent modal accelerations, did a weighted average based on node-point mass, and generated x, y, and z acceleration from which they determined the shear forces and moment distribution and the design loads. Table 33 is a typical example of loads (accelerations) obtained in these analyses. Shown are the four load cycles completed. The 5.3 indicates the Shuttle configuration used for design. ICD is the preliminary load factors placed in the interface control documents, while 5.4 is an updated Shuttle model and forcing function, and 5.7/5.8 is based on the STS-1 Shuttle configuration and forcing functions and updated Spacelab dynamic model (test verified). Load factors are given for three directions for liftoff and handling.

Notice the significant changes that have occurred in the loads as the Shuttle forcing function and model have improved. In general, the loads have gone up with each update, indicating the trend that occurs for loads from preliminary design to verification. This means that where possible the loads developed early in a program should have some conservatism added to account for changes. Obviously, once a launch vehicle has matured, most of these changes would vanish and the conservatism could be removed for subsequent analysis. With the Spacelab, one option is open instead of redesigning and fitting the structure to take the increasing loads. These load factors are based on a fully loaded generic payload complement; therefore, the actual payload contingency could be chosen to stay within the Spacelab design. This has been the path chosen for Spacelab, except in a few special cases, until a few Shuttle flights verify the environments and models. At this time, beefups can be made or flights can continue under the same offloading ground rule.

Figure 85 gives a typical Spacelab nodal response for three node points. The high dynamic content and the tuning of various frequencies is obvious in these data. This is expected since the payload has only the inertial effects from the carrier with the only static load being the longitudinal acceleration. This is not true for the basic Shuttle where thrust forces, aerodynamic forces, and control forces add directly to the dynamic response. These types of loads can be controlled somewhat and have potential for alleviation using operational procedures, etc. Payload loads are much less amenable to these alleviation techniques and must depend on isolation approaches if alleviation is required. This approach is not desirable because one ends up trading loads for deflection, etc.

The approach taken for Spacelab experiment loads had three distinct considerations: (1) load factors for experimental design were defined by MSFC using the node point accelerations obtained from the generic analysis made by Rockwell in conjunction with the 25 Hz and 35 Hz frequency constraint discussed earlier (vibroacoustic load factors were added to get the total load factor), (2) the verification of the mission complement was an all-up Shuttle, Spacelab, and (3) experiments transient load analysis conducted using the JSC/Rockwell supplied forcing functions described earlier.

The design load factors were the max/min envelope determined separately for the pallet and module mounted experiments. No alleviation was considered for the various locations within a module or on a pallet. This is shown in Tables 34 and 35.

TABLE 33. DEVELOPED LOADS IN g's ACCELERATION

	LIFTOFF			LANDING		
	N <sub>x</sub>	N <sub>y</sub>	N <sub>z</sub>	N <sub>x</sub>	N <sub>y</sub>	N <sub>z</sub>
<b>LONG MODULE</b>						
- 5.3	-6/-2.5	± 1.1	1.0/-1.3	.6/-1.0	± .5	3.1/-4
- ICD	-.3/-2.9	± 1.0	± 1.65	1.2/-1.5	± 1.1	4.1/-1
- 5.4	-.4/-2.4	± 1.4	2.1/-1.8	1.2/-1.8	± 1.5	4.2/-1
- 5.7/5.8	-.4/-3.5*	± 1.5*	2.6/-2.2*	1.0/-1.2	± 1.4*	4.51/-2.2*
<b>SINGLE PALLET</b>						
- 5.3	-.5/-2.9	± .6	.5/-6	.7/-1.1	± .5	3.7/-3
- ICD	-.2/-3.2	± .9	1.4/-1.2	1.2/-1.5	± .9	4.2/-1
- 5.4	.1/-3.1	± .4	1.3/-1.4	1.0/-1.6	± .6	3.4/-5
- 5.7/5.8	-.2/-3.8*	± .9	1.7/-2.2*	1.3/-1.2*	± .6	3.7/-1
<b>DOUBLE PALLET</b>						
- 5.3	-.6/-2.6	± .9	.5/-8	.6/-7	± .1	3.2/-1
- ICD	.0/-2.9	± 1.2	± 1.3	1.2/-1.5	± .8	4.1/-1
- 5.4	.2/-2.7	± .4	1.2/-1.0	1.1/-1.2	± .4	3.5/-7
- 5.7/5.8	-.2/-3.4	± .9	2.2/-2.3*	.9/-1.1	± .5	3.6/-8*
<b>TRIPLE PALLET</b>						
- 5.3	-.8/-2.6	± 1.0	1.1/-1.9	± .8	± .1	3.0/-0.4
- ICD	-.3/-2.9	± 1.2	1.6/-1.9	1.2/-1.5	± .8	4.1/-1
- 5.4	-.1/-3.0	± .4	3.0/-2.2	1.0/-1.9	± .4	4.1/-7
- 5.7/5.8	-.2/-3.4*	± 1.0	3.7/-3.0*	1.0/-1.1	± .4	4.5/-1.0*

\*5.7/5.8 values exceed ICD Z - 05101, Rev. C values.

COMPARISON OF SPACELAB INTERFACE FORCES, KIPS

LIFTOFF

		STAB. Z	KEEL Y	MAIN X (PORT)	MAIN X (STAR)	MAIN Z (PORT)	MAIN Z (STAR)
LONG MODULE	5.3	17.0/-19.0	22.0/-25.0	- 6.0/-30.0	- 9.0/-30.0	18.0/-20.0	13.5/-17.0
	ICD	46.4/-17.5	30.2/-30.2	15.9/-54.3	15.9/-54.3	62.9/-32.2	19.7/-17.8
	5.4	32.3/-26.3	32.0/-30.7	- 4.8/-29.2	- 3.7/-27.8	30.2/-32.8	20.6/-21.0
	5.8	41.2/-33.9*	31.9/-34.5*	- 3.8/-45.8	- 4.5/-40.3	28.4/-27.9	19.4/-23.9*
SINGLE PALLET	5.3	1.0/-13.5	5.5/-6.0	- 2.0/-13.5	- 2.0/-14.0	12.0/-1.0	13.0/-2.0
	ICD	16.4/-14.3	12.5/-12.5	6.9/-16.3	6.9/-16.3	17.8/-7.6	17.9/-7.6
	5.4	1.6/-8.6	3.5/-3.6	.6/-13.1	.0/-12.5	8.2/-2.0	8.7/-2.3
	5.8	3.0/-7.6	7.3/-7.5	.0/-16.7*	1.2/-16.7*	12.8/-7.9*	13.4/-9.6*
DOUBLE PALLET	5.3	1.5/-8.0	17.0/-17.0	- 5.0/-20.0	4.0/-20.0	8.0/-1.0	7.5/-2.0
	ICD	22.3/-15.7	19.5/-19.5	10.8/-25.0	10.8/-25.0	22.5/-10.0	25.5/-10.0
	5.4	3.4/-7.3	5.3/-5.4	1.0/-19.7	2.3/-20.3	7.9/-3.1	8.8/-3.1
	5.8	6.4/-9.9	11.2/-12.2	.0/-25.4*	- 1.6/-22.8	10.8/-7.9	11.9/-9.8
TRIPLE PALLET	5.3	14.0/-6.0	15.0/-15.0	- 4.0/-22.0	- 7.0/-23.0	2.0/-12.0	2.0/-12.0
	ICD	29.9/-15.6	± 24.1	11.4/-29.0	11.6/-29.5	22.7/-20.0	22.7/-20.0
	5.4	27.2/-15.8	6.5/-7.1	.0/24.9	1.8/-25.7	4.9/-11.8	5.5/-11.7
	5.8	29.1/-23.2*	18.5/-18.0	- 1.9/-31.3*	.0/-29.2	9.7/-11.5	9.2/-11.0

TABLE 33. LANDING LOAD FACTORS IN g's ACCELERATION

LANDING

		STAB. Z	KEEL Y	MAIN X (PORT)	MAIN X (STAR)	MAIN Z (PORT)	MAIN Z (STAR)
LONG MODULE	5.3	40.0/-2.0	11.0/-8.5	7.0/-11.0	7.0/-11.0	35.0/-0	9.0/-10.0
	ICD	46.4/-17.5	± 30.2	15.9/-54.3	15.9/-54.3	62.9/-32.2	19.7/-17.8
	5.4	41.8/-12.4	34.0/-32.8	13.9/-21.1	14.0/-20.9	45.5/-17.5	30.9/-31.8
	5.7	55.8/6*	31.9/-31.6*	14.2/-14.5	11.5/-13.6	44.7/3.2	19.8/-27.7*
SINGLE PALLET	5.3	7.4/-3.0	4.3/-3.2	3.3/-5.1	3.0/-5.2	13.0/-2.0	13.0/-1.0
	ICD	16.4/-14.3	± 12.5	6.9/-16.3	6.9/-16.3	17.8/-7.6	17.9/-7.6
	5.4	7.6/-2.0	5.0/-3.9	4.2/-6.6	4.7/-6.7	10.9/-3.2	10.7/-3.2
	5.7	9.4/-3	4.9/-4.2	5.6/-5.2	5.9/-5.1	9.0/-4.4	8.7/-3
DOUBLE PALLET	5.3	13.3/5	1.9/-1.7	4.3/-5.5	4.3/-5.5	12.5/-1.0	12.5/-1.0
	ICD	22.3/-15.7	± 19.5	10.8/-25.0	10.8/-25.0	22.5/-10.0	25.5/-10.0
	5.4	13.3/-3.7	6.4/-3.2	8.3/-8.8	8.1/-8.9	15.0/-6.2	14.8/-6.7
	5.7	13.9/-4.2	7.2/-3.1	6.2/-7.6	6.3/-7.5	13.4/-3.2	13.2/-3.1
TRIPLE PALLET	5.3	12.5/-1.0	2.0/-2.1	7.0/-6.0	7.0/-6.0	14.5/-2	14.0/-2
	ICD	29.9/-15.6	± 24.1	11.4/-29.0	11.6/-29.5	22.7/-20.0	22.7/-20.0
	5.4	18.1/-5.1	5.8/-1.8	8.6/-15.3	8.5/-15.5	16.6/-4.6	16.3/-4.4
	5.7	23.3/-9.7	8.4/-2.6	10.2/-9.6	8.4/-9.6	20.6/-7.1	20.4/-7.0

\*5.7/5.8 Values exceed 5.3 values.

	Liftoff Load Factors			Landing Load Factors		
	N <sub>x</sub> (g's)	N <sub>y</sub> (g's)	N <sub>z</sub> (g's)	N <sub>x</sub> (g's)	N <sub>y</sub> (g's)	N <sub>z</sub> (g's)
LONG MODULE						
- FRAME TOP						
- 5.3	-.35/-2.65	± 1.33	1.51/-1.71	1.40/-1.35	± .77	4.27/-.21
- 5.4	-.5/-2.68	± 1.87	3.38/-1.90	2.70/-2.10	± 2.45	4.85/-1.20
- 5.7/5.8	-.39/-3.42*	± 2.59*	3.69/-3.19*	1.29/-1.19	± 2.18*	5.42/-3.01
- FRAME SIDE						
- 5.3	-.44/-2.54	± 1.02	1.61/-1.83	.62/-95	± .60	4.43/-67
- 5.4	-.72/-2.50	± 1.51	3.22/-2.19	1.22/-1.92	± 2.64	4.86/-1.73
- 5.7/5.8	.01/-3.07*	± 1.79*	3.36/-3.03*	.84/-95*	± 1.61*	4.78/-.0*
- FRAME BOTTOM						
- 5.3	-.74/-2.58	± .81	1.32/-1.64	1.14/-1.20	± 1.14	4.18/-.19
- 5.4	-.23/-3.13	± 1.39	2.60/-2.75	2.83/-2.18	± 2.02	4.71/-2.65
- 5.7/5.8	-.22/-3.53*	± 1.85*	3.90/-3.58*	1.58/-1.73*	± 1.56*	5.94/-2.49
- RACK ATT. (FLOOR)						
- 5.3	-.72/-2.57	± .90	1.40/-1.75	.74/-1.01	± .96	4.26/-.45
- 5.4	-.40/-2.90	± 1.51	3.18/-2.20	2.43/-1.62	± 1.93	5.64/-2.0
- 5.7/5.8	-.27/-3.61*	± 1.80*	3.90/-3.62*	1.61/-1.70*	± 1.55*	5.22/-.92*
- RACK ATT. (OVERHEAD)						
- 5.3	-.25/-2.80	± 1.88	---	.96/-1.21	± 1.57	---
- 5.4	-.29/-2.66	± 3.13	---	3.96/-3.47	± 9.50	---
- 5.7/5.8	-.16/-3.82*	± 4.83*	3.93/-3.91	2.04/-1.77*	± 6.20	6.54/-2.58

\*5.7/5.8 Values exceed 5.3 values.

TABLE 33. (Concluded)

		Liftoff Load Factors			Landing Load Factors		
		$N_x(g's)$	$N_y(g's)$	$N_z(g's)$	$N_x(g's)$	$N_y(g's)$	$N_z(g's)$
LONG MODULE AIRLOCK	5.3	-3.9/-2.6	± 1.30	.72/-1.30	1.0/-1.14	± 1.05	3.75/-0.05
	5.4	-.42/-2.1	± 2.10	3.02/-2.40	1.6/-2.3	± 2.8	5.2/-2.8
	5.7/5.8	1.6/-5.5*	± 6.44*	2.6/-2.8*	9.4/-8.8*	± 11.0*	7.7/-5.6*
GN <sub>2</sub> TANK	5.3	.7/-4.3	± 1.3	1.8/-2.0	2.0/-2.7	± .9	4.5/-5.9
	5.4	1.7/-4.2	± 2.1	3.3/-3.4	8.0/-8.3	± 3.3	6.5/-5.7
	5.7/5.8	-.3/-3.02	± 2.0*	3.9/-3.0*	1.0/-1.3	± 3.1*	4.8/-1.9
TRIPLE PALLET IGLOO	5.3	.05/-4.0	± 1.2	2.5/2.8	3.4/-3.4	± .5	3.8/-1.5
	5.4	3.2/-5.7	± 1.2	6.6/-6.2	8.7/-8.9	± 1.7	6.4/-4.2
	5.7/5.8	3.0/-5.0*	± 1.6*	6.0/-5.6*	3.3/-3.1	± 3.4*	12.3/-9.5*

\*5.7/5.8 Values exceed 5.3 values

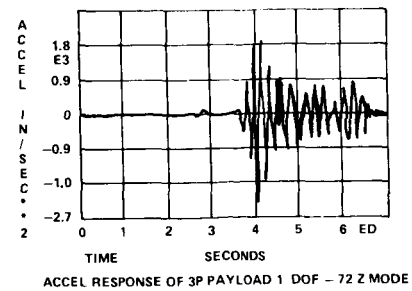
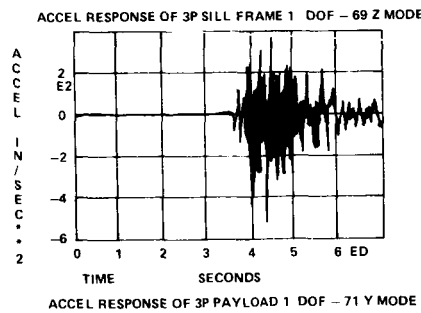
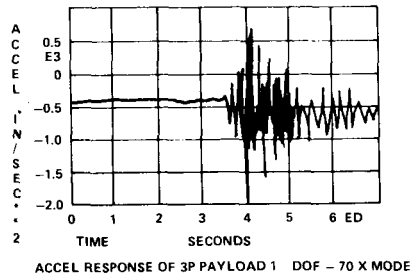


Figure 85. Typical Spacelab payload response.

TABLE 34. MODULE-MOUNTED PAYLOAD LIMIT LINEAR ACCELERATIONS (g's) DURING LIFT-OFF AND LANDING

CONDITION		LIFTOFF			LANDING		
		X (g)	Y (g)	Z (g)	X (g)	Y (g)	Z (g)
OVERHEAD CONTAINER		+ 2.8	± 7.2	+ 3.6	+ 5.6	± 7.5	+ 5.8
		- 6.0		- 3.3	- 5.3		- 3.0
AIRLOCK		+ 0.9	± 6.5	+ 2.5	+ 6.2	± 4.2	+ 7.7
		- 4.7		- 2.7	- 5.2		- 5.6
SWAA		+ 0.7	± 1.7	+ 3.3	+ 1.2	± 1.7	+ 5.2
		- 3.3		- 2.8	- 1.1		- 2.4
CENTER FLOOR RACKS		+ 0.9	± 1.8	+ 3.4	+ 2.6	± 2.3	+ 7.9
		- 3.6		- 2.9	- 1.9		- 3.9
RACKS*		+ 1.9	± 3.0	± 3.7	± 5.0	± 3.2	+ 6.0
		- 5.0					- 2.6
		+ 0.8	± 4.8	± 3.7	± 1.5	± 5.8	+ 6.0
		- 3.5					- 2.6

\*COMPONENTS MOUNTED IN RACKS MUST BE DESIGNED TO WITHSTAND BOTH SETS OF LOAD FACTORS GIVEN.

TABLE 35. PALLET-MOUNTED PAYLOAD LIMIT LINEAR ACCELERATIONS (g's) AND ANGULAR ACCELERATIONS (rad/s<sup>2</sup>) DURING LIFT-OFF AND LANDING

CONDITION		ACCELERATION						
		X (g)	Y (g)	Z (g)	Φ rad/s <sup>2</sup>	Θ rad/s <sup>2</sup>	Ψ rad/s <sup>2</sup>	
FLOOR-MOUNTED	LIFT-OFF	+ 2.0	± 1.5	+ 4.7	± 9.0	± 23.0	± 5.0	
		- 5.0		- 4.5				
	LANDING	+ 3.8	± 1.8	+ 6.0	± 7.0	± 40.0	± 3.7	
		- 4.6		- 3.0				
SIDEWALL-MOUNTED	LIFT-OFF	+ 2.0	± 3.6	+ 5.8	± 21.0	± 23.0	± 11.5	
		- 5.0		- 5.1				
	LANDING	± 6.8	± 7.2	+ 7.0	± 28.0	± 40.0	± 14.8	
				- 3.2				



In addition to the load factors, the sinusoidal vibration levels must be provided for qualification and verification testing where required. These cover the low-frequency characteristics of the responses observed in the analysis data. The time of application is determined from the predicted number of missions for the experiment. Table 36 gives these values.

TABLE 36. SINUSOIDAL VIBRATION LEVEL

	COMPONENT	FREQUENCY (HZ)	INPUT LEVEL (g 0-TO-PEAK)		
			X	Y	Z
MODULE	OVERHEAD STORAGE CONTAINERS	5 - 12	1	1	1
		12 - 35	4.3	5.4	4.1
		35 - 50	1	1	1
	AIRLOCK	5 - 12	1	1	1
		12 - 35	4.4	4.6	5.5
35 - 50		1	1	1	
SWAA	5 - 10	1	1	1	
	10 - 35	2.4	1.2	3.7	
	35 - 50	1	1	1	
RACKS	5 - 9	1	1		
	5 - 13			1	
	9 - 35	2.6	1.6		
	13 - 35			5.6	
	35 - 50	1	1	1	
RACKS	5 - 12	1	1	1	
	12 - 35	3.6	4.1	4.3	
	35 - 50	1	1	1	
PALLET	FLOOR-MOUNTED	5 - 11	1	1	1
		11 - 25	3.6	1.3	4.3
25 - 50		1	1	1	
PALLET	SIDEWALL-MOUNTED	5 - 12	1	1	1
		12 - 25	4.9	5.1	5.0
		25 - 50	1	1	1
		SWEEP RATE AT 3 OCT/MIN			
ASSUMING 1 - 10 FLIGHTS		1 SWEEP UP AND DOWN FOR EACH AXIS			
ASSUMING 10 - 50 FLIGHTS		REPEAT THE SWEEP FOR EACH ADDITIONAL INCREMENT OF 10 FLIGHTS (OR PORTIONS THEREOF)			
NOTE: THE RESPONSE IN EACH AXIS OF THE COMPONENT C, G, SHALL NOT EXCEED THE HIGHEST INPUT LEVEL OF THAT AXIS BY MORE THAN 40%.					

Spacelab Mission 1 - The first Spacelab mission has been analyzed using the all-up Spacelab module and pallet models provided by the Europeans, the experiment models provided by the SI's, and the Shuttle model and forcing functions provided by Rockwell. The analysis was run by McDonnell Douglas, the Spacelab integration contractor. Net accelerations were determined for each experiment and experiment component as well as various preliminary Spacelab structure and Spacelab-to-Orbiter interface loads. No major negative safety factors were found in this analysis when compared with the design. A typical set of values is shown in Table 37 for racks No. 1 and No. 2 for various locations of experiments. Notice that some relief in loads can be achieved by choosing the location for a given experiment. What is shown are the variations in accelerations obtained for the various experiments located in the general area. Rack No. 2 tends to have higher loads than rack No. 1 with the exception of the accelerations in the z-direction.

TABLE 37. SL-1 LOAD FACTORS FOR COMPONENTS MOUNTED IN RACKS NO. 1 AND NO. 2

COMPONENT	FLIGHT EVENT - LIFTOFF		
	LOAD FACTOR (g's)		
	N <sub>x</sub>	N <sub>y</sub>	N <sub>z</sub>
RACK 1			
COMPONENTS LOCATED FROM BOTTOM OF RACK (Z ≈ 355") TO Z = 390"	5.3/-7.0	± 3.3	4.9/-6.7
COMPONENTS LOCATED FROM Z = 390" TO Z = 425"	5.2/-7.4	± 3.6	4.8/-6.8
COMPONENTS LOCATED FROM Z = 425" TO TOP OF RACK	4.8/-7.1	± 3.7	4.6/-5.9
RACK 2			
COMPONENTS LOCATED FROM BOTTOM OF RACK (Z ≈ 355") TO Z = 390"	4.8/-7.8	± 3.8	4.3/-4.4
COMPONENTS LOCATED FROM Z = 390" TO Z = 425"	5.1/-8.7	± 4.7	4.4/-4.6
COMPONENTS LOCATED FROM Z = 425" TO TOP OF RACK	4.6/-7.4	± 5.5	4.5/-4.4

These loads are typical of the SL-1 Spacelab mission. The detail loads for the various experiments are not given for brevity's sake. Spacelab Mission 2 is in analysis using the same approach.

### SECTION III. CONCLUSIONS

Several examples of various loads analysis and loads sensitivities have been given. They are typical of the many conducted. Interested persons can get more details of the ones presented or others not presented. These results show clearly the complexity of the loads world and requirement that loads engineers be very versatile. All these aspects make for a challenging but very interesting and rewarding job.

## BIBLIOGRAPHY

- Adelfang, S. I.: Analysis of Vector Wind Change with Respect to Time for Vandenberg Air Force Base, California. NASA CR-150776, August 1978.
- Adelfang, S. I.: Analysis of Wind Bias Change with Respect to Time at Cape Kennedy, Florida, and Vandenberg Air Force Base, California. NASA CR-150777, August 1978.
- Alderson, R. G., and Wells, D. A.: Final Report on Surveyor Lunar Touchdown Stability Study. Bendix Products Aerospace Division, Report MM-66-19, July 8, 1966.
- Amos, A. K. and Goetz, R. C.: Reserarch Needs in Aerospace Structural Dynamics. AIAA Paper 79-0826, AIAA/ASME/ASCE/AHS 20th Structures, Structural Dynamics, and Materials Conference, St. Louis, Mo., April 4-6, 1979.
- Anderson, L.R. and Hallauer, Jr., W. L.: A Method of Order Reduction for Structural Dynamics. AIAA/ASME/ASCE/AMS -- 21st Structures, Structural Dynamics, and Materials Conference, Seattle, Wash., May 12-14, 1980.
- Arthurs, T. D.: Highlights 1979 Structural Dynamics. Astronautics and Aeronautics, 1979.
- Baheshko, V. A.: A New Effective Method of Dynamic Contact Problem Solution. AD-B008 803L, Army Foreign Science and Technology Center, Charlottesville, VA, May 1977.
- Bamford, R. M.: A Modal Combination Program for Dynamic Analyses of Structures. Technical Memorandum 33-290, Jet Propulsion Laboratory, Pasadena, Calif., January 1964.
- Bamford, R. M.: Application of Structural Analysis and Matrix Interpretive System. Technical Memorandum 33-399, Revision 1, Jet Propulsion Laboratory, Pasadena, Calif., March 18, 1970.
- Bamford, R. M., Wada, B. K., and Gayman, W. H.: Equivalent Mass System for Normal Modes. Technical Memorandum 33-380, Jet Propulsion Laboratory, Pasadena, Calif., February 1971.
- Bamford, R. M., Wada, B. K., Garba, J. K., and Chisholm, J.: Synthesis of Vibrating Systems. The American Society of Mechanical Engineers, New York, N. Y., November 1971.
- Bamford, R. M. and Trubert, M. R.: A Shock Spectra and Impedance Method to Determine a Bound for Spacecraft Loads. Technical Memorandum No. 33-694, Jet Propulsion Laboratory, Pasadena, Calif., September 1, 1974.

## BIBLIOGRAPHY (Continued)

- Barrett, S. and Halverson, R. M.: The Use of Coherence Functions to Determine Dynamic Excitation Sources on Launch Vehicle Payloads, NAS1-14370, June 1979.
- Bekey, I. and Naugle, J.: Just Over the Horizon in Space, Astronautics and Aeronautics, May 1980.
- Benfield, W. A. and Hruda, R. F.: Vibration Analyses of Structures for Component Mode Substitution. AIAA/ASME 11th Structures, Structural Dynamics, and Materials Conference Proceedings, Denver, CO. April 22-24, 1970.
- Blejwas, T. E. and Bresler, B.: Earthquake Response Analysis of Existing Buildings. Journal of the Structural Division ASCE, January 1980.
- Brownlee, G. R., Day, F. D., and Garba, J. A.: Analytical Prediction and Correlation for the Orbiter During the Viking Spacecraft Sinusoidal Vibration Test. The Shock and Vibration Bulletin, Bulletin 45, Part 3, Washington, D. C., June 1975, pp. 37-57.
- Card, M. F.: Trends in Aerospace Structures, Astronautics and Aeronautics, July/August 1978.
- Caughey, R. K.: Design and Subsystems in Large Structures. Technical Memorandum 33-484, Jet Propulsion Laboratory, Pasadena, Calif., 1971.
- Caughey, R. K.: Matrix Perturbation Techniques in Structural Dynamics. Technical Memorandum 33-652, Jet Propulsion Laboratory, Pasadena, Calif., September 1, 1973.
- Cerny, O. P., Foster, L. W., and Sharp, J. B.: Load Relief Attitude Control of the Skylab Launch Vehicle. Northrop-Huntsville TR-795-795, October 1970.
- Chen, J. C. and Wada, B. K.: Criteria for Analysis-Test Correlation of Structural Dynamic Systems. Journal of Applied Mechanics, June 1975.
- Chen, J. C. and Garba, J. A.: Determination of Propellant Effective Mass Properties Using Modal Test Data. The Shock and Vibration Bulletin, Bulletin 45, Naval Research Laboratory, Washington, D. C., 1975.
- Chen, J. C. and Wada, B. K.: Matrix Perturbation for Structural Dynamic Analysis. AIAA Journal, Vol. 15, August 1977, pp. 1095-1100.
- Chen, J.C., Wada, B. K., and Garba, J. A.: Launch Vehicle Payload Interface Response. Journal of Spacecraft and Rockets, Vol. 15, No. 1, January-February 1978, pp. 7-11.
- Chen, J. C., Garba, J. A., and Wada, B. K.: Estimation of Payload Loads Using Rigid-Body Interface Accelerations. Journal of Spacecraft and Rockets, Vol. 16, No. 2., March-April 1979, pp. 74-80.

## BIBLIOGRAPHY (Continued)

- Chen, J. C., Zayzebski, K. P., and Garba, J. A.: Recovered Transient Load Analysis for Payload Structural Systems. AIAA/ASME/ASCE/AMS - 21st Structures, Structural Dynamics, and Materials Conference, Seattle, Wash., May 12-14, 1980.
- Chen, J. C., Garba, J. A., Salama, M., and Trubert, M.: A Survey of Load Methodologies for Shuttle Orbiter Payloads. JPL Publication 80-37.
- Christian, D.: Space Shuttle Liftoff Dynamic Model. NASA TMX-64993, March 1976.
- Christiansen, R. G. and Cruise, D. R.: Factor Analysis on an Exploratory Tool in the Modal Analysis Of Randomly Loaded Vibrating Structures. N.W.C., China Lake, Calif. AD-906 463, December 1972.
- Craig, R. R. and Bampton, M.C.C.: Coupling of Substructures for Dynamic Analysis. AIAA Journal, Vol. 61. No. 7, July 1968, pp. 1313-1319.
- Cromer, J. C. and LaLanne, M.: Predicting and Dynamic Behavior of Complex Structures Using Part Experiment, Part Theory. Shock and Vibration Bulletin No. 46, August 1976.
- Day, F. D. and Wada, B. K.: Unique Flight Instrumentation/Data Reduction Techniques Employed on the Viking Dynamic Simulator. The Shock and Vibration Bulletin, Bulletin 45, Part 3, Naval Research Laboratory, Washington, D.C., 1975, pp. 25-35.
- Day, F. D. and Wada, B. K.: Strain Gaged Struts and Data Reduction Techniques to Maximize Quality Data from Spacecraft Flight Measurements. 21st International Instrumentation Procedures, Philadelphia, PA 1975.
- Deitrich, R. E. and Jones, R. H.: Touchdown Dynamics Study (Preliminary Report), Surveyor Spacecraft System. Report SSD 303OR, Space System Division, Hughes Aircraft Company, Culver City, Calif., January 1963.
- Devers, A. D., Harcrow, H., and Kukreti, A. R.: Coupled Base Motion Response Analysis of Payload Structural Systems. UCCE 75-2, April 1976.
- Donald, E. G.: 6.4 Percent Eastern Test Range Acoustic Model Test Program. IN-ET17-77-2.
- Drenick, R. F.: Approximation of Complex Aerospace Systems by Simpler Ones. AD.A003 754, Polytech. Inst. of New York, July 1974.
- Ernsberger, G: Wind Biasing Techniques for Use in Obtaining Load Relief. TMX-64604.
- Ernst, A. C. and Jones, B. P. J.: Vibration Transfer Functions for Base Excited Systems. 71B100441, November 1971.

## BIBLIOGRAPHY (Continued)

- Fitzgerald, Jr., P. E. and Salvage, M. : Cost as a Technology Driver. *Astronautics and Aeronautics*, October 1976.
- Fortenberry, J. and Brownlee, G.: Viking Mars Lander 1975 Dynamic Test Model/Orbiter Developmental Test Model Forced Vibration Test: Summary Report, Technical Memorandum 33-689, Jet Propulsion Laboratory, Pasadena, Calif., November 15, 1974.
- Freeland, R. E.: Mariner Mars 1971 Unique Structural Analysis and Tests. Report No. 610-176, Jet Propulsion Laboratory, Pasadena, Calif., March 26, 1971 (JPL internal document).
- Garba, J. A., Gayman, W. H., and Wada, B. K.: Computation of Torsional Vibration Modes of Ranger and Surveyor Space Vehicles. Technical Memorandum 33-277, Jet Propulsion Laboratory, Pasadena, Calif., April 1, 1968 (JPL internal document).
- Garba, J. A. and Simpson, R. D.: Orbiting Astronomical Observatory A-2 Space Vehicle Response to Transient Loading at Atlas Booster Engine Cutoff. Report No. 900-231, Jet Propulsion Laboratory, December 21, 1968 (JPL internal document).
- Garba, J. A. : Viking Orbiter Member Load Estimates for the Transonic Flight Event. Project Document 611-100, Jet Propulsion Laboratory, Pasadena, Calif., April 1974 (JPL internal document).
- Garba, J. A., Wada, B. K., and Chen, J. C.: Experiences in Using Modal Synthesis within Project Requirements. *The Shock and Vibration Bulletin*, Bulletin 46, Part 5, August 1976. Also Technical Memorandum 33-729, Jet Propulsion Laboratory, Pasadena, Calif., July 1, 1975.
- Garba, J. A.: Flight Data Obtained from Viking A During the Titan and Centaur Powered Flight. Project Document 611-126, Jet Propulsion Laboratory, Pasadena, Calif., October 1975 (JPL internal document).
- Garba, J. A.: Flight Data Obtained from Viking B During the Titan and Centaur Powered Flight. Project Document 611-128, Jet Propulsion Laboratory, Pasadena, Calif., November 1975 (JPL internal document).
- Garba, J. A., Wada, B. K., Bamford, R. and Trubert, M. R. : Evaluation of a Cost-Effective Loads Approach. *Journal of Spacecraft and Rockets*, Vol. 13, No. 11. November 1976, pp. 675-683.
- Gayman, W. H.: A Note on Boundary-Condition Simulation in the Dynamic Testing of Spacecraft Structures. Technical Report 32-938, Jet Propulsion Laboratory, Pasadena, Calif., April 15, 1966.

## BIBLIOGRAPHY (Continued)

- Gayman, W. H., Trubert, M. R., and Garba, J. A.: OGO-E Space Vehicle Response to Transient Loading at Atlas Booster Engine Cutoff. Report No. 900-128, Jet Propulsion Laboratory, Pasadena, Calif., April 1968 (JPL internal document).
- Gayman, W. H., Trubert, M. R., and Abbott, P. W.: Measurement of Structural Transfer Functions Significant to Flight Stability of the Surveyor Spacecraft. Technical Memorandum No. 33-389, Jet Propulsion Laboratory, Pasadena, Calif., May 1, 1969.
- Gayman, W. H.: Fluid Dynamics Tests of the Viking Orbiter Propellant Tank Configuration. Project Document 900-711, Jet Propulsion Laboratory, Pasadena, Calif., July 1, 1975 (JPL internal document).
- Geering, H. P.: New Methods in Substructuring. AIAA/ASME/ASCE/ASME/ASCE/AMS - 21st Structures, Structural Dynamics, and Materials Conference, Seattle, Wash., May 12-14, 1980.
- Geissler, E. D. (Editor): Wind Effects on Launch Vehicles. AGARDO-graph 115.
- Girard, A. A., Imbert, B. J. F., and Vedereane, C. M.: Payload Dynamic Behavior Study on the Ariane Launcher. International Astronautical Congress, 28th, Prague, Czechoslovakia, September 25-October 1977, 24 p.
- Gladwell, G. M. L.: Branch Mode Analysis of Vibrating Systems. Journal of Sound and Vibration, 1, January 1974, pp. 41-59.
- Glandorf, D. R.: A Generalized Attitude Control System for the Space Shuttle Ascent Mission Phase. JSC-09198, March 1976.
- Goldenberg, S. and Sharpiro, M.: A Study of Modal Coupling Procedures for the Space Shuttle, Grumman Aerospace Corp., NASA CR-112252.
- Goldman, R. I.: Vibration Analysis of Dynamic Partitioning. AIAA Journal (8), June 1969, pp. 1152-54.
- Greiner, H. G.: Influence of Vibration Modes on Control System Stabilization for Space Shuttle Type Vehicles. Convair, NASA CR-112202, November 1972.
- Guyan, R. J.: Reduction of Stiffness and Mass Matrices. AIAA Journal, Vol. 3, No. 2, February 1965.
- Hanks, B., Ibrahim, S. R., Miserentino, R., Lee, S. and Wada, B. K.: Comparison of Modal Test Methods on the Voyager Payload. SAE Paper No. 781044, San Diego, Calif., November 1978.



## BIBLIOGRAPHY (Continued)

- Harcrow, H., Jester, T., Payton, B., and Leston, D.: Skylab Payload Base Motion Analysis Report. MMC, ED-2002-1388, October 12, 1971.
- Hargis, E. E., and Levine, A.: Titan IIIE/Centaur Wind Persistency Study. Aerospace Corporation, TOR-0075 (5702-02)-1, April 1975.
- Harter, R. J. and Switz, R. J.: Analytical and Experimental Techniques Used to Establish Structural Design Loads for the Surveyor Spacecraft During Lunar Landing. Shock and Vibration Bulletin No. 35, Naval Research Laboratory, Washington, D. C., January 1966.
- Heer, E. and Trubert, M. R.: Analysis of Space Vehicle Structures Using the Transfer-Function Concept. Technical Report No. 32-1367, Jet Propulsion Laboratory, Pasadena, Calif., April 1, 1969.
- Henry, B. Z. and Decker, J. P.: Future Earth Orbit Transportation Systems/Technology Implications. Astronautics and Aeronautics, September 1976.
- Holland, W.: Response Equations for Base Motion Excitation. MSFC, March 1, 1971.
- Holland, W.: Methodology for Base Motion Response Analysis Using Incompatible Base Motion Excitation. MSFC, February 1975.
- Holland, W.: Space Shuttle-Gust Loads Study. NASA TMX-64945, July 1975.
- Hou, S. N.: Review of Modal Synthesis Techniques and a New Approach. Shock and Vibration Bulletin, Bulletin No. 40, Pt. 4, December 1969.
- Houholt, J. C.: Gust Design Procedures Based on Power Spectral Techniques. AFFDL-TR-67-74, August 1967.
- Hruda, R. F. and Jones, P. J.: Load Transformation Development Consistent with Modal Synthesis Techniques. Shock and Vibration Bulletin, No. 48, September 1978.
- Hruda, R. F. and Benfield, W. A.: Personal Conversation, MMC, Denver, CO, April 1980.
- Hurty, W. C.: Dynamic Analysis of Structural System by Component Mode Synthesis. Technical Report No. 32-530, Jet Propulsion Laboratory, Pasadena, Calif., January 15, 1964.
- Hurty, W. C.: A Criterion for Selecting Realistic Natural Modes of a Structure. Technical Memorandum 33-364, Jet Propulsion Laboratory, Pasadena, Calif., 1967.
- Hurty, W. C., Collins, J. D., and Hart, G. C.: Dynamic Analysis of Large Structures by Modal Synthesis Techniques. Computers and Structures, 1, 1971, pp. 535-63.

## BIBLIOGRAPHY (Continued)

- Ibrahim, S. R., and Mikulcik, E. C.: A Method for the Direct Identification of Vibration Parameters from the Free Response. The Shock and Vibration Bulletin, Bulletin 47, Part 4, September 1977.
- Kana, D. D. and Vargas, L. M.: Prediction of Payload Vibration Environments by Mechanical Admittance Test Techniques. AIAA/ASMA/SAE 16th Structures, Structural Dynamics, and Materials Conference, Denver, CO, May 27-29, 1975.
- King R. L.: A Computer Version of the U. S. Standard Atmosphere 1978, NASA CR-150778.
- Kingsbury, J. E.: New Works in Space. Astronautics and Aeronautics, January 1978.
- Klosterman, A. L.: On the Experimental Determination and Use of Modal Representations of Dynamic Characteristics. PhD Dissertation, Dept. and Mech. Eng., Univ. of Cincinnati, 1971.
- Knauer, C. D., Peterson, A. J., and Rencahl, W. B.: Space Vehicle Experimental Modal Definition Using Transfer Function Techniques. National Aerospace Engineering and Manufacturing Meeting, Los Angeles, Calif., November 17-20, 1975.
- Kuhar, E. J. and Stahle, C. V.: A Dynamic Transformation Method for Modal Synthesis. AIAA Paper 73-396, presented at AIAA/ASME/SAE 14th Structures, Structural Dynamics, and Materials Conference, Williamsburg, Virginia, March 1973.
- Kuhar, E. J.: Selected System Modes Using the Dynamic Transformation with Modal Synthesis. The Shock and Vibration Bulletin, No. 44, August 1974.
- Lang, T. E.: Summary of the Functions and Capabilities of the Structural Analysis and Matrix Interpretive System Computer Program. Technical Report No. 32-1075, Jet Propulsion Laboratory, Pasadena, Calif., April 1, 1967.
- Leatherwood, A. J. D.: Active Vibration Isolation for Flexible Payloads. 68X12812, January 1968.
- Leondis, A.: Viking Dynamic Simulator - Vibration Testing and Analysis Method. The Shock and Vibration Bulletin, No. 45, Part 3, Naval Research Laboratory, Washington, D. C., pp. 103-113.
- Leppert, E. L., Wada, B. K., and Miyakawa, R.: Modal Test of the Viking Orbiter. The Shock and Vibration Bulletin, No. 44, Part 2, Naval Research Laboratory, Washington, D. C., pp. 165-175; also published as JPL Technical Memorandum 33-688, July 15, 1974.

## BIBLIOGRAPHY (Continued)

- Leppert, E. L., Lee, S. H., Day, F. D., Chapman, C. P., and Wada, B. K.: Comparison of Modal Test Results: Multipoint Sine Versus Single-Point Random. SAE Paper No. 760879, San Diego, Calif., November 29-December 2, 1976.
- MacNeal, R. H.: Vibrations of Composite Systems. Air Force Office of Scientific Research, Dept. OSR TN-55-120, October 1954.
- MacNeal, R. H.: A Hybrid Method of Component Mode Synthesis. Computers & Structures, 1, 1971, pp. 581-601.
- Mageaux, Jr., H. J., Pao, M. T., Sullivan, R. F., and Sutherlin, D. W.: Load Relief Control Law Investigation and Data Report for Saturn V Apollo Launch Vehicle. Northrop-Huntsville, TR-795-8-419, September 1968.
- Marx, M. H., Adkins, A. W., Bicciortelli, L. L., Hyland, D. C.: Evaluation of Techniques for Estimating Titan III-C Flight Loads. AIAA Paper No. 70-485, Los Angeles, Calif., April 6-8, 1970.
- McCormick, C. W. (Editor): The NASTRAN User's Manual. NASA SP-222(01), Washington, D. C., May 1973.
- McDonald, R. R.: Space Vehicle Dynamics. JPL, 77W70290.
- Mangiavacchi, A., Miste, A.: Some Qualitative Considerations on the Numerical Determination of Minimum Mass Structures with Specified Natural Frequencies. Rice University, Houston, TX, AS-A053726, September 1977.
- Meiroritch, L.: Analytical Methods in Vibration. The MacMillian Company, New York, 1967.
- Melosh, R. J., Diether, P. A., and Brennan, M.: Structural Analysis and Matrix Interpretative System (SAMIS) Program Report, Revision 1. Technical Memorandum 33-307, Jet Propulsion Laboratory, Pasadena, Calif., December 15, 1966.
- Merchant, A. D. M.: Methods for Combining Payload Parameter Variations with Input Environment. Boeing Aerospace Company, Seattle, Wash., 76N28583, June 1976, 124p.
- Miller, R. H., Smith, D. B. S., Akin, D. L., and Bowden, M. L.: Men or Machines to Build in Space. Astronautics and Aeronautics, October 1980.
- Morosow, G. and Abbott, P.: Mode Selection. Synthesis of Vibrating Systems, The American Society of Mechanical Engineers, New York, N.Y., November 1971.

## BIBLIOGRAPHY (Continued)

- Morosow, G., Dublin, M., and Korces, E.: Needs and Trends in Structural Dynamics. *Astronautics and Aeronautics*, July/August 1978.
- Niblett, L. T.: The Normal Modes of Interconnected Structure. Royal Aircraft Structures, Royal Aircraft Establishment, Farnborough, England, AD-881 433L, August 1969.
- O'Hearne, C. S. and Shipley, J. W.: Structural Dynamics Computations Using an Approximate Transformation. *Shock and Vibration Bulletin*, No. 44, Part 2, August 1974.
- O'Neil, G. K., Driggers, G., and O'Leary, B.: New Routes to Manufacturing in Space. *Astronautics and Aeronautics*, October 1980.
- Payne, K. R.: An Impedance Technique for Determining Low Frequency Payload Environments. *Shock and Vibration Bulletin*, No. 49, September 1979.
- Press, H. and Steiner, R.: An Approach to the Problem of Estimating Severe and Repeated Gust Loads for Missile Operations. NACA TN 4332.
- Rheinfurth, M.: The Alleviation of Aerodynamic Loads on Rigid Space Vehicles. NASA TMX-53397, February 21, 1966.
- Richardson, D. A. and Alwang, J. R.: Engine/Airframe/Drive Train Dynamics Interface Documentation. Boeing Vertol Company, Philadelphia, PA, AS-A055 766, April 1978.
- Ross, R. G.: Synthesis of Stiffness and Mass Matrices from Experimental Vibration Modes. SAE Paper 710787, Los Angeles, Calif., September 1971.
- Rubin, S.: An Improved Component - Mode Representation. AIAA/ASME/SAE 15th Structures Conference, Las Vegas, Nevada (April 17-19, 1974, AIAA Paper No. 74.386), also Improved Component Mode Representation for Structural Dynamic Analysis, AIAA Journal Vol. 13(8), 1975, pp. 996-1006.
- Ryan, R., Jewell, R., Bugg, F., Ivey, W., McComas, R., Kiefling, L. and Jones, J.: Dynamic Testing of Large Space Structures. NASA TMX-78307, September 1980.
- Ryan, R., Schutzenhofer, L., Jones, J., and Jewell, R.: Mechanism Associated with the Space Shuttle Main Engine Oxidizer Valve Duct System, Anomalous High Amplitude Discrete Acoustical Excitation. AIAA/ASME/ASEE/ATTS Structural Dynamics and Materials Conference, Seattle, WA, May 1980.
- Ryan, R., Schutzenhofer, L., Jones, J., and Jewell, R.: Elimination of Discrete Frequency Acoustical Phenomenon Associated with the Space Shuttle Main Engine Oxidizer Valve-Duct System. 50th Shock and Vibration Symposium, Colorado Springs, CO, October 1979.

## BIBLIOGRAPHY (Continued)

- Ryan, R. (Editor): Payload Loads Survey. Government/Industry Workshop on Payload Loads Technology, MSFC, November 1978.
- Ryan, R.: Computation of Launch Vehicle System Requirements Using Hybrid Computer. Summer Computer Simulation Conference, Montreal, Canada, July 17-19, 1973.
- Ryan, R.: Structural Control Interaction. NASA TMX 64732, January 1973.
- Ryan, R.: Ascent Control Studies of the 049 Second ATP Parallel Burn Solid Rocket Motor Shuttle Configurations. NASA TMX-64720, November 1973.
- Ryan, R.: Fundamental Concepts of Structural Loading and Load Relief Techniques for the Space Shuttle. NASA TMX-64684, August 1972.
- Ryan, R.: Dynamics and Control Studies of the Parallel Burn 156-inch Solid Propellant Motors for the Space Shuttle. NASA TMX-64670, June 1972.
- Ryan, R.: Flight Loads and Control. Shuttle Technology Review, AIAA Structural Dynamics Meeting, San Antonio, TX, April 13, 1972.
- Ryan, R.: A Look at Control Law Influence on the Rigid Body Bending Moments for Boost Vehicles with Various Degrees of Aerodynamic Stability. AIAA Guidance Control and Flight Mechanics Conference, Hofstra University, Hempstead, NY, AIAA Paper 71-918, August 16-18, 1971.
- Ryan, R., Bacchus, D. L., Hall, C. E. and Mowery, D. K.: Space Shuttle Engine Gimbal Requirements. IN-AERO-71-1.
- Ryan, R.: Space Vehicle Response to Atmospheric Disturbances. Space Shuttle Symposium, Cleveland, OH, June 1970.
- Ryan, R.: Wind Induced Loads on a Launch Vehicle and Operational Procedure for Determination of Space Vehicle Response to In-flight Wind Turbulence. Fourth National Conference on Aerospace Meteorology, Las Vegas, NV, May 1970.
- Ryan, R.: Vehicle Response to Atmospheric Disturbance. Chapter 7 ADARDograph 115, Wind Effects on Launch Vehicles, E. D. Geissler, Editor, The Advisory Group for Aerospace Research and Development, NATO, February 1970.
- Ryan, R.: Dynamic Loads of a Launch Vehicle Due to Inflight Winds. New Orleans Joint AIAA Meeting, May 6, 1968.
- Ryan, R.: Use of Wind Shears in the Design of Aerospace Vehicles. Journal of Spacecraft and Rockets, November 1967.

## BIBLIOGRAPHY (Continued)

- Ryan, R.: Dynamic Problems in Space Vehicle Design. Tennessee State Science Teachers and Science Award Winners Workshop, Peabody College, Nashville, TN, August 1967.
- Ryan, R.: A Technique for Analyzing Control Gains Using Frequency Response Methods. Journal of Spacecraft and Rockets, March 1967.
- Ryan, R.: The Influential Aspects of Atmospheric Disturbances on Space Vehicle Design Using Statistical Approaches for Analysis. NASA TMX-53565, January 13, 1967, and NASA TN-D-4963, January 1969.
- Ryan, R.: Influence of Wind Shears on Space Vehicle Design. Structures and Materials Panel Meeting, NATO, Paris, France, October 4, 1966.
- Ryan, R.: A Technique for Analyzing Control Gains Using Frequency Response Methods. AIAA Meeting, Los Angeles, CA, June 28, 1966.
- Ryan, R.: A Practical Approach to the Optimization of the Saturn V Space Vehicle Control System Under Aerodynamic Loads. NASA TMX-53298, July 21, 1965.
- Ryan, R.: Stability Considerations of a Space Vehicle in Bending Oscillations for Various Control Sensors. MTP-AERO-62-64, August 20, 1962.
- Schuett, R. H., Appleby, B. A., and Martin, J. A.: Dynamic Loads Analysis of Space Vehicle Systems - Launch and Exit Phase. General Dynamics Convair Division, Report No. GDC-DDE66-012, San Diego, Calif., June 1966.
- Seymor, V. M.: Dynamic Contact Problems. Foreign Technology Division, Wright-Patterson AFB, Ohio, AD-B025 668L, December 1977.
- Sharp, J.: Attitude Control Systems for Load Relief of Saturn Class Launch Vehicles. Northrop-Huntsville, NASA CR-613575.
- Smith, O. E.: Vector Wind and Vector Wind Shear Models 0-27 Km Altitude for Cape Kennedy, Fla., and Vandenberg AFB, Calif. NASA TMX-73319, July 1976.
- Sobieszczanski-Sobreski, J. and Goetz, R. C.: Synthesis of Aircraft Structures Using Integrated Design and Analysis Methods - Status Report. NASA Langley.
- Sperling, F. and Garba, J.: A Treatise on the Surveyor Lunar Landing Dynamics and an Evaluation of Pertinent Telemetry Data Returned by Surveyor I. Technical Report 32-1035, Jet Propulsion Laboratory, Pasadena, Calif., August 15, 1967.
- Stetson, K. A., Morrison, I. R., Cassenti, B. N.: Redesign of Structural Vibration Modes by Finite Element Inverse Perturbation. U. T. R. C., East Hartford, Conn., AD-1057662, May 1978.

## BIBLIOGRAPHY (Continued)

- Stone, C. R., Chase, T. W., Kiziloz, B. M., Kelly, E. D., Stein, G., And Ward, M. D.: Development of Control Systems for Space Shuttle Vehicles. NASA CR-1899.
- Szu, C.: Vibration Analysis of Structures Using Fixed-Interface Component Modes. Shock and Vibration Bulletin, No. 46, August 1976.
- Tatom, F., Fichtl, G. and Smith, S. R.: Simulation of Atmospheric Turbulent Gusts and Gust Gradients. 19th AIAA Aerospace Science Meeting, January 1980.
- Trautwein, W.: Load Relief and Gust Alleviation Control Study. Lockheed-Huntsville, HREC-7009-1.
- Trubert, M. R.: Use of Ranger Flight Data in the Synthesis of a Torsional Acceleration Transient for Surveyor Vibration Qualification Testing. Technical Memorandum 33-237, Jet Propulsion Laboratory, Pasadena, Calif., April 19, 1966.
- Trubert, M. R.: A Fourier Transform Technique for the Prediction of Torsional Transients for a Spacecraft from Flight Data of Another Spacecraft Using the Same Booster. Technical Memorandum 33-350, Jet Propulsion Laboratory, Pasadena, Calif., October 15, 1967.
- Trubert, M. R., Chisholm, J. R., and Gayman, W. H.: Use of Centaur/Spacecraft Flight Data in the Synthesis of Forcing Functions at Centaur Main Engine Cutoff During Boost of Mariner 1969, OAO-II, and ATS Spacecraft: Analysis, Evaluation, and Computer Plots. Technical Memorandum 33-487, Volumes I and II, Jet Propulsion Laboratory, Pasadena, Calif., June 21, 1971.
- Trubert, M. R.: A Practical Approach to Spacecraft Structural Dynamics Problems. Journal of Spacecraft and Rockets, Vol. 9, No. 11, November 1972, pp. 818-824.
- Trubert, M. R. and Eqwuatu, A.: Helios TC-2 Stage Zero Ignition Pulse Reconstruction for MJS '77 Load Analysis. Project Document 618-426, Jet Propulsion Laboratory, Pasadena, Calif., August 1976 (JPL internal document).
- Trubert, M. R.: A Fourier Transform Technique for the Prediction of Torsional Transients for a Spacecraft from Flight Data of Another Spacecraft Using the Same Booster. Technical Memorandum 33-350, Jet Propulsion Laboratory, Pasadena, Calif., October 15, 1976.
- Trubert, M. R., and Salama, M.: A Generalized Shock Spectra Method for Spacecraft Loads Analysis. JPL Publication 79-2, Jet Propulsion Laboratory, Pasadena, Calif., March 15, 1979; to be published in AIAA Journal, Vol. 18 (September 1980) and in the Journal of Spacecraft and Rockets.

## BIBLIOGRAPHY (Continued)

- Toelle, R. G., Blackwell, D. L., and Lott, L. N.: Space Shuttle Launch Vehicle Performance Trajectory, Exchange Ratios, and Dispersion Analysis. NASA TMX-64919, March 1975.
- Ugale, M., Volkert, K., and Fortenberry, J.: Viking Orbiter 75 Test Report, Static Ultimate Type Approval Test, Jet Propulsion Laboratory Project Document 611-117, Pasadena, Calif., October 11, 1974 (JPL internal document).
- Wada, B. K.: Viking Orbiter - Dynamics Overview. The Shock and Vibration Bulletin, Bulletin 44, Part 2, Naval Research Laboratory, Washington, D. C., February 12, 1962.
- Wada, B. K.: Stiffness Matrix Structural Analysis. Technical Report 32-774, Jet Propulsion Laboratory, Pasadena, Calif., October 31, 1965.
- Wada, B. K., Bamford, R., and Garba, J. A.: Equivalent Spring Mass System: A Physical Interpretation. The Shock and Vibration Bulletin, Bulletin 42, Naval Research Laboratory, Washington, D. C., January 1972, pp. 215-225.
- Wada, B. K., Garba, J. A., and Chen, J. C.: Development and Correlation: Viking Orbiter Analytical Dynamic Model with Modal Test. The Shock and Vibration Bulletin, Bulletin 44, Part 2, Naval Research Laboratory, Washington, D. C., pp. 125-164, also published as JPL Technical Memorandum 33-690, June 1, 1974.
- Wada, B. K.: Modal Test: Measurement and Analysis Requirements. SAE Paper No. 751066, Los Angeles, Calif. November 17-20, 1975.
- Wada, B. K. and Garba, J. A.: Dynamic Analysis and Test Results of the Viking Orbiter. ASME 1975 Winter Annual Meeting, ASME Paper 75-WA/Aero7, Houston, TX, November 30-December 4, 1975.
- Wada, B. K.: Design of Space Payloads for Transient Environments. Paper presented at the ASME 1979 Winter Annual Meeting, December 2-7, 1979, New York, N.Y.
- Wada, B. K.: Design of Space Payloads for Transient Environments. Survival of Mechanical Systems in Transient Environments, AMD- Vol. 36, ASME.
- Wade, D. C.: Influence of Structural Dynamics on Space Shuttle Design. AIAA Paper 77-436, AIAA/ASME 18th Structures, Structural Dynamics, and Materials Conference, San Diego, CA, March 21-23, 1977.
- White, C. W. and Maytum, B. D.: Eigensolution Sensitivity to Parametric Model Perturbations. Shock and Vibration Bulletin, No. 46, Part 5, August 1976.
- White, C. W.: Personal Conversation. MMC, Denver, CO, April 1980.



## BIBLIOGRAPHY (Continued)

- Wiggins, J. H., Company: Review and Development of Modal Synthesis Techniques. Tech. Report 1073-1, May 1972.
- Wilkerling, H. D. and Paulson, B. A.: Operational Procedure for Determining Space Vehicle Response to Wind Turbulence. NASA Contract NAS8-21325, Martin Denver Contract Reports.
- A Generalized Modal Shock Spectra Method for Spacecraft Loads Analysis. Publication 79-2, JPL, Pasadena, Calif., March 15, 1979.
- A Method for Determining the Response of the Space Shuttle to Atmospheric Turbulence. General Dynamics Report Vol., Contract NAS8-26363, November 1971.
- A Report of Advancements in Structural Dynamic Technology Resulting from Saturn 5 Programs. 70B10710, Langley Research Center, December 1970.
- C-5A System Analysis and Synthesis, Aircraft Load Alleviation, and Mode Stabilization. Boeing and Honeywell, D3-7901-2.
- Configuration Management Requirements, Level II Program Definition and Requirements. JSC 07700, Volume IV.
- Controller Design Technology for the Space Shuttle Vehicle. Honeywell Document 12738-1R1, NASA Contract NAS8-25708.
- Effects of Structural Flexibility on Launch Vehicle Control System. NASA SP-8036, NASA Space Vehicle Design Criteria.
- Introduction to Load Problems in Spacecraft Structures. Boeing Aerospace Corporation, Seattle, Wash., 78N78237, March 1974, 59 p.
- Inversion of First-Order Perturbation Theory and Its Application to Structural Design. AIAA Journal, Vol. 14, April 1976, pp. 454-460.
- Large Space Structure - Challenge of the Eighties. 7 articles, Astronautics and Aeronautics, October 1978.
- OFT-1 Flight Requirements Document. JSC 10780.
- Project Manager's Guide for STS Payload Environmental Measurements. DATE Working Group, National Aeronautics and Space Administration, Washington, D. C., April 1978.
- Project Plan for Dynamic Acoustic, Thermal Environments (DATE) Experiment. Goddard Space Flight Center, Greenbelt, Maryland, October 1979.

## BIBLIOGRAPHY (Continued)

- Propellant Slosh Loads. NASA SP-8009, NASA Space Vehicle Design Criteria.
- Shuttle OFT Flight - Program Requirements Document. JSC No. 11891.
- Space Shuttle Program Requirements Document, Level I and II.
- Space Shuttle Abort Baseline and Criteria Document. Rockwell International, SD 76-SH-0133A.
- Space Shuttle Flight and Ground System Specification, Level II Program Definition and Requirements. JSC 07700, Vol. X.
- Space Shuttle Level II Program Definition and Requirements. Volume XIV. Space Shuttle System Payload Accommodation, JSC 0770, Vol. XIV.
- Staging Loads. NASA SP-8022, NASA Space Vehicle Design Criteria.
- Stiffness Matrix Structural Analysis. Technical Memorandum 33-75, Jet Propulsion Laboratory, Pasadena, Calif. February 12, 1962.
- Structural Design Criteria Applicable to a Space Shuttle. NASA SP-8057, NASA Space Vehicle Design Criteria.
- Structural Dynamics Payload Loads Estimates. MMC Technical Proposal, P79-48144-1, February 1979.
- Structural Interaction with Control System. NASA SP-8079, NASA Space Vehicle Design Criteria.
- Terrestrial Environment (Climatic) Criteria Guidelines for Use in Aerospace Vehicle Development. TMX-64757.
- The Simulation of Elastic Mechanisms Using Kinematic Constraints and Lagrange Multipliers. Proceedings, 6th Applied Mechanisms Conference, Denver, CO, October 1979.
- Transient Loads from Thrust Excitation. NASA SP-8030, NASA Space Vehicle Design Criteria.
- Wind Loads During Ascent. NASA SP-8035, NASA Space Vehicle Design Criteria.

## REFERENCES

1. Ryan, R.: Computation of Launch Vehicle System Requirements Using Hybrid Computer. Summer Computer Simulation Conference, Montreal, Canada, July 17-19, 1973.
2. Ryan, R.: Structural Control Interaction. NASA TMX 64732, January 1973.
3. Ryan, R.: Ascent Control Studies of the 049 Second ATP Parallel Burn Solid Rocket Motor Shuttle Configurations. NASA TMX-64720, November 1973.
4. Ryan, R.: Fundamental Concepts of Structural Loading and Load Relief Techniques for the Space Shuttle. NASA TMX-64684, August 1972.
5. Ryan, R.: Dynamics and Control Studies of the Parallel Burn 156-inch Solid Propellant Motors for the Space Shuttle. NASA TMX-64670, June 1972.
6. Ryan, R.: Flight Loads and Control. Shuttle Technology Review, AIAA Structural Dynamics Meeting, San Antonio, TX, April 13, 1972.
7. Ryan, R.: A Look at Control Law Influence on the Rigid Body Bending Moments for Boost Vehicles with Various Degrees of Aerodynamic Stability. AIAA Guidance Control and Flight Mechanics Conference, Hofstra University, Hempstead, NY, AIAA Paper 71-918, August 16-18, 1971.
8. Ryan, R., Bacchus, D. L., Hall, C. E., and Mowery, D. K.: Space Shuttle Engine Gimbal Requirements. IN-AERO-71-1.
9. Ryan, R.: Space Vehicle Response to Atmospheric Disturbances. Space Shuttle Symposium, Cleveland, OH, June 1970.
10. Ryan, R.: Wind Induced Loads on a Launch Vehicle and Operational Procedure for Determination of Space Vehicle Response to In-flight Wind Turbulence. Fourth National Conference on Aerospace Meteorology, Las Vegas, NV, May 1970.
11. Ryan, R.: Vehicle Response to Atmospheric Disturbance. Chapter 7 ADARDograph 115, Wind Effects on Launch Vehicles, E. D. Geissler, Editor, The Advisory Group for Aerospace Research and Development, NATO, February 1970.
12. Ryan, R.: Dynamic Loads of a Launch Vehicle Due to Inflight Winds. New Orleans Joint AIAA Meeting, May 6, 1968.
13. Ryan, R.: Use of Wind Shears in the Design of Aerospace Vehicles. Journal of Spacecraft and Rockets, November 1967.
14. Ryan, R.: Dynamic Problems in Space Vehicle Design. Tennessee State Science Teachers and Science Award Winners Workshop, Peabody College, Nashville, TN, August 1967.

15. Ryan, R.: A Technique for Analyzing Control Gains Using Frequency Response Methods. *Journal of Spacecraft and Rockets*, March 1967.
16. Ryan, R.: The Influential Aspects of Atmospheric Disturbances on Space Vehicle Design Using Statistical Approaches for Analysis. NASA TMX-53565, January 13, 1967, and NASA TN-D-4963, January 1969.
17. Ryan, R.: Influence of Wind Shears on Space Vehicle Design. Structures and Materials Panel Meeting, NATO, Paris, France, October 4, 1966.
18. Ryan, R.: A Technique for Analyzing Control Gains Using Frequency Response Methods. AIAA Meeting, Los Angeles, CA, June 28, 1966.
19. Ryan, R.: A Practical Approach to the Optimization of the Saturn V Space Vehicle Control System Under Aerodynamic Loads. NASA TMX-53298, July 21, 1965.
20. Ryan, R.: Stability Considerations of a Space Vehicle in Bending Oscillations for Various Control Sensors. MTP-AERO-62-64, August 20, 1962.
21. Adelfang, S. I.: Analysis of Vector Wind Change with Respect to Time for Vandenberg Air Force Base, California. NASA CR-150776, August 1978.
22. Adelfang, S. I.: Analysis of Wind Bias Change with Respect to Time at Cape Kennedy, Florida, and Vandenberg Air Force Base, California. NASA CR-150777, August 1978.
23. Toelle, R. G., Blackwell, D. L., and Lott, L. N.: Space Shuttle Launch Vehicle Performance Trajectory, Exchange Ratios, and Dispersion Analysis. NASA TMX-64919, March 1975.
24. A Method for Determining the Response of the Space Shuttle to Atmospheric Turbulence. General Dynamics Report Vol., Contract NAS8-26363, November 1971.
25. Controller Design Technology for the Space Shuttle Vehicle. Honeywell Document 12738-1R1, NASA Contract NAS8-25708.
26. Holland, W.: Space Shuttle-Gust Loads Study. NASA TMX-64945, July 1975.
27. Structural Design Criteria Applicable to a Space Shuttle. NASA SP-8057, NASA Space Vehicle Design Criteria.
28. Wind Loads During Ascent. NASA SP-8035, NASA Space Vehicle Design Criteria.
29. Effects of Structural Flexibility on Launch Vehicle Control System. NASA SP-8036, NASA Space Vehicle Design Criteria.
30. Structural Interaction with Control Systems. NASA SP-8079, NASA Space Vehicle Design Criteria.

31. Transient Loads from Thrust Excitation. NASA SP-8030, NASA Space Vehicle Design Criteria.
32. Propellant Slosh Loads. NASA SP-8009, NASA Space Vehicle Design Criteria.
33. Staging Loads. NASA SP-8022, NASA Space Vehicle Design Criteria.
34. Geissler, E. D. (Editor): Wind Effects on Launch Vehicles, AGARDograph 115.
35. Smith, O. E.: Vector Wind and Vector Wind Shear Models 0-27 Km Altitude for Cape Kennedy, Fla., and Vandenberg AFB, Calif. NASA TMX-73319, July 1976.
36. Terrestrial Environment (Climatic) Criteria Guidelines for Use in Aerospace Vehicle Development. TMX-64757.
37. Ernsberger, G.: Wind Biasing Techniques for Use in Obtaining Load Relief. TMX-64604.
38. Chen, J. C. and Wada, B. K.: Criteria for Analysis-Test Correlation of Structural Dynamic Systems. Journal of Applied Mechanics, June 1975.
39. Chen, J. C. and Garba, J. A.: Determination of Propellant Effective Mass Properties Using Modal Test Data. The Shock and Vibration Bulletin, Bulletin 45, Naval Research Laboratory, Washington, D.C., 1975.
40. Chen, J. C. and Wada, B. K.: Matrix Perturbation for Structural Dynamic Analysis. AIAA Journal, Vol. 15, August 1977, pp. 1095-1100.
41. Chen, J. C., Wada, B. K., and Garba, J. A.: Launch Vehicle Payload Interface Response. Journal of Spacecraft and Rockets, Vol. 15, No. 1, January-February 1978, pp. 7-11.
42. Chen, J. C., Garba, J. A., and Wada, B. K.: Estimation of Payload Loads Using Rigid-Body Interface Accelerations. Journal of Spacecraft and Rockets, Vol. 16 No. 2, March-April 1979, pp. 74-80.
43. Chen, J. C., Zayzebski, K. P., and Garba, J. A.: Recovered Transient Load Analysis for Payload Structural Systems. AIAA/ASME/ASCE/AMS - 21st Structures, Structural Dynamics, and Materials Conference, Seattle, Wash., May 12-14, 1980.
44. Chen, J. C., Garba, J. A., Salama, M., and Trubert, M.: A Survey of Load Methodologies for Shuttle Orbiter Payloads. JPL Publication 80-37.
45. Trubert, M. R., and Salama, M.: A Generalized Shock Spectra Method for Spacecraft Loads Analysis. JPL Publication 79-2, Jet Propulsion Laboratory, Pasadena, Calif., March 15, 1979; to be published in AIAA Journal, Vol. 18 (September 1980) and in the Journal of Spacecraft and Rockets.

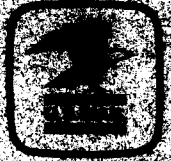
46. Wada, B. K.: Design of Space Payloads for Transient Environments. Paper presented at the ASME 1979 Winter Annual Meeting, December 2-7, 1979, New York, N. Y.
47. Wada, B. K.: Design of Space Payloads for Transient Environments. Survival of Mechanical Systems in Transient Environments, AMD-Vol. 36, ASME.
48. Ryan, R. (Editor): Payload Loads Survey. Government/Industry Workshop on Payload Loads Technology, MSFC, November 1978.
49. Henry, B. Z. and Decker, J. P.: Future Earth Orbit Transportation Systems/Technology Implications. Astronautics and Aeronautics, September 1976.
50. Amos, A. K. and Goetz, R. C.: Research Needs in Aerospace Structural Dynamics. AIAA Paper 79-0826, AIAA/ASME/ASCE/AHS 20th Structures, Structural Dynamics, and Materials Conference, St. Louis, Mo., April 4-6, 1979.
51. Bekey, I. and Naugle, J.: Just Over the Horizon in Space. Astronautics and Aeronautics, May 1980.
52. Card, M. F.: Trends in Aerospace Structures, Astronautics and Aeronautics, July/August 1978.
53. Kingsbury, J. E.: New Works in Space. Astronautics and Aeronautics, January 1978.
54. Morosow, G., Dublin, M., and Korces, E.: Needs and Trends in Structural Dynamics. Astronautics and Aeronautics, July/August 1978.
55. Space Shuttle Abort Baseline and Criteria Document. Rockwell International, SD 76-SH-0133A.
56. Space Shuttle Program Requirements Document, Level I and II.
57. Space Shuttle Flight and Ground System Specification, Level II Program Definition and Requirements. JSC 07700, Vol. X.

1. REPORT NO. NASA TP-1950		2. GOVERNMENT ACCESSION NO.		3. RECIPIENT'S CATALOG NO.	
4. TITLE AND SUBTITLE SYSTEM ANALYSIS APPROACH TO DERIVING DESIGN CRITERIA (LOADS) FOR SPACE SHUTTLE AND ITS PAYLOADS VOLUME II - TYPICAL EXAMPLES				5. REPORT DATE December 1981	
				6. PERFORMING ORGANIZATION CODE	
7. AUTHOR(S) Robert S. Ryan, Tulon Bullock, Wayne B. Holland, Dennis A. Kross, and Larry A. Kiefling				8. PERFORMING ORGANIZATION REPORT #	
9. PERFORMING ORGANIZATION NAME AND ADDRESS  George C. Marshall Space Flight Center Marshall Space Flight Center, AL 35812				10. WORK UNIT NO. M-359	
				11. CONTRACT OR GRANT NO.	
				13. TYPE OF REPORT & PERIOD COVERED  Technical Paper	
12. SPONSORING AGENCY NAME AND ADDRESS  National Aeronautics and Space Administration Washington, D.C. 20546				14. SPONSORING AGENCY CODE	
15. SUPPLEMENTARY NOTES  Prepared by Systems Dynamics Laboratory, Science and Engineering					
16. ABSTRACT  Derivation of a set of design loads criteria for a space system that provides a specified launch or operational probability, adequate lifetime, and safety factors and, at the same time, meet low-cost, high-performance (low weight in general) requirements is the major problem facing engineering and program personnel. Stated another way, how do you achieve an optimized design from the system standpoint under the low-cost, high risk constraints of the present day environment? The answer to this question is compounded by the complex mission models and structural configurations which have strong interaction or coupling between structures, control, propulsion, thermal, aeroelastic, and performance. Basic to this question is how to treat vehicle system parameters and environment uncertainties. Space Shuttle, the most complex transportation system designed to date, illustrates the requirement for an analysis approach that considers all major disciplines simultaneously. Its unique cross coupling and high sensitivity to aerodynamic uncertainties and high performance requirements dictated a less conservative approach than those taken in prior programs. Analyses performed for the Space Shuttle and certain payloads, Space Telescope and Spacelab, are used as examples in Volume 2. These illustrate the requirements for system analysis approaches and criteria, including dynamic modeling requirements, test requirements, control requirements, and the resulting design verification approaches. A survey of the problem, potential approaches available as solutions, implications for future systems, and projected technology development areas are addressed in this report. This report is divided into two independent volumes. Volume 1 deals with the philosophy and general loads analysis approaches. Volume 2 gives the Shuttle examples. Readers can read both or choose either, since they are written to be independent.					
17. KEY WORDS  Aerospace vehicle design loads Load alleviation techniques Structural dynamics			18. DISTRIBUTION STATEMENT  Unclassified - Unlimited  Subject category: 15		
19. SECURITY CLASSIF. (of this report) Unclassified		20. SECURITY CLASSIF. (of this page) Unclassified		21. NO. OF PAGES 118	22. PRICE A06

National Aeronautics and  
Space Administration  
Washington, D.C.  
20546  
Official Business  
Penalty for Private Use, \$300

THIRD CLASS BULK RATE

Postage and Fees Paid  
National Aeronautics and  
Space Administration  
NASA-467



**NASA**

POSTMASTER: If Undeliverable (Section 110  
Postal Manual) Do Not Return

---